


2012

Mesoporous Silicates: Materials Science and Biologica Applications

Robert Anthony Roggers
Iowa State University

Follow this and additional works at: <https://lib.dr.iastate.edu/etd>

 Part of the [Biomedical Commons](#), [Chemistry Commons](#), and the [Mechanics of Materials Commons](#)

Recommended Citation

Roggers, Robert Anthony, "Mesoporous Silicates: Materials Science and Biologica Applications" (2012). *Graduate Theses and Dissertations*. 12630.
<https://lib.dr.iastate.edu/etd/12630>

This Dissertation is brought to you for free and open access by the Iowa State University Capstones, Theses and Dissertations at Iowa State University Digital Repository. It has been accepted for inclusion in Graduate Theses and Dissertations by an authorized administrator of Iowa State University Digital Repository. For more information, please contact digirep@iastate.edu.

Mesoporous silicates: Materials science and biological applications

by

Robert Anthony Rogers

A dissertation submitted to the graduate faculty in
partial fulfillment of the requirements for the degree of

DOCTOR OF PHILOSOPHY

Major: Chemistry

Program of Study Committee

Brian G. Trewyn, Co-Major Professor

Keith Woo, Co-Major Professor

Nicola Pohl

Edward Yu

Marek Pruski

Iowa State University

Ames, Iowa

2012

Copyright © Robert Anthony Rogers, 2012. All rights reserved.

Table of Contents

ABBREVIATIONS.....	v
ACKNOWLEDGEMENTS.....	viii
ABSTRACT.....	ix

CHAPTER 1. MESOPOROUS SILICA PARTICLES IN BIOLOGICAL APPLICATIONS

I.	Introduction.....	1
II.	Toxicity Studies and Mesoporous Silicates.....	2
	a. <i>In Vitro</i> Studies.....	4
	b. <i>In Vivo</i> Studies.....	8
III.	Strategies for Controlled Release.....	14
	a. Controlled Release with Cellular Stimuli.....	14
	b. Controlled Release with External Stimuli.....	20
IV.	Actively Targeted MSP Systems.....	24
	a. Folic Acid.....	25
	b. Saccharides.....	28
	c. Small Molecules.....	31
	d. DNA, RNA and Antibody Targeting.....	32
V.	Analytical Applications.....	35
	a. Separations.....	35
	b. Imaging Applications.....	37
VI.	Conclusion.....	41
VII.	References.....	41

CHAPTER 2. LIPID BILAYER COATED MESOPOROUS SILICA

I.	Chemically Reducible Lipid Bilayer Functionalized Mesoporous Silica:
----	--

Biocompatibility and Controlled Release	46
a. Introduction.....	46
b. Experimental.....	49
c. Results and Discussion.....	52
d. Conclusions.....	60
II. Haemocompatibility of Lipid Bilayer Functionalized Large-Pore Mesoporous Silica...	62
a. Introduction.....	62
b. Experimental.....	64
c. Results and Discussion.....	67
d. Conclusions.....	72
III. References.....	73

CHAPTER 3: SYNTHESIS OF NEW MATERIALS USING THE HYDROLYSIS AND CONDENSATION OF ALKOXYSILANE PRECURSORS

a. General Introduction.....	78
I. Synthesis of a New Mesoporous Silica Particle from Water in Oil Emulsion.....	79
a. Introduction.....	79
b. Experimental.....	80
c. Results and Discussion.....	81
II. Synthesis and Morphology Control of a Periodic Mesoporous Organosilica Derived from Benzobisoxazole-Bridged Alkoxysilanes.....	87
a. Introduction/Experimental/Results.....	87
b. Conclusions.....	92
III. References.....	92

CHAPTER 4: THE DESIGN OF A SOLID SUPPORTED N-HETEROCYCLIC CARBENE CATALYST

I. Introduction.....	95
II. Experimental.....	105

III.	Results and Discussion.....	108
IV.	Conclusions.....	111
V.	References.....	111
CHAPTER 5: GENERAL CONCLUSIONS.....		114
APPENDICES		
Appendix A: ToxRTool (Klimisch criteria) and glossary of selected terms.....		117
Appendix B: Supplemental Data: Chemically Reducible Lipid Bilayer Functionalized Mesoporous Silica: Biocompatibility and Controlled Release.....		120
Appendix C: Synthesis Conditions and Additional TEM/SEM images, XRD plots: Synthesis of a New Mesoporous Silica Particle from Water in Oil Emulsion.		127
Synthesis results of PMO: Synthesis and Morphology Control of a Periodic Mesoporous Organosilica Derived from Benzobisoxazole-Bridged Alkoxysilanes.....		137
Appendix D: Structures of featured ligands in the introduction of “The design of a Solid Supported N-Heterocyclic Carbene Catalyst		138
(Appendices are located in a supplemental file)		

Abbreviations

- 3-GPTES – 3-glycidoxypropyl triethoxysilane
 3-ICPTES – 3-isocyanatopropyl triethoxysilane
 3-IPTES – 3-iodopropyl triethoxysilane
 AA – anisamide
 ACA – 9-anthracene carboxylic acid
 ALT – alanine aminotransferase
 AMP – adenosine monophosphate
 AP – aminopropyl
 AR – aspect ratio
 AST – aspartate aminotransferase
 ATP – adenosine triphosphate
 BBO - benzobisoxazole
 BET – Brunauer-Emmett-Teller method
 BHEEEN - 5-bis[2-(2-(2-hydroxyethoxy)ethoxy)ethoxy)naphthalene
 BTB – 1,3,5-benzyltrimethoxybenzene
 bpy - bipyridyl
 C7U – cucurbit[7]uril
 cAMP – cyclic adenosine monophosphate
 CBPQT - cyclobis(paraquat-*p*-phenylene)
 CIL – cell interaction layer
 CL - cardiolipin
 Cp – camptothecin
 CuAAC – copper mediated azide/alkyne cross-coupling
 CTAB – cetyltrimethylammonium bromide
 DAG - diacylglycerol
 DC – direct current
 DCC – dicyclohexylcarbodiimide
 DEA - diethylamine
 DHLA – dihydroxylicipoic acid

DMSO - dimethylsulfoxide
 DNA – deoxyribonucleic acid
 DP-MSN – dipalmitoyl functionalized mesoporous silica nanoparticles
 DPPC – dipalmitoyl phosphatidylcholine
 DTPA – diethyltriammine pentaacetic acid
 DTT – dithiothreitol
 DOX – doxorubicin
 FA – folic acid
 GN – gold nanorod
 GSH – glutathione
 HA – hyaluronic acid
 HC – heterogeneous catalysis
 IR - infrared
 ICP-MS – inductively coupled plasma mass spectrometry
 LA - lactobionic acid
 LB – lipid bilayer
 LB-MSN – lipid bilayer functionalized mesoporous silica nanoparticles
 MALDI-TOFMS – matrix-assisted laser-desorption ionization time-of-flight mass spectrometry
 MASBB - 2,6-bis(methyl(3-aminopropyltriethoxy-silane))benzo(1,2-d,4,5-d')bisoxazole
 MOF – metal organic framework
 MPTMS – 3-mercaptopropyl trimethoxysilane
 MRI – magnetic resonance imaging
 MS – mesoporous silicate
 MSN – mesoporous silica nanoparticle
 MSP – mesoporous silica particle
 MTT – methotrexate
 NADH – nicotinamide adenine dinucleotide
 NHBE – normal human bronchial epithelial cells
 NHC – N-heterocyclic carbene

NIR – near-infrared
NLC – normal liver cells
NMR – nuclear magnetic resonance
PA – phosphatidic acid
PBS – phosphate buffered saline
PC – phosphatidylcholine
PE – phosphatidylethanolamine
PCR – polymerase chain reaction
PEG – polyethyleneglycol
PEI – polyethyleneimine
PLD – phospholipase D
PMO – periodic mesoporous organosilicate
PNIPAM – poly(N-isopropylacrylamide)
RBC – red blood cell
RNA – ribonucleic acid
ROS – reactive oxygen species
SEM – scattering electron microscopy
siRNA – signal interference ribonucleic acid
TBTA – tris-(benzyltriazolylmethyl)amine
TCEP – tris(2-carboxyethyl)phosphine
TDPP – 1-thiol-2,3-dipalmitoyl propane
TED – tetraacetic acid diethylamine
TEM – transmission electron microscopy
TEP – Tolman electronic parameter
TEOS - tetraethylorthosilicate
TPD – 1-thiol-2,3-propanediol
TGA – thermogravimetric analysis
W/O – water-in-oil emulsion
XRD – X-ray diffraction

Acknowledgments

This thesis is dedicated to the things that make life worth living.

My wife, who has stood by me and worked with me for the duration of this work.

My daughter, who always has a smile and can make me feel important and needed.

My friends, who have offered spiritual counsel, scientific advice and opportunity for general mischief in times of need.

Man cannot survive on bread and science alone.

ABSTRACT

This thesis dissertation presents the collective research into the advancement of mesoporous silicate particles as biointerface devices, the development of new materials and the application of these particles as solid supports for heterogeneous catalysis.

Mesoporous silica has been utilized in the aforementioned applications due to several reasons; the first being the ability to achieve high surface areas ($500 - 1000 \text{ m}^2 \text{ g}^{-1}$) with controlled pore sizes and particle morphology. Another reason for their popularity is their robustness in applications of heterogeneous catalysis and readily functionalizable surface with a wide variety of organic groups. In the field of biointerface devices, mesoporous silica nanoparticles represent a class of materials that exhibit high biocompatibility. In addition, the ability to functionalize the surfaces (outer surface and pore interiors) allows the particles to be targeted to specific cell types as well as optimized to release many different therapeutic molecules under specific stimuli.

A unique particle coating consisting of a chemically cleavable lipid bilayer that allows for the encapsulation of a fluorescent molecule and increases the biocompatibility of the particle has been developed. The lipid bilayer coated mesoporous silica nanoparticle (LB-MSN) was characterized using X-ray diffraction, transmission electron microscopy and nitrogen 'sorption isotherms. The finished LB-MSN was then incubated with mammalian cells in order to demonstrate their biocompatibility. Confocal micrographs demonstrate the endocytosis of the particles into the cells. In addition the micrographs also show that the LB-MSNs are separate from the endosomal compartments, however due to the lipophilic nature of the dye used to label the endosome there is some debate regarding this conclusion. The lipid bilayer coating was then applied to a large pore MSN (l-MSN) which had been previously shown to cause lysis of red blood cells (RBCs) at low concentrations of particles. The lipid bilayer allowed the LB-MSN to interface with RBCs without resulting in haemolysis. It was observed however, that spiculation (damage) of the RBCs still occurred despite the lack of cell lysis. During the course of the study, the composition of the outer

leaflet of the lipid bilayer was altered to more closely match that of the outer leaflet of RBCs. This alteration proved to make the LB-I-MSN particle extremely compatible with RBCs in that spiculation of the cells was reduced by more than 50 % according to observations by scanning electron microscopy.

A new synthetic route to mesoporous silica nanoparticles (MSNs) was developed using water in oil (W/O) emulsions. This method relies on the presence of an amphiphilic stabilizer molecule to control the size and quality of the spherical morphology of the particles. Partitioning of the oil phase into cetyltrimethylammonium bromide surfactant molecules is implicated in expanding the size of the mesopores from the standard 3 nm pore to 7 nm. This material is extensively characterized using X-ray diffraction techniques and TEM microscopy. Chapter 3 also outlines the synthesis of a new periodic mesoporous organosilica (PMO) in which the bridging organic group is a benzobisoxazole molecule synthesized in the research group of Dr. Malika Jeffries-EL. While no immediate application of this new particle was proven, we propose this structure as the basis for a new class of light harvesting or light emitting diode material based on the performance of the polymers containing these benzobisoxazole moieties and functionalized dyes.

The final project was the initial development of an N-heterocyclic carbene ligand based on an imidazole framework. This project represents significant synthetic challenges in that the pattern of substitution on the imidazole framework has not been reported in the literature to the best of our knowledge. Despite the synthetic challenges, significant progress has been made towards the goal of generating an MSN with a functional group capable of coordinating a wide variety of metals for an extensive array of catalytic reactions. Additionally, N-heterocyclic carbenes have been shown to have anti-bacterial and anti-tumor capabilities. We propose that these new ligands may also represent a significant advancement in the field of biomedical applications of MSNs.

Chapter 1: Mesoporous Silica Particles in Biological Applications

I. Introduction

Mesoporous silica particles (MSPs) have been used for over a decade to affect changes and analyze biological systems. These particles exhibit characteristics such as high surface area capable of accepting diverse functionalization, relatively large internal volumes for storage of different molecules and the ability to selectively functionalize either the inner or outer surface areas of the particle. In addition, particle size and morphology can also be successfully tuned to match specific needs of the application.

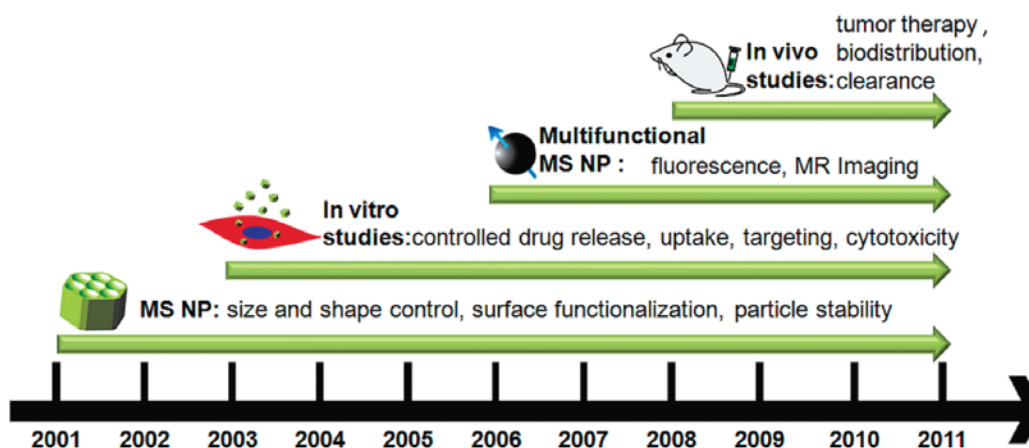


Figure 1. Timeline of different studies using MSP systems. Reprinted with permission from Lin, Y.-S.; *et al. Phys. Chem. Lett.* **2012**, 3, 364 – 274. Copyright 2012 American Chemical Society.

The combinations of these attributes can lead to a dizzying array of parameters that should be known if the MSP system is to be properly evaluated for effectiveness. One recent review focused exclusively on the synthetic aspect of MSPs and concluded that the majority of systems developed for use in biological applications do not meet many of the physical criteria required to go from bench top to bedside.^[1] These criteria include particle size, pore structure, aggregation of particles and biodegradability. While controlling synthetic conditions to provide the optimal particle for the application is one necessity of bio-destined MSPs, another is adopting the correct particle characterization techniques and assays for

evaluating the performance and toxicity of the MSP in the biological system being studied. Bio-destined MSPs have been under development for over 10 years and are showing potential as possible therapeutic devices and delivery agents. With this in mind, it is important that researchers studying the biological applications of MSPs (and indeed nanoparticles in general) adopt a set of criteria which will enable the fair evaluation for all future work done in this field. This will be the focus of section III of the review, wherein the strictly toxicological studies of MSPs will be evaluated. Further sections of this review will attempt to provide some perspective on the diversity of MSP systems that are available to study.

II. Toxicity Studies and Mesoporous Silicates

One of the greatest challenges facing researchers designing MSPs for drug delivery lies in understanding the toxicology and development of a uniform set of standards for determining the safety and effectiveness of MSPs. Recently the journal *Nature* published a short editorial on the inadequacies of several *in vivo* and *in vitro* methods claiming that 15 of 21 animal studies failed to meet the highest criteria of the Klimisch test.^[2, 3] The article goes on to state “Of 10 parameters that... should be in a nanotoxicity study, such as particle size, shape and surface chemistry, more than half were missing from the 14 animal studies.” This study was brought about in part by a paper in the *European Respiratory Journal* in which Song *et al.* report that seven Chinese factory workers developed pleural granulomas (aggregations of immune cells in the lung lining) and excessive discolored fluid in the lung lining.^[4] All cases examined were found to have high concentrations of ≈ 30 nm polyacrylate ester particles in the lung fluid and tissue. A second editorial in *Nature* points out that several experts regard the study as being inconclusive regarding nanoparticles being the cause of respiratory distress in the workers; however it was stated that the evidence “raises the bar for doing appropriate research... when working with nanomaterials”.^[5] A reply made by an author of one of the evaluated studies points out that much of the data that is missing in the study is actually available in previous papers published by their research group, however this is akin to a pharmaceutical company claiming that two batches of drug have identical

properties without doing any physical analyses, which would not be allowed under FDA guidelines.

This section is devoted to a serious review of toxicological studies of MSPs for use in biological systems and an attempt to quantify the quality of data coming from several toxicological studies, the Klimisch criteria will be applied and a ranking of reports will be provided (Klimisch criteria are available in appendix A). While it is true that all Klimisch score criteria are not precisely defined, this approach presents the most uniform method for evaluating a large number of studies. In addition, inconsistencies regarding *in vitro* toxicity evaluation methods have already been observed by several groups and these will be discussed in an attempt to determine the best method(s) for assessing toxicity.

Over the last five years, several groups have attempted to quantify the toxicity and bioaccumulation of MSPs and nanoparticles in general. The majority of work describing the cytotoxicity of MSPs involves unfunctionalized nanoparticles and attempts to correlate the toxicity with physical parameters such as particle size, pore size and particle morphology. Silica particles bearing absorbed or grafted polyethylene glycol (PEG) groups are also evaluated for their toxicity, owing to the relatively recent findings that many materials, when coated with PEG do not actively interact with cells and do not participate in non-specific protein binding. One broad review on nanoparticles suggests that reproducibility in data may be affected by interference of nanoparticles with read-out systems commonly used to determine cytotoxicity.^[6, 7] Indeed, false data have been observed in a number of studies in which methotrexate (MTT) was employed, including one report where it was discovered that a standard MTT assay gave falsely high compatibility results due to reduction of MTT at the surface of an MSP instead of through normal cellular metabolism.^[8] A further study reported that MTT data was unreliable due to the ability of MSPs to increase the rate of formazan (MTT metabolite) exocytosis, falsely increasing the biocompatibility of MSPs.^[9] Despite this finding, MTT is still widely applied to determine toxicity of nanomaterials, perhaps due to the availability and cost of kits and the fact that only a fluorometer is necessary for data collection.

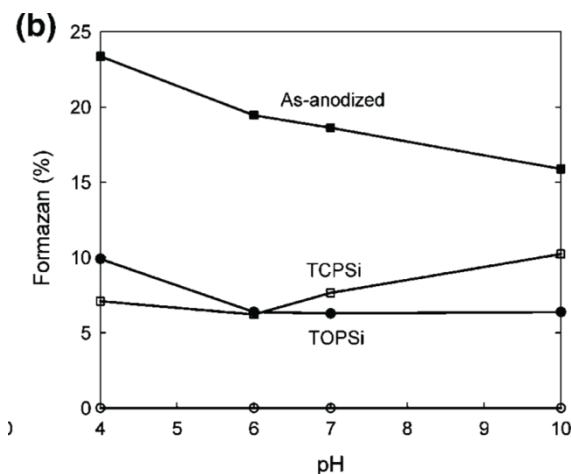


Figure 2. Graph representing the percentage of formazan detected from the reduction of (3-[4,5-dimethylthiazol-2-yl]-2,5-diphenyltetrazolium bromide) (MTT) in the presence of MSPs. Anodized = Si-C surface, TOPSi = thermally oxidized (calcined), TCPSi = thermally carbonized. The sample TOPSi represents the surface most similar to the MSPs reviewed in this chapter. Reprinted with permission from Laaksonen, T.; *et al.*, *Chemical Research in Toxicology* **2007**, 20 (12), 1913-1918. Copyright 2007 American Chemical Society

Unfortunately, due to the number of earlier studies that rely on MTT assays for toxicity measurements, much of our knowledge regarding the toxicity of MSPs must be carefully examined and studies using MTT must include a clear negative control group in which MTT and MSPs are co-incubated in growth media to ensure validity of observations.

Toxicity of MSPs *in vitro*

In order to bypass some of the problems found in their earlier studies, Heikkila *et al.* have chosen several assays that rely on different metabolic indicators to determine overall toxicity of sieved particle aggregates.^[10] Different kits for measuring cell viability were used, including protease activity, ATP luminescence, and caspase 3/7 activity in addition to flow cytometry and ROS detection in order to ensure accurate results of individual methods. Protease and ATP-luminescence (**Fig. 3**) assays gave remarkably similar results for percent cell viability and the caspase 3/7 assay for apoptosis activity results showed that in experiments with less cell viability, the caspase 3/7 activity was increased. The peroxide

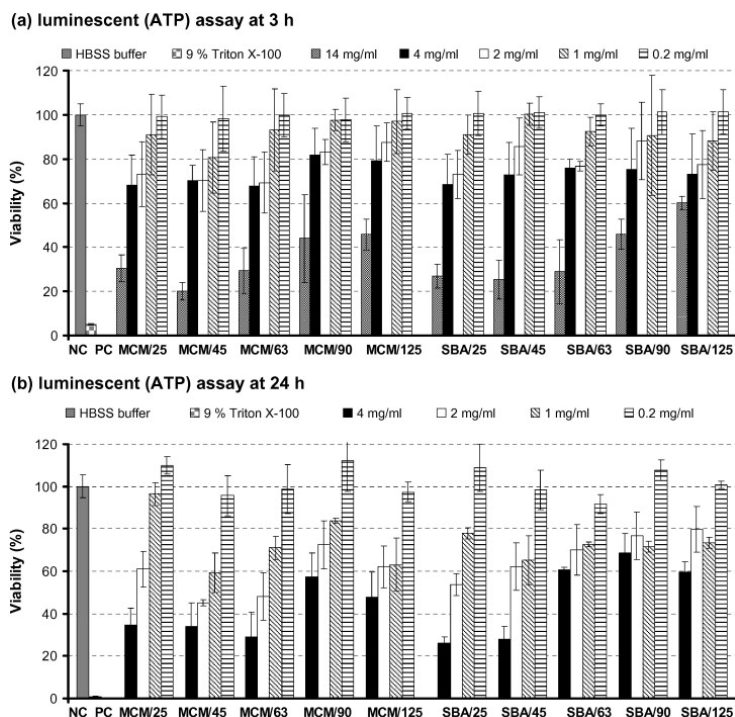


Figure 3. Results of the ATP luminescence assay in Caco-2 cells. Deemed the most accurate and sensitive indicator of cell viability. Reprinted with permission from Heikkilä, T.; *et al.*, *Euro. J. Pharma Biopharma* **2010**, *74* (3), 483-494. Copyright 2010 Elsevier Publishing.

A study by Al Shamsi *et al.* uses a novel method of examining the oxygen consumption of excised mouse organ tissue; this is believed to be the only example utilizing this oxygen consumption technique with MSPs.^[11] In this work the authors determined that MCM-41 and SBA-15 type MSPs are biocompatible under specific conditions *in vitro*. One thing to note in this study is the large diameter and broad size distribution (600 to 1000 nm) of MCM-41 particles examined. In most systems describing MCM-41 type MSPs the average particle size is approximately 200 nm \pm 50 nm. As the size of a particle is widely accepted as one of the main determining factors of toxicity, care must be exercised when attempting to correlate the findings of this study with other toxicological studies of MCM-41 type particles. Huang and coworkers examined the toxicity of MSPs with different morphologies but similar diameters using such diverse assays as cytoskeleton formation, cell adhesion, Western blot, cell migration, PCR-assisted protein quantification, annexin V apoptosis assay and MTT assay.^[12] The majority of findings in this study indicate that particles with higher aspect ratios (i.e. rod-shaped particles) interfere more with cellular processes such as adhesion, cytoskeletal organization and protein synthesis than spherical particles resulting in an

approximately 10 -20% increase of cells undergoing apoptosis over the control group. In contrast to the latter findings, the MTT assay for viability showed that almost all particle types and exposure concentrations resulted in cells that were at or above 100% viability and the particles were judged non-toxic based on this evidence.

Another study on the effects of particle size on cell viability by He and coworkers shows similar results for the MTT assay as the previous study.^[13] Additionally, this study showed that the toxicity of particles where the templating surfactant has been removed

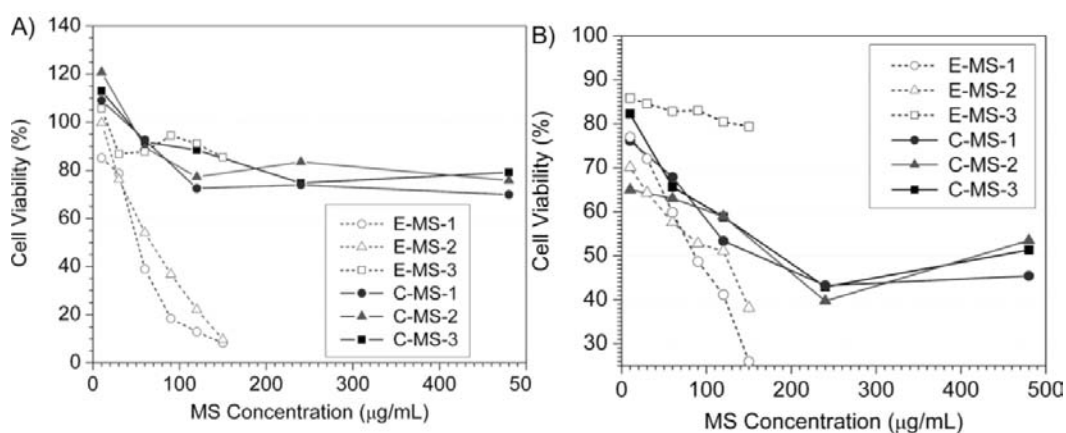


Figure 4. Results of the viability assays for MAD-MB-468 cells (A) and COS-7 cells (B). E-MS and C-MS refer to solvent extracted (soxhlet) and calcined MSPs respectively.

through solvent extraction is markedly increased compared to particles that have been calcined (**Fig. 4**). However, upon examination of the experimental evidence, the solvent extracted particles have an unusually high mass percentage of surfactant remaining compared with the majority of MSP publications. Control experiments with free surfactant were carried out; however a questionable correlation is drawn between the ζ -potential of the particles and the effect that surfactant *within* the pores of the particle plays on this measurement.^[14] Zeta-potential measurements examine the charge at a defined distance from the surface of a solid. This distance is defined by the thickness of the inner and outer Helmholtz layers and the thickness of the slip plane (Figure X) which are all affected, in part, by the surface charge of the solid, pH, ionic strength and type of counter-ion as well as small amounts of impurity in solution. The distance of the MSP surface hypothetically altered by the presence of surfactant is too far from the slip plane to reasonably affect the measurement of ζ -potential if it is

assumed that diffusion of surfactant during extraction leads to the absence of surfactant at the pore openings.

An important concern about the validity of toxicological studies is raised in a study by Zhang *et al.*^[15] They point to the fact that most cell lines used for *in vitro* toxicity assays are genetically transformed and that there are numerous problems including cells without natural phenotype, different numbers of chromosomes, and differences in signaling and viability pathways between transformed and non-transformed cells. These differences, the authors state, result in large differences between *in vivo* and *in vitro* studies. To test an example of this hypothesis the authors use differentiated versus undifferentiated (primary) bronchial epithelial cells and compare cell viability after exposure to MSPs. Zhang *et al.* shows that there are measurable differences in toxicity for polyethyleneimine functionalized MSPs for differentiated and undifferentiated normal human bronchial epithelial (NHBE) cells. The increase in toxicity of MSPs toward differentiated NHBE cells result from increased binding of positively charged MSPs to negatively charged syndecan-1 proteins present on the surface of the differentiated cells. This finding was confirmed by treating NHBE cell lines with heparinase to cleave syndecan-1 from the surface of the cells, resulting in reduced MSP uptake and binding similar to that of undifferentiated NHBEs. The results of these assays suggest that MSPs may become increasingly toxic after cells have differentiated *in vivo*.

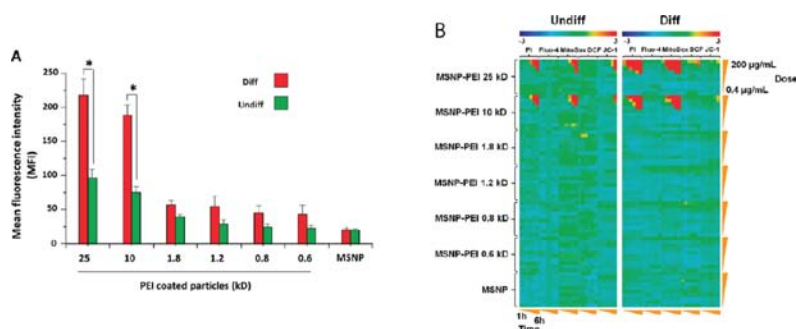


Figure 5. Assay of the mean fluorescence intensity (A) of fluorescein labeled MSPs. Differentiated cells show greater than 2 fold increase in intensity when larger PEI chains are used to coat the MSP. (B) Multiparametric heat map consisting of assays of calcium flux (Fluoro-4), superoxide generation (Mitoxox), H₂O₂ generation (DCF) and mitochondrial membrane depolarization (JC-1). Reprinted with permission from Zhang, H.; *et al.* *ACS Nano* **2011**, 5 (4), 2756-2769. Copyright 2011 American Chemical Society

Toxicity of MSPs *in vivo*

Findings by Kohane and coworkers shows that various MSPs have highly variable *in vivo* toxicity depending on particle type and administration route.^[16] Intraperitoneal administration resulted in the death of all test subjects for all particle types within 24 hours, while intravenous administration resulted in the death of all subjects within 15 minutes. Examination of lung tissue from deceased subjects indicated severe pulmonary thrombi and emboli. Subcutaneous delivery resulted in no death of subjects; this was hypothesized to be due to slow distribution of particles from the administration site. Histology revealed that materials administered subcutaneously remained in the region of administration for a period of up to 3 months and that splenic deformation could be observed for 2 -3 months after exposure to MSPs.

Similar findings were reported by Liu *et al.* with regards to 110 nm hollow MSPs in ICR mice at similar concentrations of particles (≈ 1200 mg/kg).^[17] Liver enzymes alanine aminotransferase (ALT) and aspartate aminotransferase (AST), both important indicators of liver health were found to be elevated in mice receiving over 80 mg/kg continuous intravenous dosages and liver necrosis, microgranulation and lymphocytic infiltration were observed for mice receiving a 1280 mg/kg bolus. Additionally, white blood cell count increased in mice receiving over 500 mg/kg doses of MSPs and in those receiving continuous intravenous doses

Table 1. Details of a 90 day study on mortality rates of rats exposed to MSPs

Material ^a	Mortality ^b	Time to death ^c	Numbers of animals euthanized for necropsy, by time point				
			4 days	2 weeks	1 month	2 months	3 months
MCM-41cal	1 of 8	2 days	2	2	-	2	2
MCM-41ref	1 of 6	3 days	2	2	1	1	-
SBA-15	0 of 14	-	4	4	1	3	2
MCF	0 of 14	-	4	4	1	3	2

^a 60 mg of MSP injected subcutaneously and at the sciatic nerve in the same animal

^b From presumed MSP toxicity

^c In animals that died from MSP toxicity

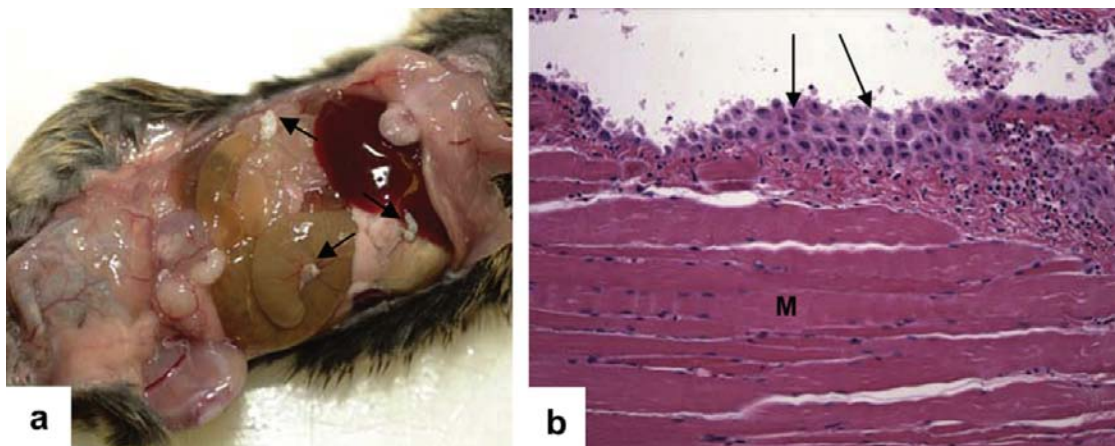


Figure 6. (a) Exposed peritoneum in mouse 24 hr post-injection of MSPs. Arrows indicate pockets of MSP residue. (b) Light microscopy image of mouse peritoneum, despite the presence of pockets of MSPs, mesothelial cells (arrows) do not appear to be damaged. Both table and figure are reprinted with permission from Hudson, S. P.; Padera, R. F.; Langer, R.; Kohane, D. S., *Biomaterials* **2008**, 29 (30), 4045-4055. Copyright 2008 Elsevier Publishing.

above 20 mg/kg, though not at levels outside of normal range until doses of 80 mg/kg were administered. The bioaccumulation of MSPs were also studied and found that MSPs are present for up to 4 weeks in the spleen and liver post administration.

In contrast to the unfunctionalized MSPs examined in the previous studies; MSPs functionalized with the tumor targeting ligand, folic acid were evaluated for *in vivo* toxicity by Lu *et al.*^[18] Results of histology and silicon ICP-MS showed that folate-functionalized MSPs preferentially accumulate in tumor cells during the first 24 hours of the experiment. During the following 24 hours, folate functionalized MSPs migrate from the tumor sites (2-fold decrease in MSP concentration in tumors) to the lung, spleen and intestine. After this time period MSPs are excreted ($\approx 94.4\%$ of the initial bolus) in the urine and feces of mice tested. A control study of untargeted MSPs showed an approximately 50% decrease in the amount of particles observed in tumors. During the course of this study several liver enzymes were also examined demonstrating elevated liver enzyme activity of alanine aminotransferase (ALT) and aspartate aminotransferase in mice receiving 0.5 mg bolus of MSPs though not in mice receiving 1.0 mg bolus, despite earlier findings that toxicity generally increases with particle concentration. Since exact times of subject analysis were included in this report, one

explanation of this result could be that ALT has a normal diurnal variation in concentration. Both ALT and AST are indicators of normal liver health. Liver enzymes were elevated again in mice receiving 2.0 mg bolus; however this concentration of MSPs was not used during the regular experiments. The number of eosinophils and neutrophils (types of white blood cells) were also observed to be elevated in the mice receiving 0.5 mg bolus and not in mice receiving 1.0 mg bolus. To determine long-term toxicity mice were administered two doses of MSPs per week for 8 weeks (18 injections total), body weight and observations for ascites were carried out every day and final histology results showed no systematic toxicity despite previous reports.

Huang and coworkers recently expanded their previous *in vitro* work with an *in vivo* toxicology study detailing the biodistribution, clearance and toxicity of unfunctionalized and PEGylated rod shaped MSPs.^[19] Silicon concentrations in the organs of test subjects were determined 2 hours, 24 hours and 7 days after receiving intravenous injections of MSPs (20 mg/kg) either coated with PEG groups or unfunctionalized and possessing aspect ratios of 1.5 or 5 (AR1.5 and AR 5 respectively). Results of this assay indicate that the short term kinetics of biodistribution are more dependent upon the aspect ratios of the particles than the presence or absence of surface PEG groups. Particles with AR 1.5 were found more often in the liver, kidney and blood 2 hours after injection. Two surprising pieces of data were that PEGylated particles with AR5 were found in the lungs at levels twice that of all other particle types and that uncoated particles with AR5 were found in the spleen at levels four times that of the other particle

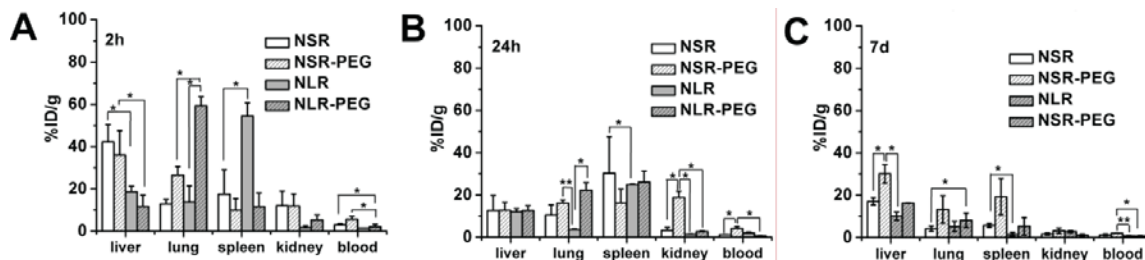


Figure 7. Quantitative analysis of silicon concentration in tissue type by ICP-OES of near spherical (NSR) and long rod mesoporous silicates (NLR) and the PEGylated analogues, NSR-PEG and NLR-PEG. Reprinted with permission from Huang, X.; *et al.*, *ACS Nano* **2011**, 5 (7), 5390-5399. Copyright 2011 American Chemical Society

types. Within 24 hours, MSP levels in all organs and blood had essentially become equal except for the disproportionately high level of uncoated AR1.5 MSPs in the kidney. Lung tissue showed almost complete clearance of uncoated AR5 particles though PEGylated AR5 particles were found at similar concentrations to other MSP types. After 7 days appreciable concentrations of all MSP types were found in the liver and concentrations of PEGylated AR1.5 MSPs were elevated in spleen and lung tissue. Total excretion percentage was not able to be determined due to fluctuating silicon levels in feces and urine of test subjects however, the majority of renal clearance occurs within 2 hrs post-injection followed by low levels in both urine and feces at 24 hours post-injection. After 7 days the majority of particles are found in test subject feces however the exact mechanisms under which excretion occurs remains unknown. All hematological test results came back within accepted normal ranges of controls for both 24 hour and 18 day test groups. Liver enzymes were found to be altered slightly, total bilirubin was lower than the control subjects after 24 hour but elevated in the 18 day test group. The 18 day test group also showed decreased creatine concentrations and blood urea nitrogen was elevated for all particle types but more so for AR1.5 MSPs. The results of these studies indicate that at least at the lower concentrations examined, MSPs do not result in any short term or systematic toxicity in test subjects.

He and coworkers have also recently examined the biodistribution and toxicity of both PEGylated and unPEGylated spherical MSPs with different diameters (80, 120, 200, and 360 nm).^[20] Biodistribution results for mice intravenously injected with 20 mg/kg dosages of MSPs are uniform across all time points and particle sizes. The general trend is as follows; after 30 minutes a spike in silicon concentration is observed in the spleen and liver followed by a gradual decline over the course of the study. Unfortunately, information on concentrations of silica in control populations is unavailable for this study though it can be observed that both the liver and spleen retain a significant percentage of both PEGylated and unPEGylated MSPs with diameters of 80 nm and 120 nm after 30 days. In contrast to the MSP rods studied in the previous report, all MSPs were rapidly, though not completely, cleared from the lungs within 24 hours. Blood silicon concentrations were examined in order to determine the mean retention times (MRT) of MSPs. PEGylated particles showed a general increase of approximately 15 minutes over unPEGylated MSPs. Histopathology of all

subjects after 30 days post-injection showed no edema or erythema at the injection sight and fluorescence microscopy of organ tissue was deemed to show no acute pathological damage.

Much research has been accomplished in proving at least a limited biocompatibility of MSPs in cells and *in vivo*. However, through evaluation of reports utilizing standardized criteria for toxicity evaluation (i.e. the Klimisch test) and careful examination of the reports summarized, only the most general conclusion can be reached about the toxicity of MSPs; that MSPs are biocompatible at low dosages and can be effectively cleared from tissue with limited exposures. The lack of a more specific conclusion is due to several factors including differing particle synthesis, *in vitro* studies in a variety of cell types, and *in vivo* studies. Examining the data in Table 1 shows that out of the 9 studies evaluated, there were 7 different particle types and no two studies have used the same cell lines. While this differing information may make it difficult to see what MSPs are capable of or which one is the “best” or most biocompatible, the positive message is that all of the MSPs evaluated have at least a modicum of biocompatibility and that the framework SiO₂ of MSPs is not overtly toxic. The future of MSPs in biological applications remains strong, in further sections of this chapter we will see specific examples of why MSPs are few systems available with the ability to be chemically tuned to provide to provide different types of drug release, cellular targeting, and diagnostic information all from the same framework.

Particle	In Vitro Assay	Cell Type	In Vivo Assay	Organism	Author's Evaluation	Klimisch Score	Reference
MCM-41/SBA-15	Various	CaCo-2 (human colon carcinoma)	-	-	Toxicity at small particle size	I(1)*	Heikkila, Teemu ¹⁰
MCM-41/SBA-15	O ₂ metabolism/histology	Lung, Liver, Spleen, Kidney, Pancreas (excised tissues)	-	-	Reasonable biocompatibility of calcined materials	I(1)*	Shamsi, Mariam ¹¹
modified MCM-41	Various/ MTT	A375 (epithelial malignant melanoma)	-	-	Rod-shape particles show some metabolic disturbance. No tox.	2(3)*	Huang, Xinglu ¹²
MSP	MTT	MDA-MB-468 (human breast cancer); COS-7 (monkey kidney)	-	-	low toxicity below 25 µg/mL; no size dependance	2(3)*	He, Qianjun ¹³
MSN - polyethyleneimine	Multiparametric fluorescence assay	normal human bronchial epithelial	-	-	Toxicity towards differentiated cells increased	I(1)*	Zhang, Haiyuan ¹⁵
MCM-41/SBA-15/MCF	MTT	mesothelial/macrophage	histology	Rat/ Mouse	Severe systematic toxicity	2(3)*, 2(2)†	Hudson, Sarah ¹⁶
Hollow mesoporous spheres	-	-	Hematology histology/ biomarker	Mouse	low single does toxicity moderate systematic toxicity	I(1)†	Liu, Tianlong ¹⁷
MCM-41 (MSN-type)	-	-	Biomarkers/ histology	Mouse	mild to no toxicity	2(3)†	Lu, Jie ¹⁸
MSP	-	-	Histology	Mouse/Rat	no acute pathological damage	I(3)†	He, Qianjun ²⁰

Table 2. Results of applying the Klimisch criteria to studies in which evaluating MSP toxicity are the main focus. Scores denoted with * are *in vitro* studies, † are *in vivo* studies. Results in paranthesis () are scores adjusted for the absence of critical data.

III. Strategies for Controlled Release

The ability to release cargo molecules in a controlled fashion upon the action of some stimulus has been a driving force behind mesoporous silicates (MSs) research as drug delivery devices. Ideally, a drug delivery system is designed to carry a pharmaceutical compound to a specific location in the body and release the pharmaceutical molecule in response to a unique set of stimulus found only at the target site. In this way many of the problems with current pharmaceutical technology can be remediated including drug toxicity and environmental contamination due to clearance of unmetabolized drug molecules.^[21, 22] The types of stimuli that have been shown to cause the release of a cargo molecule can include chemical stimuli in the form of molecules and enzymes and physical stimuli such as light, heat pH, and magnetic fields. Reliable controlled release at physiological conditions is a challenging endeavor and the stimulus must be chosen carefully for a particular application.^[23, 24] Many of the stimuli studied are present in cells and tissue at concentrations adequate to cause release of the cargo. Systems utilizing cellular stimuli will be reviewed first. External release stimuli are usually dual purpose for example, in cancer cells, heating above 42°C causes cell death which can be combined with chemotherapy drug release. Similarly, magnetic fields may also be applied to cause local heating of “frustrated” magnetic particles resulting in both heating of the cell and sustained release of a therapeutic compound. In this section we will review the methods by which controlled release is affected in MSP systems. MSP systems whose controlled release is dependent on external stimuli are summarized in the last part of this section.

Controlled Release with Cellular Stimuli

Disulfide cleavage represents one of the largest areas of study with regards to MS-based drug delivery devices; this may be due to its place as one of the first such systems discovered in 2003.^[25-27] In regards to biological stimuli, disulfide reducing agents such as glutathione, are nearly ubiquitous in all animal cell types and exist at concentrations of up to 2 mM, making them ideal candidates as guest-release triggering molecules.^[28] Methods for synthesis of disulfide-linked compounds and macromolecules also proceeds orthogonally

with other types of synthesis, making them reliable functional groups that are compatible and will not interfere with other functional groups found on capping molecules. Tolerance of other functional groups allows disulfide bonds to be used in multi-functional systems, such as systems that are capable of targeting specific cell types or systems that can

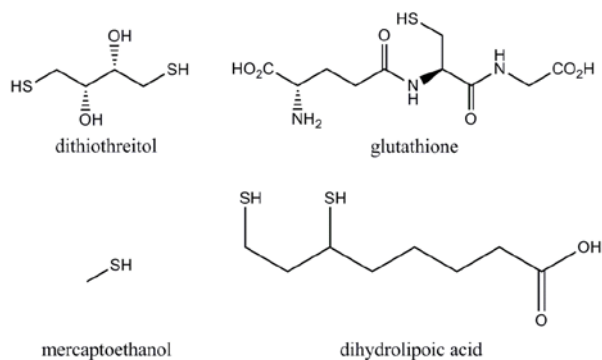


Figure 8. Examples of disulfide reducing agents used in the literature to affect controlled release.

A second strategy for achieving controlled release under biological conditions is to use pH-sensitive moieties as linkers between the caps and particles. Sensitivity towards pH allows scientists to use a variety of biological systems for affecting the release of a cargo molecule such as the pH change between stomach and small intestine, the pH of the endosome/lysosome and the increased pH of cancer cells.^[38-42] Most of the controlled release activity in these systems is a result of the generation or elimination of ionic charges. The charges either attract or repel caps and pharmaceutical molecules which cause encapsulation or release of the pharmaceutical respectively. Several examples of this type of control can be seen when the drug doxorubicin (dox) is used as the entrapped pharmaceutical molecule. The amine group of doxorubicin can be associated with negatively charged groups like carboxylic acids and thus retained at pH below ≈ 8.0 and released upon deprotonation of dox and/or protonation of the carboxylic acid.^[43] Alternatively, molecules such as polyethyleneimine can be utilized for their ability to conjugate dox at pH ≈ 8.0 , when placed into media of lower pH, both dox and the polyethyleneimine can be protonated resulting in Coulombic release cargo under several different stimuli.^[33, 37] Table 2 summarizes some of the MS systems that more prominently feature disulfide cleavage as their preferred method of affecting controlled release. repulsion and subsequent release of dox from the particle system.^[44]

Table 3. Examples of MSPs utilizing disulfide-linked capping agents capable of controlled release of a guest molecule

MS Particle	Cap	Stimulus	Conc. [Stimulus]	Reference
Wormhole	β -Cyclodextrin	GSH/DTT	1 mM/1 mM	Kim, C. ^[29]
MCM-41	α -cyclodextrin/ cucurbit[6]uril	EtSH/DTT	Excess	Ambrogio M.W. ^[30]
MCM-41	collagen	DTT	Unreported	Luo, Z. ^[31]
MCM-41	none	NADH/DTT/ DHLA/ GSH	1 mM	Mortera, R ^[32]
MCM-41	Cadmium Sulfide	EtSH/DTT	50 mM	Lai, C.-Y ^[25]
MCM-41	β -Cyclodextrin	DTT	35 mM	Liu, R. ^[33]
Core/Shell	Dye Molecules	GSH	10 mM	Sauer, A ^[34]
MCM-41	RAFT polymer	DTT	20 mM	Wan, X. ^[35]
MCM-41	PAMAM / Cadmium Sulfide	EtSH/DTT/ TCEP	5 mM	GruenHagen, J. ^[36]
MCM-41	Fe ₃ O ₄ particle	DTT	315 μ M	Giri, S. ^[27]

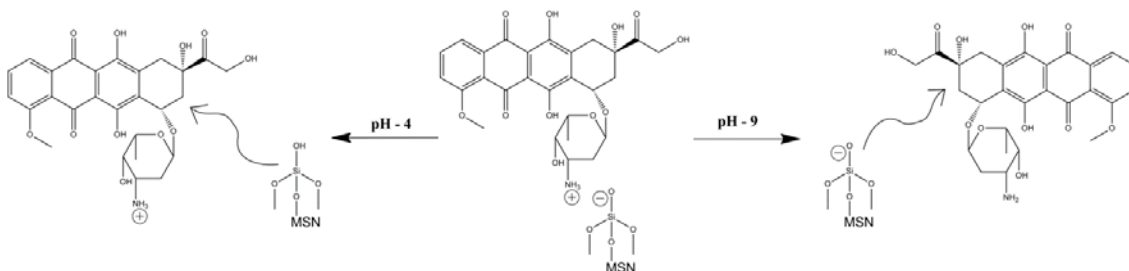


Figure 9. Doxorubicin release from the pore of MSPs with varying pH. Around physiological pH doxorubicin is bound via static charge to the surface of the MSN.

A review of some of pH active controlled release MS systems is summarized in table Y.

Controlled release systems that depend on pH are usually responsive to other stimuli such as ionic strength. Casasús *et al.* has developed a system that in which a protonated polyamine cap counters the release of a squaraine dye by using Coulombic repulsion to prevent the dye

from passing the cap. The cap can then be removed either by raising the pH to ≥ 5.0 or by adding anions such as chloride, sulfate, or ATP to neutralize the charged caps, allowing squaraine to be released.^[45] A second dual response system relies on a poly(N-isopropylacrylamide) polymer (PNIPAM) to cap the pores of the MS particles.^[46] Observation by dynamic light scattering techniques at physiological temperatures shows that the polymer coating contracts around the surface of the particle, forming a tightly capped network. When the pH is lowered to 6 and then to 5, the amount of carboxylate groups in the polymer decreases and electrostatic repulsions swell the polymer network, allowing or the release of dox *in vivo* .

Boronic acids have also been utilized for pH dependant controlled release by Gan *et al.*^[48] In this system Fe_3O_4 is linked to an 4-aminophenylboronic acid ($\text{pK}_a \approx 8.3$), and the boronic acid is used to form a well known diol complex with a poly-ol functionally grafted to the MS particle.^[56] One of the surprising attributes of this system is the persistence of the diol-boronic acid complex at pH below the pK_a of the boronic acid, though this complexation behavior has been observed previously. The strength of the boronic acid/diol bonds such that release of cargo molecules is not observed until the pH of the solution is below 4. Another interesting attribute of this system is the reversible nature of the capping and uncapping reaction. In release experiments, the pH is adjusted to 3 and then to 7, at which time release of cargo molecules ceases until the pH is lowered to 3 again. A similar system was developed by Zhao *et al* in which insulin is functionalized with boronic acids and linked to the surface of MCM-41 particles using a similar strategy as the last report. Boronic acids also show specific binding affinity for different monosaccharides which has been utilized to release insulin in response to elevated glucose concentrations in this study.^[57] Glucose responsive release occurs at biologically relevant concentrations for those suffering from diabetes. The pores of the MSP was also utilized to carry cyclic AMP (cAMP), which was released after the insulin caps dissociated from the particle.

Table 4. Summary of MSP systems capable of controlled release of a guest molecule from the pore in response to a change in pH

MS Particle	Cap	pH-Active Functionality	Release Location	Release pH	Reference
-------------	-----	-------------------------	------------------	------------	-----------

MCM-41	None	Ammonium	Colon	≥ 7.4	Lee, C.-H. ^[47]
MCM-41	Fe ₃ O ₄	4-aminophenyl-boronic acid	MC3T3 - Bone Osteoblast	2 - 4	Gan, Q. ^[48]
MCM-41	None	Carboxylic Acid	MCF-7 - Breast Cancer	5.5 - 7.4	Gu, J. ^[49]
SBA-15	PMMA	Carboxylic Acid	HeLa - Cancer	7.0	Kim, T.-W. ^[50]
MCM-41	triamine	Ammonium	Buffer only	5 - 6	Casasu, R. ^[45]
Silica Nanotubes	poly-electrolyte	Amine (doxorubicin)	MCF-7 - Breast Cancer	1 - 4	Yang, Y.-J. ^[43]
MCM-41	none	Amine	Cancer Cells	≥ 8.0	Sun, G. ^[51]
MCM-41	none	Carboxylic Acid	HeLa - Cancer	5.0	Park, H.-S. ^[52]
MCM-41	polyethylene-imine	Amine (doxorubicin)	KB-V1 (mdr HeLa line)	5.0	Meng, H. ^[53]
MCM-41	β -cyclodextrin	Imine	Buffer only	≤ 6.0	Zhao, Y.-L. ^[54]
MCM-41	β -cyclodextrin	Benzimidazole	THP-1 (leukemia)	≤ 6.0	Meng, H. ^[44]
MCM-41	None	Hydrazone	Hep-G2 (liver cancer)	≤ 4.5	Lee, C. ^[55] -H.
MCM-41	PNIPAM	Carboxylic Acid	HeLa - Cancer	6.0 - 5.0	Chang, B. ^[46]

The last class of MSPs to rely on available cellular stimuli are systems that utilize enzymes to cleave the capping molecule from the particle to generate release. Very few reports of enzyme mediated controlled release are available, probably owing to the expense of many of the enzymes and the difficulty inherent in designing a molecule which can interact with the enzyme while still associated with the cap and particle. In one of the earliest examples, Patel *et al.* highlights the use of a previously reported α -cyclodextrin cap held in place with an ester-linked adamantyl group.^[58] The study shows that porcine liver esterase can effectively cleave the adamantyl-ester bond causing α -cyclodextrin to diffuse away from the particle and affecting the release of the molecular cargo.

Carbohydrate polymers are also targets for enzymatic cleavage, Bernardos *et al.* have designed a system that relies on the disaccharide lactose as a cap. This system was designed with oral drug delivery in mind and initial reports show that there is no release of cargo under simulated gastric pH, however upon exposure to β -D-galactosidase, lactose is cleaved into glucose and galactose resulting in the release of encapsulated rhodamine B.^[59] This work was expanded upon, where it was found that MS particles functionalized with a lactose 4-mer had the one of the highest loadings of dye molecules while maintaining the ability to release its cargo upon addition of β -D-galactosidase. Systems with shorter lactose chains had much smaller dye uptake values and systems with longer lactose chains were unable to effectively cap the mesopores resulting in cargo leaching.^[60] The last system reviewed does not use an enzyme to directly cleave the cap from the particle, instead, Liu and coworkers have shown that cadaverine, generated from lysine and lysine decarboxylase can be used to competitively bind the cap, cucurbit[7]uril (C7U), and cause the release of encapsulated calcein.^[61] Essentially, the authors show that cadaverine is a competitor for the pore of C7U and that cadaverine concentrations can be increased using enzymatic degradation of lysine to the point where the caps are released from the MSPs.

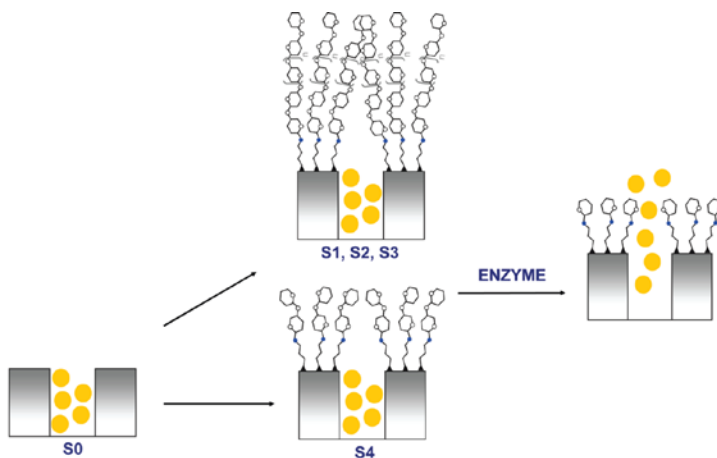


Figure 10. Schematic representation of the synthesis of trehalose groups on the surface of the MSP followed by cleavage by an enzyme. Reprinted with permission from Bernardos, A.; *et al.*, *ACS Nano* **2010**, *4* (11), 6353-6368. Copyright 2010 American Chemical Society

Controlled Release with External Stimuli

In many cases, a viable internal stimulus cannot be found to affect controlled release in MS systems, leading to the use of a stimulus delivered from outside of the cell or body. One such stimulus that is currently under investigation is photo-assisted release. The most common method for photon-mediated release is to use a cap-particle linking molecule that is labile at a specific wavelength or sensitive to photo-generated electrons to cause the dissociation of a capping molecule. One of the first examples of photon-mediated release comes for the Zink and coworkers.^[62] During the course of this study it was discovered that the 1:1 capping complex of [BHEEEN+CBPQT]⁴⁺ (BHEEEN = 1,5-bis[2-(2-(2-hydroxyethoxy)ethoxy)ethoxy)naphthalene and CBPQT = cyclobis(paraquat-*p*-phenylene) could be sensitized to light by incorporating the photoresponsive molecule 9-anthracene carbocyclic acid (ACA) and Ru(bpy)₂(bpy(-CH₂OH)₂). When irradiated with the appropriate wavelength (364 nm and 457 nm, respectively) both ACA and Ru(bpy)₂(bpy(-CH₂OH)₂) are able to transfer an electron to CBPQT⁴⁺, reducing its formal charge to 3+ and causing the rotaxane to diffuse away from the pores allowing the release of the guest molecules. Lin and coworkers designed a photo-labile system using a previously reported gold-MSN cap-particle system with a gold-linker molecule from the Rotello group.^[63, 64] Irradiation at 365 nm for 10 minutes was sufficient to release the drug paclitaxel from the MSN pore and cause a decrease greater than 50% in the viability of human liver cells. No significant cell death was reported for controls in which paclitaxel was not loaded into the pore. A third type of MS particle explored here does not feature a photo-labile cap, instead the drug molecule, chlorambucil, is linked to a surface-grafted coumarin functional group through an ester bond.^[65] One of the advantages to using coumarin as the photo-excitable molecule is that it can be activated in a single photon mechanism at 420 nm and in a double photon mechanism at 800 nm which is in the near-IR region of the electromagnetic spectrum. Near IR wavelengths of light can pass through several centimeters of tissue and can be utilized to affect the release of a drug molecule, making the system much promising for use as a real drug-delivery system.

An alternative method for photon-mediated release of cargo is to use molecules that act as impellers to cause fluid flow within the pores and subsequently release the

encapsulated guest molecule. Azo derivatives are used extensively in this area as they are frequently photo-isomerizable at visible wavelengths of light.^[66] This area of research is largely dominated by the work of Jeff Zink and coworkers, their work in free particles has shown that molecules such as benzene and 1,3,5- benzyltrimethoxybenzene (BTB) can be conjugated to an azo linker which results in a material sensitive to 457 nm light.^[67] Upon exposure to this wavelength of light, the guest molecule (coumarin) can be observed to leave the pores of the MS particles. An experiment was carried out in which the photon source was switched on and off periodically which resulted in stepwise release of coumarin only when the photon source was switched on. Further advances on this system include the replacement of azobenzene and azo-BTB impellers with a 4-phenylazoaniline impeller excitable at 413 nm.^[68] The study showed that the anticancer-drug camptothecin would exit the pore upon photo-irradiation of cells exposed to the particle system, inducing cell apoptosis. One of the advantages to using a nano-impeller system over a photo-cleavable/electron donating system is that cis-trans isomerization of azo-bonds works well in aqueous conditions. Photo-cleavable molecules may or may not work in aqueous systems and is entirely dependent on molecular architecture; however those systems that rely on generation and transfer of an excited electron often have that excitation mechanism quenched in aqueous media.

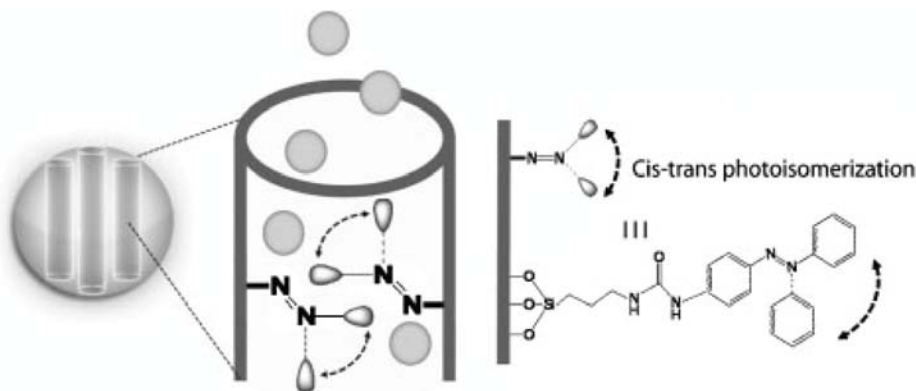


Figure 11. Schematic diagram of azo-impellers in the pores of MSPs and the type of motion available to the molecule during photoisomerization. Reprinted with permission from Lu, J.; Choi, E.; Tamanoi, F.; Zink, J. I., *Small* **2008**, 4 (4), 421-426. Copyright 2008 John Wiley & Sons.

Overall there does not seem to be much application of photon-mediated release systems within the body, as biological tissue is opaque to visible light wavelengths; however products such as slow release sunscreen, acne medication and other topical pharmaceuticals may benefit from release systems of this type.

One of the more quickly expanding areas of MS drug delivery systems are those that include some sort of magnetic functionality. In many cases the inclusion of magnetic functionality has been shown to provide a way of physically moving or sequestering the nanoparticles under static magnetic fields.^[69] More relevant to the field of therapeutics is the property that when MS-magnetic hybrid systems are placed in a rapidly alternating magnetic field, heat is generated through frustration of one of the hypothesized relaxation mechanisms.^[70] Heating in this fashion, termed magnetic hyperthermia is also an effective method for releasing cargo molecules. Chen and coworkers have shown that Fe_3O_4 nanoparticles coordinated with a carboxylate terminated linker molecule can successfully cleave the linker using heat generated during exposure to a magnetic field.^[71] The heat caused lyses of the organic linker molecule, allowing the cargo molecule to diffuse from the pore. No leaching of cargo molecules was observed in the absence of a magnetic field. One of the most recent reports of magnetic MS systems uses Fe_2O_3 particles embedded in the MS matrix, the MS particle is then coated with PNIPAM to form a thermally responsive cap.^[72] Upon application of an alternating magnetic field, the heat generated causes the polymer cap to swell and release the contents of the pores. The system was also heated to 45°C in order to cause the swelling of the PNIPAM cap, release of guest molecules in this fashion was directly comparable to the amount released under magnetic field.

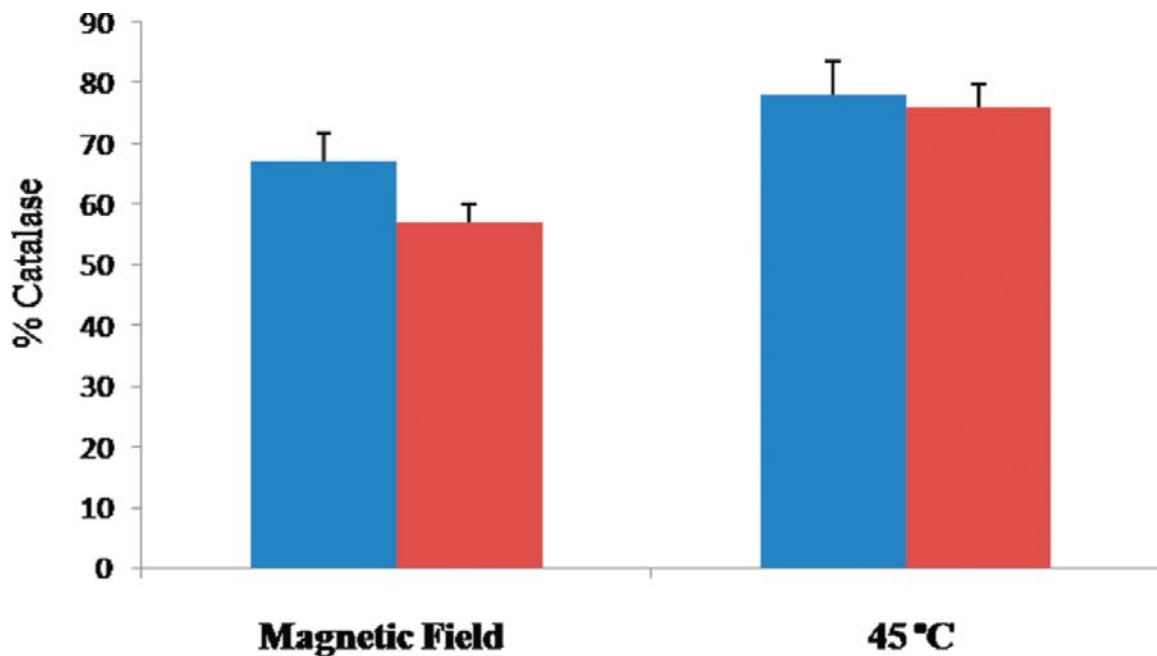


Figure 12. The total release of catalase from magnetic MSPs (blue) and the enzymatic activity of caspase (red). Release of caspase from MSP under alternating magnetic field and traditional temperature increases have been studied. Reprinted with permission from Baeza, A.; *et al.*, *Chemistry of Materials* **2012**, *24* (3), 517-524. Copyright 2012 American Chemical Society.

Several other methods have been developed to allow controlled drug release from MS particles which rely on external stimuli. Electric fields have been used to release guest molecules in two different systems; the first used an electrically conducting polymer to cap the pores of the particle while the second system employed dipolar molecules under an alternating magnetic field as impellers.^[73, 74] In the former study MS particle is embedded in a polypyrrole film. Upon application of a DC electric field, release of a nerve growth factor is increased by almost 2-fold above controls. This increase in released nerve growth factor results in an approximately 25% increase in the number of healthy increase in rat adrenal PC-12 cells. The latter study utilizes cyanophenyl moieties, which possess strong dipolar moments along the long axis of the molecule. This attribute allows the molecule to reorient itself quickly with an alternating electric field, creating the impeller effect. By applying the alternating electric field, a 40% increase in the release of ibuprofen was observed and the time for total release could be lowered nearly 25%. Nanoparticle systems utilizing the thermo-responsive nature of PNIPAM as a capping strategy have also been reported.^[75, 76] In both examples, PNIPAM is directly grafted onto the surface of MS particles and the guest

molecule release profile is examined at 20°C and 40°C. Both systems show that only slow and incomplete leaching of guest molecules occur at 20°C temperature while mixtures in 40°C solutions demonstrates rapid and almost total release of the guest molecule.

The last stimulus examined is that of ultrasonication. Depan *et al.* have shown that mesoporous silica can be capped with the biopolymer chitosan to effectively slow the release of ibuprofen.^[77] The application of ultrasound to particle solutions results in a 2-fold increase of ibuprofen release with approximately 75% of the initially loaded drug being released after 24 hours. This system is not particularly unique, but recent advances in ultrasonic surgery techniques means that a system such as the one described above could be introduced prior to surgery and entrapped therapeutic molecules released during the procedure. In this way anti-cancer compounds could potentially be introduced at tumor sites to ensure complete eradication of tumor or neuronal growth factors could be employed to facilitate healing of nerve tissue and promote differentiation of nerve cells. Indeed a similar system has been developed to facilitate surgery in which an MRI contrast agent is entrapped within MSPs and is used to guide the ultrasound beam.^[78]

IV. Actively Targeted MSP Systems

Early research into drug delivery applications of MSPs focuses almost entirely on the conveyance of anti-cancer pharmaceuticals. The theoretical impetus for the research being that particles carrying anti-cancer pharmaceuticals would achieve greater concentrations in cancer cells due to passive endocytotic uptake. This increased uptake is due to the fact that cancer cell metabolism is faster than the normal tissue and endocytosis of particles occurs at an increased rate in these cell types. However, particles could still be effectively endocytosed by non-cancerous cells potentially resulting in some of the same side effects seen with traditional oral and intravenous delivery of these pharmaceuticals. To this effect many MSP systems have been developed with surface bound targeting ligands to further improve the biodistribution of MSPs.^[79]

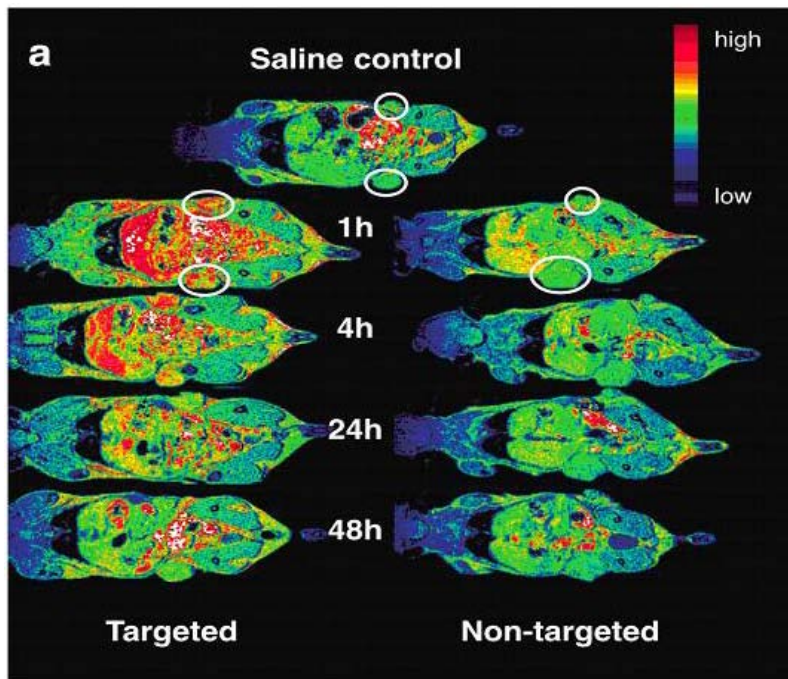


Figure 13. This image shows the MRI scan of a gadolinium-based dendritic contrast agent which has been functionalized with folate molecules (left side) and left unfunctionalized (right side). The circles represent areas of grafted tumors in female mice. The functionalized material shows a much higher contrast in tumors than the unfunctionalized gadolinium carrier. Reprinted with permission from Swanson, S. D.; *et al.*, *Int. J. Nanomedicine*; **2008**, 3(2), 201 – 210. Copyright 2008 Dovepress

Folic Acid

Initial reports of targeted MSP systems used small molecules such folic acid to improve endocytotic uptake in cancer cells. Folic acid based targeting of MSPs remains one of the most popular methods of showcasing the ability of MSPs to be targeted to specific cell types. The first of these studies appeared in 2007 by Pasqua and coworkers.^[80] In this work MSPs were functionalized with dendritic polyethyleneimine (PEI) molecules and end-capped with folic acid (FA). This approach proved successful towards increasing the amount of particles that were endocytosed by the MCF and HeLa cancer cell lines under investigation. These results were quickly followed by work from the groups of Zink and Dubernet in which folic acid functionalized MSPs were found to cause cell death with greater efficiency than non-targeted MSPs.^[81, 82]

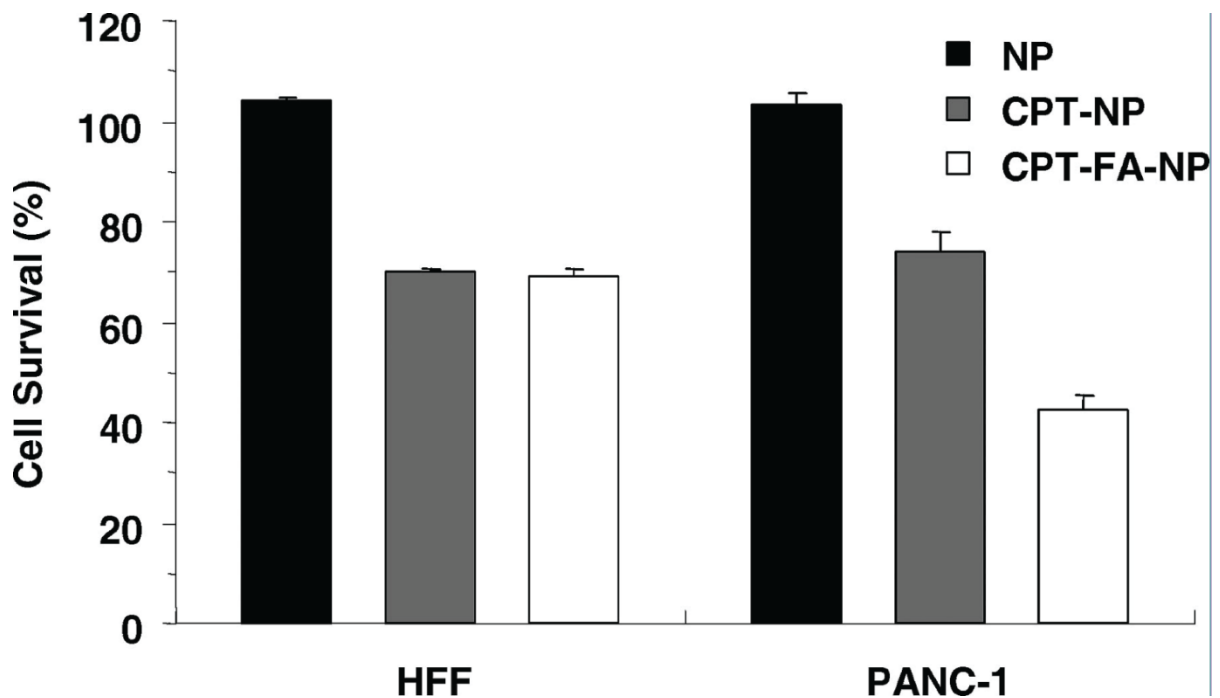


Figure 14. Results of cell growth inhibition assay of folate modified MSPs in HFF and PANC-1 cells. Cells were treated with bare nanoparticles (NP), camptothecin loaded nanoparticles (CPT-NP), or camptothecin-loaded folate-functionalized nanoparticles (CPT-FA-NP). Reprinted with permission from Liang, M.; *et al.*, *ACS Nano* **2008**, 2 (5), 889-896. Copyright 2008 American Chemical Society.

Linden *et al.* published a second report on the PEI-folic acid functionalized MSPs. In this study the authors showed that the endocytosis of FA MSPs increased five-fold in HeLa cells over the non-cancerous human embryonic kidney 293 cell line. The difference of MSP concentrations in the two cell lines is explained as a property of the number of folate receptors on the surface of the cells; the HeLa cell line having considerably more FA receptors than HEK-293 cells. Linden and coworkers expanded the ability of their PEI-FA MSPs to show that they could also carry pharmaceutical molecules into cancer cells, further increasing the amount of cell death by approximately 30% over controls (anticancer drug and FA-MSP controls).^[83]

In addition to PEI coatings, folic acid has also been employed in MSP systems with phospholipid coatings. Wang and coworkers synthesized a hydrophobic MSP and coated the particle with folate-PEG conjugate before associating phospholipids with the external surface of the particles.^[84] Folic acid proved to be an effective targeting agent in HeLa cells when compared with untargeted, PEGylated MSPs. Additional studies in A549 cells expressing

normal amounts of folate receptors show only 40% of the cell population has endocytosed MSPs as compared to 99% of HeLa cells. The study also demonstrates, via FITC-IgG conjugate adsorption that PEGylation of MSPs results in lower non-specific protein binding than unfunctionalized MSPs. There are no control experiments of MSP-phospholipid interactions with cells or endocytosis which are necessary for establishing the nature of the interaction between the MSP and the cell. Additionally, the endocytosis data are not backed up by a competitive binding assay in which free folic acid is added to the media to bind FA receptors and prevent signal-specific endocytosis of MSPs, this test would help to validate the precise endocytosis mechanism by which the author's MSPs enter the cells.

The groups of Kaskel, Salvetat, Wu and Pasqua have all followed suit and developed their own MSP systems that rely on FA to achieve cancer cell specific targeting.^[85-88] Kaskel *et al.* synthesize a Fe₃O₄ nanoparticle around which mesoporous silica was generated. The Fe₃O₄ nanoparticle is hypothesized to allow the MSP system to be targeted via an external magnetic field. The pores of the MSPs are then loaded with dox and showed increased ability to kill cancer cells; approximately 20% less cell population between free dox and FA functionalized MSPs loaded with dox in 24 hours. Salvetat *et al.* showed that MSPs functionalized with folate ligands are endocytosed more effectively than MSPs with a PEG coating. However, the effectiveness was not quantified and only the mean fluorescence intensity is reported.

Wu and coworkers have synthesized a system in which dox is linked to the MSP via a pH-sensitive hydrazone linker and folic acid is grafted onto the MSP surface to provide targeting. In this study the viability of three cell lines (HeLa, L929, A549) was evaluated against exposure to free dox, dox-MSPs and FA targeted dox-MSPs. Experimental findings clearly indicate that L929 and A549 (FA-negative) cell lines have roughly the same viability with either targeted or untargeted MSP systems. In the case of HeLa cells (FA-positive), targeted MSPs prove more effective at killing cells than untargeted MSPs, however viabilities for both MSP tests are higher than for the control group in which cells are exposed to free dox in solution. The results may be explained in part due to the employment of a

MTT assay as the viability measuring experiment and the potential discrepancies as outlined in Section II.

The study performed by Pasqua *et al.* examined the difference in uptake of folic acid modified MSPs between one normal human cell line (HEK293) and two cancer cell lines (MCF-7, T47D, and HeLa). The cell lines HEK 293 and MCF-7 are not characterized by an overexpression of folate receptors and correspondingly the data involving particle uptake in these two lines shows that endocytosis of folate modified and unmodified MSPs are nearly identical. While in the two cell lines that do show overexpression of folic acid receptors, HeLa and T47D, MSP endocytosis is clearly enhanced for particles modified with folic acid. The study also shows that in HEK 293 cells, free camptothecin (Cp) kills the same amount of cells as Cp loaded in MSPs, while for HeLa cells, MSP loaded with Cp was much more effective at killing cells than free Cp after 24 hours.

Saccharides

Monosaccharides have also been recognized as being able to direct MSPs to different cell types. Mannosylated MSPs first appeared in the literature in 2008 in a study by Park *et al.* on MSP-mediated gene delivery.^[89] In this report mannose was covalently attached to a polyethyleneimine polymer to allow receptor mediated endocytosis of MSPs in HeLa and Raw 264.7 cells (leukaemic monocyte macrophage). Endocytosis of MSPs was quantified by examining the amount of DNA delivered to the cells. Surprisingly, mannosylation did not result in higher DNA concentrations in HeLa cells while results for Raw 264.7 cells clearly showed an increase in DNA concentrations for mannosylated MSPs, especially when the polymer to DNA weight ratio was below 10. A competition assay in which Raw 264.7 cells were exposed to free mannose in growth media resulted in decreased amount of DNA delivered to the target cells. This result indicated that mannose receptor mediated endocytosis played a role in increasing the transfection efficiency of the DNA-MSP system.

The field of saccharide targeting of MSPs has largely been the domain of Durand and coworkers.^[90-93] They have utilized mannose in four publications in order to prove the

effectiveness of targeted MSPs in cancer research. Their system consists of MSPs functionalized with porphyrin or fluorene molecules in order to convert near IR (NIR) wavelengths of light to excited electrons which are then transferred to adventitious oxygen, resulting in the generation of toxic species (singlet oxygen radicals, peroxides and other reactive oxygen species (ROS)) followed by cell death. Initial studies for these systems were carried out in MDA-MB-231 breast cancer cells and showed that the combination of NIR radiation and mannose-mediated targeted led to the death of all cells in the culture. Control experiments from ^[90] show that irradiation did not kill a significant proportion of cells and that MSPs alone could only account for 20 – 40% of cell death. In the most recent studies by this group, breast cancer cell lines MCF-7 and MDA-MB-231 and colon cancer cells HCT-116 are treated with fluorene containing MSPs that have covalently grafted mannose on the particle surface. The newer system ^[92] shows less toxicity in MDA-MB-231 cells (67% cell death as opposed to 100%) although the overall toxicity of the galactosylated MSPs is at least 20 % greater than MSPs with fluorene alone. In addition, the MSP functionalized with the fluorene derived sensitizer has also been tested *in vivo* on xenografted (HCT-116) mice. Excised tumors in mice that received both MSPs and 760 nm laser irradiation were less than 30% mass of the untreated and MSP only controls. Mice with full treatment also showed no metastases in the liver or colon as compared to the control groups in which 50% of individuals showed metastases in either the liver or colon.

A system employing a polysaccharide targeting agent has been developed by the group of Durand *et al.*^[93] In this study they use their previously developed porphyrin-based photosensitizing MSP coupled with a hyaluronic acid (HA). Human colorectal cancer cells (HCT-116), when exposed to MSPs coupled with HA show approximately 30 % and 0 % viability after two and three days respectively. This is a 40 % and 30 % decrease in cell survival over cells treated with unfunctionalized MSPs or irradiated with NIR laser light alone. It should be noted that viability was quantified using the MTT assay so the actual values may not be accurate.

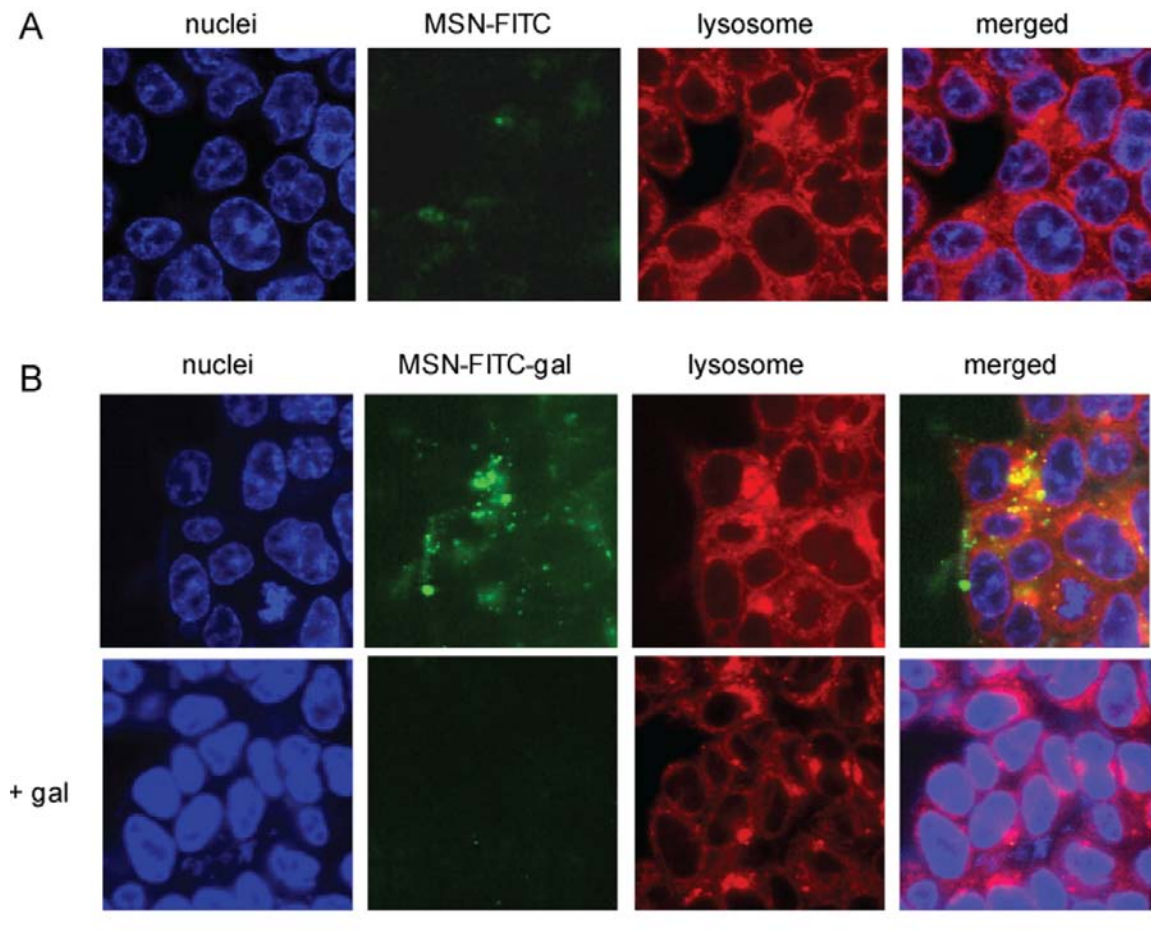


Figure 15. Confocal images of living HCT-116 colorectal cancer cells incubated with FITC-MSP (A) or FITC-MSP with targeting galactose (B) in the absence (top row) or presence of free galactose (bottom row, 10 mM). Images show the preferential uptake of the galactose targeted MSPs and that endocytosis is dependent on receptor mediated endocytosis.

Though no *in vivo* studies involving HA polymer and MSP are currently published, based on the Durand's earlier record of publications a study of this nature should not be far behind. Hyaluronic acid represents one of the most promising new capping/targeting agents in the field of MSP drug delivery devices. This is due to three main factors, first is the role that HA plays in tumor progression. Overproduction of hyaluronidase HYAL-1 by cancer cells results in the degradation of the extracellular HA matrix. Matrix fragments of HA are known to promote angiogenesis and thus tumor growth.^[94,95] Cancer cells also express an abundance of CD44 hyaluronan receptors in order to ensure that enough HA is available to degrade and continue angiogenesis. The second factor is the ability of HA encapsulated virus to escape phagocytosis and avoid activating the immune system.^[96] The third factor involves

the normally fast turnover rate of HA in a healthy human, approximately one third of the total HA per day.^[97] All of these attributes have the potential to combine into a drug delivery system capable of directed targeting to cancer cells, rapid degradation of the cap which would lead to release of any potential cargo and the ability to be rapidly cleared from the body by an easily accessible and plentiful degradation pathway.

Small Molecules

Reports of other MSP systems utilizing small molecules for to engage receptor mediated endocytosis mechanisms are currently lacking in the literature. Vivero-Escoto *et al.* have recently developed a system for MRI contrast in which anisamide (AA) is covalently bound to a PEG chain and tethered to the MSP surface.^[98] Human pancreatic carcinoma cells (AsPC-1) are exposed to AA functionalized and unfunctionalized MSPs. Confocal images of cells exposed to these nanoparticles were interpreted to have a larger concentration of AA functionalized MSPs within the cell bodies than unfunctionalized MSPs. The cell lines studied were exposed to particles for 24 hours, removing the possibility of time dependent endocytosis as the result of these differences. However these results are said to correspond to ICP quantification of Gd in the centrifuged cell pellet, but this data is unavailable in the full paper.

Luo *et al.* have designed and characterized a targeted MSP in which the collagen, also acts as the pore capping agent and the small molecule, lactobionic acid (LA) is the targeting molecule.^[31] Collagen is linked to the surface of the MSP via a disulfide bond, making the cap potentially labile to reducing conditions found in the cell. In this study the authors affected the release of the collagen cap via addition of DTT to cell growth media. After the addition of collagen, LA was grafted to the matrix on the surface of the MSP. The authors then observed an approximate 2-fold increase of cells that endocytosed LA targeted MSPs over untargeted control in HepaG2 cells. A second experiment in which the endocytosis of targeted MSPs in cancer cells was compared with the uptake in normal cells showed an approximate 2-fold increase in the concentration of MSPs in cancer cells. No controls were

available to determine whether the increase in targeted MSP concentration was due to LA or due to targeting from RGD fragments native to the collagen matrix. Additionally, collagen is a biomolecule well known for activating the immune system and autoimmune response in collagen induced arthritis.^[99-101] This effect is more pronounced when the source of the collagen is foreign to the living system being studied. These factors make the continued use of collagen as a capping agent unclear and certainly unadvisable in certain patients until careful *in vivo* studies are carried out to confirm or dispute immune system activation.

DNA, RNA and Antibody Targeting

Macromolecular targeting agents, like small molecule targeting agents for cancer therapy generally rely on the overexpression of certain cell surface receptors common to several cell types to increase endocytosis of MSPs. In contrast DNA, RNA and antibody derived targeting moieties can provide an increased level of cell-specific stimuli for mediating MSP association and/or endocytosis. This could potentially mean that MSPs targeted with DNA, RNA and antibodies could one day be entirely specific for cell type and potentially from individual to individual.

The small peptide RGD is one of the most studied molecules of its kind for affecting the endocytosis of MSPs into cancer cells. This is due to the fact that the RGD sequence binds with several different types of integrins and can be modified and cyclized to bind to specific integrin sequences.^[102] While RGD-based targeting abilities have been recognized for some time, one of the first comprehensive MSP systems developed to take advantage of this was by Cheng *et al.*^[103] In their study, an MSP was developed with a NIR contrast agent enabling imaging of the particle and a NIR active palladium porphyrin complex for photodynamic therapy. The MSP was evaluated for its ability to kill two cancer cell lines, U87MG glioblastoma cells and MCF-7 cells. It was observed that in experiments with U87MG cells, known to have an elevated level of $\alpha_v\beta_3$ integrin receptors, that MSPs with RGD functionalization provided excellent toxicity with less than 10% of cells surviving after MSP treatment and laser light irradiation. In contrast, MSPs functionalized only with PEG

only destroyed 20 to 30% of cells as compared to the negative control. In MCF-7 cells, RGD functionalization proved as effective as PEGylated MSPs resulting in approximately 20 – 30% cell death as compared to negative control.

The difference in uptake between primary cancer cells and metastatic cancer cells of MSPs functionalized with RGD or transferrin (Tf) was observed and reported by Ferris *et al.*^[104] In this work MSPs were either functionalized with cyclic RGD or transferrin and then loaded with CPT and evaluated for cell killing ability. In cell lines expressing an abundance of Tf receptors (Panc-1 and BT-549) Tf-functionalized MSPs would kill up to 60% of cells.

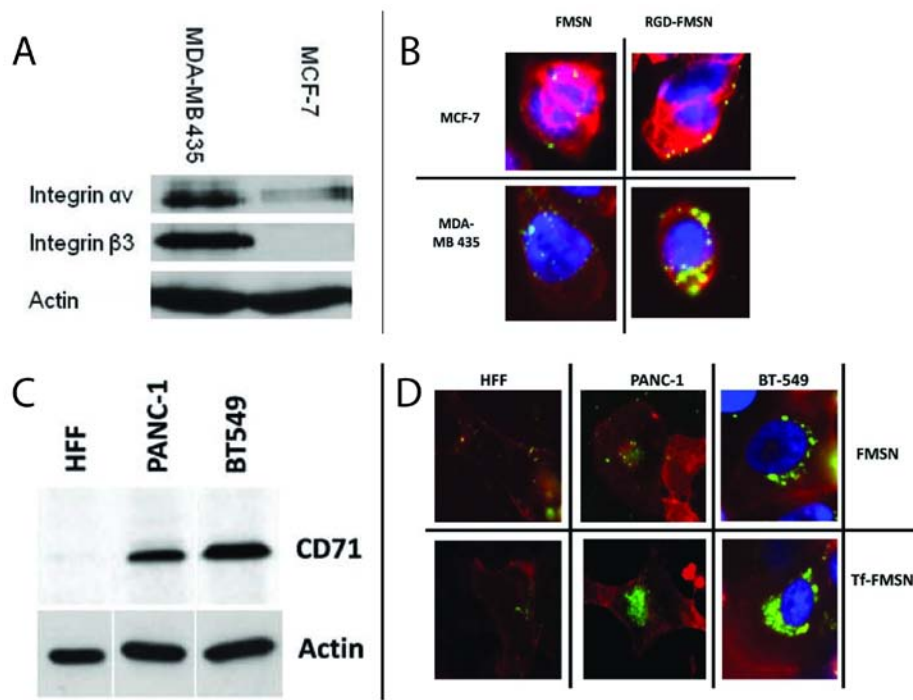


Figure 16. (A) Gel-electrophoresis of MDA-MB-435 and MCF-7 cells and confocal images (B) of the cells having been exposed to FITC-labeled MSPs expressing either folate or cyclic RGD targeting molecules. (C) Gel-electrophoresis of HFF, PANc-1 and BT549 cells to confirm the presence of the folate receptor CD71. (D) Confocal images of cells having been exposed to FITC labeled MSPs expressing folate or unmodified. Particles appear green in panels B and D, the amount of green observed in the micrographs can be roughly correlated with the amount of cell-surface receptor found through electrophoresis

MSPs bearing RGD functionalization would kill up to 50% of cell populations in MDA-MB cells. Confocal images of MSPs in cells presents a picture that targeting molecules RGD and Tf behave as expected in examined cells lines. However, well quantified results for endocytosis efficiencies are not available in this study.

In a study by Ashley *et al.* siRNA was again employed as a therapeutic molecule and an MSP supported lipid bilayer with a targeting group, SP94 and an endosomolytic peptide, H5WYG.^[105] It was observed that siRNA containing MSPs are effective in halting production of their target proteins and arresting the cell cycle in the G₁/G₀ and G₂/M phases. Furthermore, western blot analysis of cyclin A2 (Appendix A) concentrations revealed that siRNA loaded MSPs do not target healthy liver cells but do target and effectively decrease cyclin A2 concentrations in Hep3B liver carcinoma cells. Analysis of apoptosis markers also confirms this, 100% of Hep3B liver carcinoma cells are positive for apoptosis markers while less than 10% of normal liver cells express these markers after the same time period. A study of annexin V and PI concentrations in Hep3B and normal hepatocytes after exposure to targeted siRNA lipid bilayer protocells or lipid bilayer MSPs reveals that protocells are still better at targeting and killing Hep3B cells while leaving the normal cells undamaged.

In a 2009 study by Zhu and coworkers reported an MSP system functionalized with polyelectrolyte monolayers and a cancer cell specific DNA aptamer for cellular targeting.^[106] The aptamer was shown to effectively increase toxicity of the MSP system in HeLa cells which express the receptor. A second cell line QGY 7703, to which the aptamer is not targeted did show doxorubicin related toxicity, but no more than the control experiment in which MSPs were loaded with dox absent of the aptamer. While the amount of HeLa cells killed by targeted MSPs was given as 58% versus control, this is only 30% greater than untargeted MSPs, indicating that even though the targeting molecule is specific for one cell type; other types of endocytosis are available for access by the MSP. This is especially evident in the studies of QGY 7703 studies in which both targeted and untargeted MSPs killed approximately 40% of the control cell populations.

V. Analytical Applications

In addition to their ability to deliver drugs directly to cells of interest, MSPs have also been developed to aid in the analysis of diseases, contrast agents, and for biochemical separations. Many of the systems described here are multi-function in that they combine

several of the attributes previously discussed e.g. controlled release and targeting with some new functionality conferring analytical importance to the MSP. Indeed, it should be seen as necessary for any successful MSP based analytical system to have clearly defined roles for all of the easily accessible areas of the particle, external surface area, internal (pore) surface area, and pore volume. Biochemical separations with MSPs may be excluded from such criteria, however a different set of criteria such as the need for tightly controlling locality/density of functional groups and physical parameters of the particles like pore size, pore volume, and framework stability.

Separations

In the field of biochemical separations, there are two reasons why MSPs stand out, the first is the ability to selectively sequester biomolecules based on their size in the pores and the second is the ease at which functional groups can be added to the particle, either through post-synthesis grafting or *in-situ* co-condensation techniques. These attributes allow MSPs to sequester a large number of proteins of a particular size and to increase protein loading and orientation through addition of functional groups on the MSP. In a recent study, Fan *et al.* utilized SBA-15 type (8 nm pore) MSPs for the sequestration and proteolysis of myoglobin.^[107] Trypsin digest of proteins is a common method for developing a protein “fingerprint” of molecular fragments having different masses however this method suffers from problems related to incomplete digests and extended reaction times. Experiments in this study show that all myoglobin was rapidly sequestered and subsequent digestion with trypsin occurred without protein leaching. Additionally, it was observed by the authors of this study that proteolysis occurred in approximately 10 minutes in myoglobin entrapped in MSP as compared to 12 hours for digestion in solution. The samples digested in MSPs also had equal or higher sequence coverage than solution digested samples. This implies that proteolysis occurs only at specific areas when proteins are in MSPs, generating fewer unidentifiable fragments as opposed to solution experiments. The authors cite previous, unpublished works in which the surface of a different MSP system was able to unfold a target protein which caused the efficiency of digestion to increase in that study as well. One other interesting experiment showed that different types of surface (calcined, extracted, functional groups)

were evaluated for their sequestration and digestion abilities. Acid extracted MSPs and the acid extracted thiol-functionalized MSPs had a two-fold increase in the occurrence of protein sequence matching over controls.

A second example of biomolecular separation with MSPs comes from the group of Zou *et al.*^[108] In this study MSPs were functionalized with titanium phosphonate for the selective enrichment of phosphorylated peptides. Specific phosphorylation events due to cancer metabolism can be detected in the bloodstream, so effective enrichment of these phosphorylated peptides by MSPs may potentially be utilized to detect cancer with a simple serum screening. In model experiments, the authors clearly show that titanium MSPs (Ti-MSPs) will selectively adsorb only the phosphorylated peptide sequences of β -casein and fibrinogen. The results of MALDI-TOFMS showed clean spectra with only phosphorylated

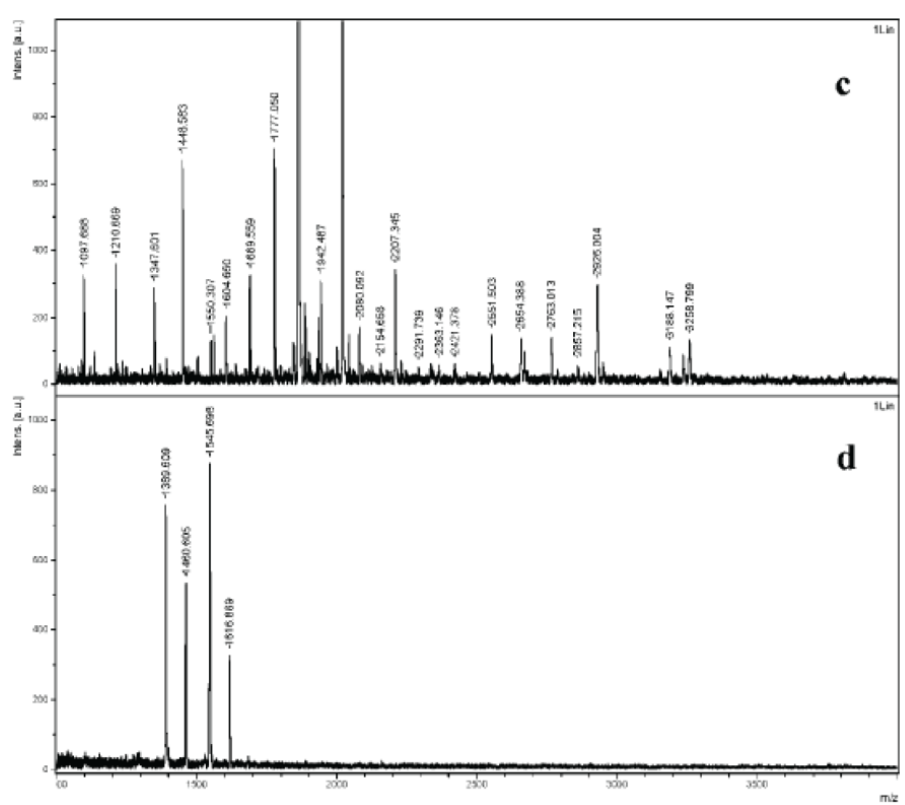


Figure 17. Analysis of protein in human blood serum by MALDI-TOF. The results in panel (C) show the mass-spec analysis of unpurified blood serum while the results from panel (D) show only those phosphorylated proteins present in the blood serum sample. Reprinted with permission from Hu, L.; et al., *Analytical Chemistry*; **2009**, *81* (1), 94-104. Copyright 2009 American Chemical Society.

peptide peaks present. A second study was carried out in which blood from humans with hepatocellular carcinoma (HCC) and healthy individuals (HI) was subjected to MSP sequestration and MALDI-TOFMS in order to determine if significant differences in protein concentrations could be observed. The results of this study clearly showed a difference in concentrations of four different phosphorylated peptides between of HCC and HI test populations. While this system may not have detected all available phosphorylated biomarkers; the fact that significantly varying peptide concentrations were observed from the mixture of human serum is excellent proof of concept.

A third study in which pore size, surface functionalization and particle type was varied to determine the best system for protein enrichment of blood plasma and urine was carried out by Terracciano *et al.*^[109] This study looks at the protein profiles captured from human plasma and urine in order to develop the most effective MSP for the sample conditions. All of the MSPs examined in this work were found to be capable of significantly enriching the protein contents of urine and plasma, however MSPs functionalized with aminopropyl (AP) groups excelled in plasma studies while tetraacetic acid diethylamine (TED) functionalized material were better at enriching urine protein. Both AP and TED functionalized MSPs were able to increase the number of detected peaks from approximately a dozen in controls to over 160 (plasma) and 199 (urine) respectively. Reproducibility analysis showed that while m/z values were highly consistent between experiments, and though the peaks heights varied by as much as 33% for some peptide sequences, the overall variance was less than 15% for all tested MSPs.

Imaging Agents

During the course of the previous decade numerous reports of MSP-based imaging agents have been published. Imaging studies using MSPs have tended to fall into two categories, MRI contrast agents and NIR imaging agents. Many systems also tout the ability to be detected via particle fluorescence, however fluorescence imaging is really only applicable in cell culture or tumor-grafted mice as the penetration depth of visible light is less than 10 mm and MSPs bearing only visible-spectrum fluorescent reports are not considered here (though these systems may be employed in biopsy).^[110, 111] Similar to drug delivery

devices, MSPs can potentially be targeted to specific cell types which can lead to the detection or confirmation of disease, the majority of current work of this type is designed for tumor imaging. Also similar to drug delivery devices, active targeting would theoretically lower the concentration of imaging agent needed in a given patient. Protection from the biological environment and clearance conferred by capped pores may also allow for longer half lives of imaging agents. The pores of MSPs used for imaging are often at least partially empty allowing future systems the ability to carry therapeutic molecules, once again, in those systems where the therapy/imaging combination is carried out, the work is done in tumor cells.

A system developed by Gianotti *et al.* was shown to be effective in carrying a NIR-active molecule into cells and protect the imaging molecule from degradation in the lysosome.^[112] An aggregate-producing synthesis for MSPs from fumed silica was utilized resulting in 100 – 300 nm clusters which were subsequently loaded with the imaging agent, IRIS3. The clusters were then ultrasonicated to produce particles between 2 and 20 nm. Despite the lack of covalent attachment between the IRIS3 and the silica framework, the material was observed to retain fluorescence for 24 hours while exposed to cells. This indicates that no leaching of IRIS3 was observed even after 24 hours exposure to cellular environments. Additionally, IRIS3 was protected from the degradation processes in the lysosome by the pores of the MSPs. The MSPs were observed to accumulate in the lysosome and neither acidic pH nor neutral pH of chloroquine treated lysosomes had any effect on the fluorescence of the IRIS3.

A second system to utilize the NIR end of the spectrum employs gold nanorods instead of small photoactive molecules.^[113] Utilization of MSPs to carry gold nanorods (GNs) helps to remove several of the problems associated with gold nanoparticles including low particle stability and high cytotoxicity. In order to remediate problems related to stability, GNs are routinely coated in cetyltrimethylammonium bromide, which is known to be extremely toxic in and of itself and does not form stable small assemblies at lysosomal pH (4.0 - 5.0). The synthesis of the gold-MSP material by Zan *et al.* results in monodisperse GNs surrounded by mesoporous silica coatings. The design of this system provides three

improvements; the first is stability as the GNs are now surrounded by a robust silica shell and protected from the environment. The second improvement results in improved extinction coefficient due to the fact that GNs encased in silica can no longer participate in self-quenching events. The last advantage is striking increase of biocompatibility of GN-MSPs over the CTAB-GNs. In order to prove that imaging ability is not lost upon functionalization of the silica network, antibodies were conjugated to the particles using electrostatic interactions and then the antibody-GN-MSP system was tested in MCF-7 breast cancer cells. The results of this study show that GNs may be targeted to specific cell types and can then be used to generate an image using localized surface plasmon resonance.

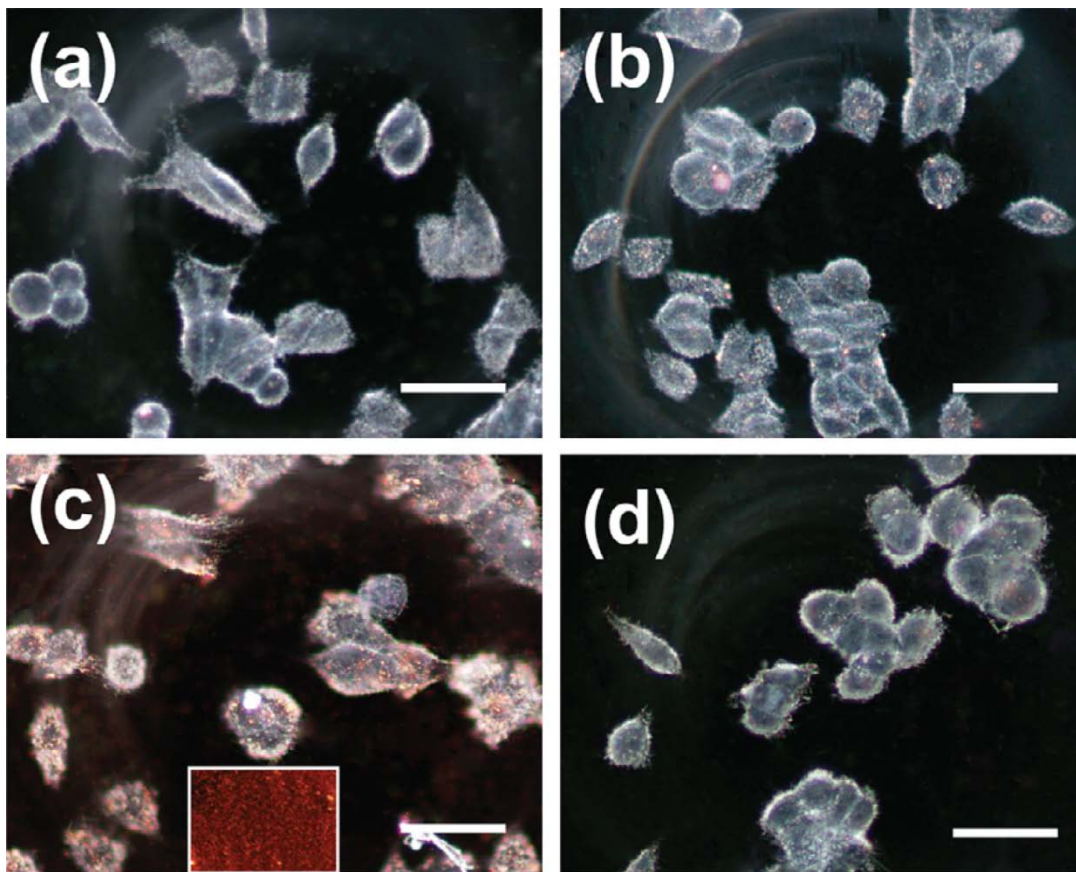


Figure 18. Dark field images of MCF cells without treatment (a), treated with GN-MSPs (b), treated with anti-HER2-conjugated GN-MSPs (positive targeting ligand) (c), and anti-CEA8-conjugated GN-MSPs (negative targeting ligand) (d). The GN-MSP composites appear red in the images. Reprinted with permission from He, Q.; et al., *Nanotechnology* **2010**, *21* (5), 055704. Copyright 2010 IOP Science.

The imaging technique garnering the most attention from MSP researchers over the past decade is MRI. One of the first accounts of MRI capable MSPs was published in 2004 by the

group of Mou *et al.*^[114] In this study gadolinium atoms were incorporated directly into the framework of the MSP (Gd-MSP) as evidenced by the lack of crystalline peaks in wide angle powder X-ray diffraction experiments and TEM images. The system was to provide enhanced contrast over the currently used gadolinium diethyltriammine pentaacetic acid (Gd-DTPA). By increasing the concentration of Gd-MSPs, the solid supported system proved to be more effective at providing contrast for T_1 and T_2 relaxivities than Gd-DTPA at similar concentrations (concentrations were recorded in terms of Gd present). Mou *et al.* followed their first publication with one for another MRI contrast agent based on Fe_3O_4 particles embedded in the MSP framework.^[115] The relaxation time for Fe_3O_4 embedded in MSP is $r_2 = 153 \text{ mM}^{-1} \text{ s}^{-1}$, this nearly doubles the $r_2 = 82.3 \text{ mM}^{-1} \text{ s}^{-1}$ value for Gd-MSPs that was observed in their earlier work. In 2007, Mou collaborated with D.-M. Huang of the Center for Nanomedicine Research in Taiwan for an *in vivo* study of MSPs functionalized with Gd-coordinated DTPA.^[116] While this system had smaller r_1 and r_2 values than the Gd-MSP original developed, the measured $r_1 = 23 \text{ mM}^{-1} \text{ s}^{-1}$ and $r_2 = 34 \text{ mM}^{-1} \text{ s}^{-1}$ which are respectively 5 and 8 times higher than Gd-DTPA by itself. The author's also demonstrated the long term biocompatibility and imaging ability of the MSP system by exposing human mesenchymal stem cells (hMSCs) to Gd-DTPA-MSPs. In one study the hMSCs are placed in media with specific growth factors and the cells can be observed to properly differentiate. The second study involving hMSCs showed that cells exposed to Gd-DTPA-MSPs and injected into a mouse brain still demonstrated contrast imparted by the MSP system after 14 days. Importantly, no migration of Gd-DTPA-MSPs away from the tumor site was observed.

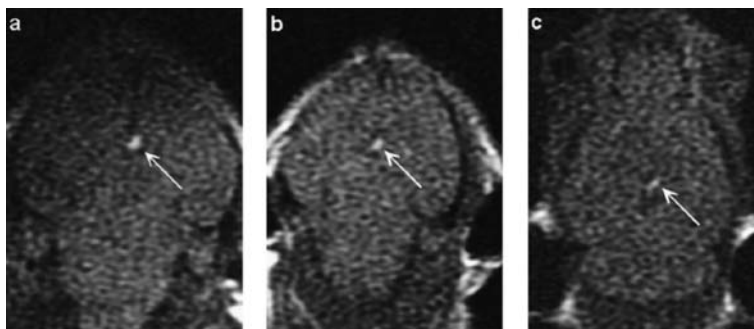


Figure 19. Images show the brain of a single mouse at 0 days (a), 7 days (b), and 14 days (c) post injection with Gd-DTPA-MSP. The arrow indicates the site of particle injection, contrast from the MSP system is still visible 14 days post injection and has not migrated. Reprinted with permission from Hsiao, J.-K.; et al., *Small* **2008**, *4* (9), 1445-1452. Copyright 2008 John Wiley & Sons.

VI. Conclusion

Mesoporous silica particles represent one of the most variable material frameworks currently being researched. The ability to functionalize the surface of the MSPs with a vast array of different organic and inorganic molecules allows for MSPs to be utilized in an almost equally vast number of applications. One of the most important applications of MSPs and one of the hottest research areas are biological applications for specific disease therapy. Recent advances in the literature have begun to move MSPs away from proof-of-concept studies and more towards the clinical evaluation of MSPs *in vivo* for an actual therapy or imaging device. This coupled with recent reports on the toxicity of nanoparticles in general increases the importance for researchers seeking to do serious evaluations of their MSPs biocompatibility to rely on a single well-accepted set of criteria. In addition to criteria for biological applications, the parallel review by Haynes and coworkers outlines necessary parameters for the physical properties of the MSPs being used to affect change biological systems. These events indicate the maturation of MSP research from scientific hypothesis to technological proposal, as such our methods and criteria for MSP evaluation must now move from bench-top criteria to clinical criteria.

VII. References

- [1] Y.-S. Lin, K. R. Hurley, C. L. Haynes *The Journal of Physical Chemistry Letters*. **2012**, 3, 364-374.
- [2] E. S. Reich *Nature*. **2011**, 480, 160 - 161.
- [3] J. W. Card, T. S. Jonaitis, S. Tafazoli, B. A. Magnuson *Critical Reviews in Toxicology*. **2011**, 41, 20 - 49.
- [4] Y. Song, X. Li, X. Du *European Respiratory Journal*. **2009**, 34, 559-567.
- [5] N. Gilbert *Nature*. **2009**, 460, 937.
- [6] B. Fadeel, A. E. Garcia-Bennett *Advanced Drug Delivery Reviews*. **2009**, 62, 362-374.
- [7] N. Lewinski, V. Colvin, R. Drezek *Small*. **2008**, 4, 26-49.
- [8] T. Laaksonen, H. Santos, H. Vihola, J. Salonen, J. Riikonen, T. Heikkilä, L. Peltonen, N. Kumar, D. Y. Murzin, V.-P. Lehto, J. Hirvonen *Chemical Research in Toxicology*. **2007**, 20, 1913-1918.
- [9] M. Fisichella, H. Dabboue, S. Bhattacharyya, M.-L. Saboungi, J.-P. Salvétat, T. Hevor, M. Guerin *Toxicology in Vitro*. **2009**, 23, 697-703.
- [10] T. Heikkilä, H. A. Santos, N. Kumar, D. Y. Murzin, J. Salonen, T. Laaksonen, L. Peltonen, J. Hirvonen, V.-P. Lehto *European Journal of Pharmaceutics and Biopharmaceutics*. **2010**, 74, 483-494.
- [11] M. Al Shamsi, M. T. Al Samri, S. Al-Salam, W. Conca, S. Shaban, S. Benedict, S. Tariq, A. V. Biradar, H. S. Penefsky, T. Asefa, A.-K. Soud *Chemical Research in Toxicology*. **2010**, 23, 1796-1805.
- [12] X. Huang, X. Teng, D. Chen, F. Tang, J. He *Biomaterials*. **2010**, 31, 438-448.

- [13] Q. He, Z. Zhang, Y. Gao, J. Shi, Y. Li *Small*. **2009**, 5, 2722-2729.
- [14] A. V. Delgado, F. González-Caballero, R. J. Hunter, L. K. Koopal, J. Lyklema *Journal of Colloid and Interface Science*. **2007**, 309, 194-224.
- [15] H. Zhang, T. Xia, H. Meng, M. Xue, S. George, Z. Ji, X. Wang, R. Liu, M. Wang, B. France, R. Rallo, R. Damoiseaux, Y. Cohen, K. A. Bradley, J. I. Zink, A. E. Nel *ACS Nano*. **2011**, 5, 2756-2769.
- [16] S. P. Hudson, R. F. Padera, R. Langer, D. S. Kohane *Biomaterials*. **2008**, 29, 4045-4055.
- [17] T. Liu, L. Li, X. Teng, X. Huang, H. Liu, D. Chen, J. Ren, J. He, F. Tang *Biomaterials*. **2011**, 32, 1657-1668.
- [18] J. Lu, M. Liong, Z. Li, J. I. Zink, F. Tamanoi *Small*. **2010**, 6, 1794-1805.
- [19] X. Huang, L. Li, T. Liu, N. Hao, H. Liu, D. Chen, F. Tang *ACS Nano*. **2011**, 5, 5390-5399.
- [20] Q. He, Z. Zhang, F. Gao, Y. Li, J. Shi *Small*. **2011**, 7, 271-280.
- [21] E. Zuccato, D. Calamari, M. Natangelo, R. Fanelli *The Lancet*. **2000**, 355, 1789-1790.
- [22] E. E. Agency in Pharmaceuticals in the Environment, Vol. (Ed.^Eds.: Editor), Office for Official Publications of the European Communities, City, **2010**, pp.1-33.
- [23] V. S.-Y. Lin, C.-Y. Lai, S. Jeftinija, D. M. Jeftinija in Capped mesoporous silicates for drug delivery, Vol. (Ed.^Eds.: Editor), (Iowa State University Research Foundation, Inc., USA). City, **2005**, pp.129 pp.
- [24] Y. Cho, R. Shi, A. Ivanisevic, R. Borgens in A mesoporous drug delivery system using an electrically conductive polymer, Vol. (Ed.^Eds.: Editor), (Purdue Research Foundation, USA). City, **2010**, pp.27pp.
- [25] C.-Y. Lai, G. Trewyn Brian, M. Jeftinija Dusan, K. Jeftinija, S. Xu, S. Jeftinija, S. Y. Lin Victor *Journal of the American Chemical Society*. **2003**, 125, 4451-4459.
- [26] D. R. Radu, C.-Y. Lai, K. Jeftinija, E. W. Rowe, S. Jeftinija, V. S. Y. Lin *Journal of the American Chemical Society*. **2004**, 126, 13216-13217.
- [27] S. Giri, B. G. Trewyn, M. P. Stellmaker, V. S. Y. Lin *Angewandte Chemie, International Edition*. **2005**, 44, 5038-5044.
- [28] P. Monostori, G. Wittmann, E. Karg, S. Túri *Journal of Chromatography B*. **2009**, 877, 3331-3346.
- [29] H. Kim, S. Kim, C. Park, H. Lee, H. J. Park, C. Kim *Advanced Materials (Weinheim, Germany)*. **2010**, 22, 4280-4283.
- [30] M. W. Ambrogio, T. A. Pecorelli, K. Patel, N. M. Khashab, A. Trabolsi, H. A. Khatib, Y. Y. Botros, J. I. Zink, J. F. Stoddart *Org. Lett.* **2010**, 12, 3304-3307.
- [31] Z. Luo, K. Cai, Y. Hu, L. Zhao, P. Liu, L. Duan, W. Yang *Angew. Chem., Int. Ed.* **2011**, 50, 640-643, S640/641-S640/648.
- [32] R. Mortera, J. Vivero-Escoto, I. I. Slowing, E. Garrone, B. Onida, V. S. Y. Lin *Chemical Communications (Cambridge, United Kingdom)*. **2009**, 3219-3221.
- [33] R. Liu, Y. Zhang, P. Feng *J. Am. Chem. Soc.* **2009**, 131, 15128-15129.
- [34] A. M. Sauer, A. Schlossbauer, N. Ruthardt, V. Cauda, T. Bein, C. Braeuchle *Nano Letters*, 10, 3684-3691.
- [35] X. Wan, D. Wang, S. Liu *Langmuir*, 26, 15574-15579.
- [36] J. A. Gruenhagen, C.-Y. Lai, D. R. Radu, V. S. Y. Lin, E. S. Yeung *Appl. Spectrosc.* **2005**, 59, 424-431.
- [37] Z. Luo, K. Cai, Y. Hu, L. Zhao, P. Liu, L. Duan, W. Yang *Angewandte Chemie, International Edition*. **2011**, 50, 640-643, S640/641-S640/648.
- [38] A. Patel, P. Heussen, J. Hazekamp, K. P. Velikov *Soft Matter*. **2011**, 7, 8549-8555.
- [39] L. Zhao, J. Ding, P. He, C. Xiao, Z. Tang, X. Zhuang, X. Chen *Journal of Controlled Release*. **2011**, 152, Supplement 1, e184-e186.

- [40] A. Rivinoja, N. Kokkonen, I. Kellokumpu, S. Kellokumpu *J. Cell. Physiol.* **2006**, 208, 167-174.
- [41] F. McCarty Mark, J. Whitaker *Altern Med Rev.* **2010**, 15, 264-272.
- [42] R. V. Benjaminsen, H. Sun, J. R. Henriksen, N. M. Christensen, K. Almdal, T. L. Andresen *ACS Nano.* **2011**, 5, 5864-5873.
- [43] Y.-J. Yang, X. Tao, Q. Hou, Y. Ma, X.-L. Chen, J.-F. Chen *Acta Biomaterialia*, 6, 3092-3100.
- [44] H. Meng, M. Liong, T. Xia, Z. Li, Z. Ji, J. I. Zink, A. E. Nel *ACS Nano.* **2010**, 4, 4539-4550.
- [45] R. Casasus, M. D. Marcos, R. Martinez-Manez, J. V. Ros-Lis, J. Soto, L. A. Villaescusa, P. Amoros, D. Beltran, C. Guillem, J. Latorre *Journal of the American Chemical Society.* **2004**, 126, 8612-8613.
- [46] B. Chang, X. Sha, J. Guo, Y. Jiao, C. Wang, W. Yang *J. Mater. Chem.* **2011**, 21, 9239-9247.
- [47] C.-H. Lee, L.-W. Lo, C.-Y. Mou, C.-S. Yang *Advanced Functional Materials.* **2008**, 18, 3283-3292.
- [48] Q. Gan, X. Lu, Y. Yuan, J. Qian, H. Zhou, X. Lu, J. Shi, C. Liu *Biomaterials.* **2011**, 32, 1932-1942.
- [49] J. Gu, S. Su, Y. Li, Q. He, J. Zhong, J. Shi *Journal of Physical Chemistry Letters.* **2010**, 1, 3446-3450.
- [50] T.-W. Kim, I. I. Slowing, P.-W. Chung, V. S.-Y. Lin *ACS Nano.* **2010**, 5, 360-366.
- [51] G. Sun, Y. Chang, S. Li, Q. Li, R. Xu, J. Gu, E. Wang *Dalton transactions (Cambridge, England 2003).* **2009**, 4481-4487.
- [52] H. S. Park, C. W. Kim, H. J. Lee, J. H. Choi, S. G. Lee, Y.-P. Yun, I. C. Kwon, S. J. Lee, S. Y. Jeong, S. C. Lee *Nanotechnology.* **2010**, 21, 225101/225101-225101/225109, S225101/225101-S225101/225103.
- [53] H. Meng, M. Xue, T. Xia, Y.-L. Zhao, F. Tamanoi, J. F. Stoddart, J. I. Zink, A. E. Nel *Journal of the American Chemical Society*, 132, 12690-12697.
- [54] Y.-L. Zhao, Z. Li, S. Kabehie, Y. Y. Botros, J. F. Stoddart, J. I. Zink *Journal of the American Chemical Society.* **2010**, 132, 13016-13025.
- [55] C.-H. Lee, S.-H. Cheng, I. P. Huang, S. Souris Jeffrey, C.-S. Yang, C.-Y. Mou, L.-W. Lo *Angewandte Chemie (International ed. in English).* **2010**, 49, 8214-8219.
- [56] J. Yan, G. Springsteen, S. Deeter, B. Wang *Tetrahedron.* **2004**, 60, 11205-11209.
- [57] P. J. Duggan, D. A. Offermann *Tetrahedron.* **2009**, 65, 109-114.
- [58] K. Patel, S. Angelos, W. R. Dichtel, A. Coskun, Y.-W. Yang, J. I. Zink, J. F. Stoddart *Journal of the American Chemical Society.* **2008**, 130, 2382-2383.
- [59] A. Bernardos, E. Aznar, M. D. Marcos, R. Martinez-Manez, F. Sancenon, J. Soto, J. M. Barat, P. Amoros *Angewandte Chemie, International Edition.* **2009**, 48, 5884-5887, S5884/5881-S5884/5887.
- [60] A. Bernardos, L. Mondragon, E. Aznar, M. D. Marcos, R. Martinez-Manez, F. Sancenon, J. Soto, J. M. Barat, E. Perez-Paya, C. Guillem, P. Amoros *ACS Nano.* **2010**, 4, 6353-6368.
- [61] J. Liu, X. Du, X. Zhang *Chemistry--A European Journal.* **2010**, 17, 810-815, S810/811-S810/816.
- [62] T. D. Nguyen, K. C. F. Leung, M. Liong, Y. Liu, J. F. Stoddart, J. I. Zink *Advanced Functional Materials.* **2007**, 17, 2101-2110.
- [63] J. L. Vivero-Escoto, I. I. Slowing, C.-W. Wu, V. S. Y. Lin *Journal of the American Chemical Society.* **2009**, 131, 3462-3463.
- [64] G. Han, C.-C. You, B.-j. Kim, R. S. Turingan, N. S. Forbes, C. T. Martin, V. M. Rotello *Angewandte Chemie International Edition.* **2006**, 45, 3165-3169.
- [65] Q. Lin, Q. Huang, C. Li, C. Bao, Z. Liu, F. Li, L. Zhu *Journal of the American Chemical Society*, 132, 10645-10647.
- [66] E. Luboch, R. Bilewicz, M. Kowalczyk, E. Wagner-Wysiecka, J. F. Biernat *Adv. Supramol. Chem.* **2003**, 9, 71-162.
- [67] S. Angelos, E. Choi, F. Vögtle, L. De Cola, J. I. Zink *The Journal of Physical Chemistry C.* **2007**, 111, 6589-6592.
- [68] J. Lu, E. Choi, F. Tamanoi, J. I. Zink *Small.* **2008**, 4, 421-426.

- [69] S. Laurent, D. Forge, M. Port, A. Roch, C. Robic, L. Vander Elst, R. N. Muller *Chemical Reviews*. **2008**, 108, 2064-2110.
- [70] R. H. a. S. D. a. R. M. a. M. Zeisberger *Journal of Physics: Condensed Matter*. **2006**, 18, S2919.
- [71] P.-J. Chen, S.-H. Hu, C.-S. Hsiao, Y.-Y. Chen, D.-M. Liu, S.-Y. Chen *J. Mater. Chem.* **2011**, 21, 2535-2543.
- [72] A. Baeza, E. Guisasola, E. Ruiz-Hernández, M. Vallet-Regí *Chemistry of Materials*. **2012**, 24, 517-524.
- [73] Y. Cho, R. Shi, A. Ivanisevic, R. B. Borgens *Nanotechnology*. **2009**, 20, 275102/275101-275102/275112.
- [74] Y. Zhu, H. Liu, F. Li, Q. Ruan, H. Wang, M. Fujiwara, L. Wang, G. Q. Lu *Journal of the American Chemical Society*, 132, 1450-1451.
- [75] Y. Yang, X. Yan, Y. Cui, Q. He, D. Li, A. Wang, J. Fei, J. Li *Journal of Materials Chemistry*. **2008**, 18, 5731-5737.
- [76] Y. Zhu, S. Kaskel, T. Ikoma, N. Hanagata *Microporous and Mesoporous Materials*. **2009**, 123, 107-112.
- [77] D. Depan, L. Saikia, R. P. Singh *Macromolecular Symposia*, 287, 80-88.
- [78] Y. Chen, H. Chen, Y. Sun, Y. Zheng, D. Zeng, F. Li, S. Zhang, X. Wang, K. Zhang, M. Ma, Q. He, L. Zhang, J. Shi *Angewandte Chemie International Edition*. **2011**, 50, 12505-12509.
- [79] Y.-W. Yang *MedChemComm*. **2011**, 2, 1033-1049.
- [80] L. Pasqua, C. Morelli, F. Testa, D. Sisci, E. Brunelli, R. Aiello, S. Ando, J. B. Nagy *Studies in Surface Science and Catalysis*. **2007**, 170B, 1956-1962.
- [81] M. Liong, J. Lu, M. Kovoichich, T. Xia, S. G. Ruehm, A. E. Nel, F. Tamanoi, J. I. Zink *ACS Nano*. **2008**, 2, 889-896.
- [82] V. Lebret, L. Raehm, J.-O. Durand, M. Smahi, M. H. V. Werts, M. Blanchard-Desce, D. Methy-Gonnod, C. Dubernet *Journal of Sol-Gel Science and Technology*. **2008**, 48, 32-39.
- [83] J. M. Rosenholm, E. Peuhu, L. T. Bate-Eya, J. E. Eriksson, C. Sahlgren, M. Linden *Small*. **2010**, 6, 1234-1241.
- [84] L.-S. Wang, L.-C. Wu, S.-Y. Lu, L.-L. Chang, I. T. Teng, C.-M. Yang, J.-a. A. Ho *ACS Nano*. **2010**, 4, 4371-4379.
- [85] Y. Zhu, Y. Fang, S. Kaskel *J. Phys. Chem. C*. **2010**, 114, 16382-16388.
- [86] M. Fisichella, H. Dabboue, S. Bhattacharyya, G. Lelong, M.-L. Saboungi, F. Warmont, P. Midoux, C. Pichon, M. Guerin, T. Hevor, J.-P. Salvetat *Journal of Nanoscience and Nanotechnology*. **2010**, 10, 2314-2324.
- [87] J. Fan, G. Fang, X. Wang, F. Zeng, Y. Xiang, S. Wu *Nanotechnology*. **2011**, 22, 455102/455101-455102/455111, S455102/455101-S455102/455117.
- [88] C. Morelli, P. Maris, D. Sisci, E. Perrotta, E. Brunelli, I. Perrotta, M. L. Panno, A. Tagarelli, C. Versace, M. F. Casula, F. Testa, S. Ando, J. B. Nagy, L. Pasqua *Nanoscale*. **2011**, 3, 3198-3207.
- [89] I. Y. Park, I. Y. Kim, M. K. Yoo, Y. J. Choi, M.-H. Cho, C. S. Cho *International Journal of Pharmaceutics*. **2008**, 359, 280-287.
- [90] D. Brevet, M. Gary-Bobo, L. Raehm, S. Richeter, O. Hocine, K. Amro, B. Look, P. Couleaud, C. Frochot, A. Morere, P. Maillard, M. Garcia, J.-O. Durand *Chem. Commun. (Cambridge, U. K.)*. **2009**, 1475-1477.
- [91] O. Hocine, M. Gary-Bobo, D. Brevet, M. Maynadier, S. Fontanel, L. Raehm, S. Richeter, B. Look, P. Couleaud, C. Frochot, C. Charnay, G. Derrien, M. Smahi, A. Sahmoune, A. Morere, P. Maillard, M. Garcia, J.-O. Durand *International Journal of Pharmaceutics*. **2010**, 402, 221-230.

- [92] M. Gary-Bobo, Y. Mir, C. Rouxel, D. Brevet, I. Basile, M. Maynadier, O. Vaillant, O. Mongin, M. Blanchard-Desce, A. Morere, M. Garcia, J.-O. Durand, L. Raehm *Angew. Chem., Int. Ed.* **2011**, 50, 11425-11429, S11425/11421-S11425/11417.
- [93] M. Gary-Bobo, O. Hocine, D. Brevet, M. Maynadier, L. Raehm, S. Richeter, V. Charasson, B. Loock, A. Morère, P. Maillard, M. Garcia, J.-O. Durand *International Journal of Pharmaceutics.* **2012**, 423, 509-515.
- [94] A. L. Raines, M. Sunwoo, A. A. Gertzman, K. Thacker, R. E. Guldberg, Z. Schwartz, B. D. Boyan *Journal of Biomedical Materials Research Part A.* **2011**, 96A, 575-583.
- [95] A. Benitez, T. J. Yates, L. E. Lopez, W. H. Cerwinka, A. Bakkar, V. B. Lokeshwar *Cancer Research.* **2011**, 71, 4085-4095.
- [96] M. R. Wessels, A. E. Moses, J. B. Goldberg, T. J. DiCesare *Proceedings of the National Academy of Sciences.* **1991**, 88, 8317-8321.
- [97] S. Robert *European Journal of Cell Biology.* **2004**, 83, 317-325.
- [98] J. L. Vivero-Escoto, K. M. L. Taylor-Pashow, R. C. Huxford, J. Della Rocca, C. Okoruwa, H. An, W. Lin, W. Lin *Small.* **2011**, 7, 3519-3528.
- [99] D. D. Brand, K. A. Latham, E. F. Rosloniec *Nat. Protocols.* **2007**, 2, 1269-1275.
- [100] C. Chunxia, Z. Peng, P. Huifang, R. Hanli, H. Zehua, W. Jizhou *Journal of Ethnopharmacology.* **2011**, 133, 573-582.
- [101] M. G. Patino, M. E. Neiders, S. Andreana, B. Noble, R. E. Cohen *Journal of Periodontal Research.* **2003**, 38, 458-464.
- [102] E. Ruoslahti *Annual Review of Cell and Developmental Biology.* **1996**, 12, 697-715.
- [103] S.-H. Cheng, C.-H. Lee, M.-C. Chen, J. S. Souris, F.-G. Tseng, C.-S. Yang, C.-Y. Mou, C.-T. Chen, L.-W. Lo *J. Mater. Chem.* **2010**, 20, 6149-6157.
- [104] D. P. Ferris, J. Lu, C. Gothard, R. Yanes, C. R. Thomas, J.-C. Olsen, J. F. Stoddart, F. Tamanoi, J. I. Zink *Small.* **2011**, 7, 1816-1826.
- [105] C. E. Ashley, E. C. Carnes, G. K. Phillips, D. Padilla, P. N. Durfee, P. A. Brown, T. N. Hanna, J. Liu, B. Phillips, M. B. Carter, N. J. Carroll, X. Jiang, D. R. Dunphy, C. L. Willman, D. N. Petsev, D. G. Evans, A. N. Parikh, B. Chackerian, W. Wharton, D. S. Peabody, C. J. Brinker *Nature Materials.* **2011**, 10, 389-397.
- [106] C.-L. Zhu, X.-Y. Song, W.-H. Zhou, H.-H. Yang, Y.-H. Wen, X.-R. Wang *Journal of Materials Chemistry.* **2009**, 19, 7765-7770.
- [107] J. Fan, W. Shui, P. Yang, X. Wang, Y. Xu, H. Wang, X. Chen, D. Zhao *Chemistry--A European Journal.* **2005**, 11, 5391-5396.
- [108] L. Hu, H. Zhou, Y. Li, S. Sun, L. Guo, M. Ye, X. Tian, J. Gu, S. Yang, H. Zou *Analytical Chemistry (Washington, DC, United States).* **2009**, 81, 94-104.
- [109] R. Terracciano, L. Pasqua, F. Casadonte, S. Frasca, M. Preiano, D. Falcone, R. Savino *Bioconjugate Chemistry.* **2009**, 20, 913-923.
- [110] J. P. Celli, B. Q. Spring, I. Rizvi, C. L. Evans, K. S. Samkoe, S. Verma, B. W. Pogue, T. Hasan *Chemical Reviews.* **2010**, 110, 2795-2838.
- [111] C. Ran, Z. Zhang, J. Hooker, A. Moore *Molecular Imaging and Biology*, 1-7.
- [112] E. Gianotti, C. A. Bertolino, C. Benzi, G. Nicotra, G. Caputo, R. Castino, C. Isidoro, S. Coluccia *ACS Applied Materials & Interfaces.* **2009**, 1, 678-687.
- [113] Q. Z. a. J. Q. a. X. L. a. S. He *Nanotechnology.* **2010**, 21, 055704.
- [114] Y.-S. Lin, Y. Hung, J.-K. Su, R. Lee, C. Chang, M.-L. Lin, C.-Y. Mou *Journal of Physical Chemistry B.* **2004**, 108, 15608-15611.

- [115] Y.-S. Lin, S.-H. Wu, Y. Hung, Y.-H. Chou, C. Chang, M.-L. Lin, C.-P. Tsai, C.-Y. Mou *Chemistry of Materials*. **2006**, 18, 5170-5172.
- [116] J.-K. Hsiao, C.-P. Tsai, T.-H. Chung, Y. Hung, M. Yao, H.-M. Liu, C.-Y. Mou, C.-S. Yang, Y.-C. Chen, D.-M. Huang *Small*. **2008**, 4, 1445-1452.

Chapter 2: Lipid Bilayer Coated Mesoporous Silica

I. Chemically Reducible Lipid Bilayer Functionalized Mesoporous Silica: Biocompatibility and Controlled Release.

A modified version of this section has been submitted for publication in *Molecular Pharmaceutics*.

INTRODUCTION

The development of mesoporous silica nanoparticle (MSN) technology for controlled release of pharmaceutical molecules has become a major research direction in the last decade. Recent developments have demonstrated that the high surface area, tunable pore sizes, and ordered mesostructure of functionalized MSNs all contribute to this controlled release property.^[1, 2] In addition to pharmaceuticals, MSNs have been shown to deliver many types of biologically-relevant molecules including DNA, RNA and small proteins into cells. The release of these molecules by stimuli responsive methods, including several different capping and uncapping schemes are currently under development. The types of capping materials involve the use of quantum dots, iron oxide nanoparticles, dendrimer and several “molecular machine” caps.^[3-9]

Combinatorial techniques have allowed researchers to greatly expand the existing library of potential drug molecules since the mid 1980's.^[10] While there are millions of potential target molecules available, it is vital to note how few actually are approved for human use. In many cases the overall toxicity of the target molecule; insolubility and instability in biological systems, and undesired interactions (side effects) of the pharmaceutical can lead to the termination of promising clinical trials.^[11] In order to meet many of these challenges, various strategies are under development in order to encapsulate

pharmaceuticals to ensure delivery to the affected tissue and avoidance of detrimental side-effects.

With the unique pore structure of MSNs, guest molecules can be loaded and protected with these stimuli-responsive controlled release systems. In addition to the mechanisms of controlled release listed above, liposomes have recently been introduced as potential supramolecules to assist in utilizing MSN for drug delivery devices.^[12-18] Their use as potential carriers of bioactive molecules has rapidly become apparent and several liposome-derived pharmaceuticals have been developed and are already in use.^[19] There are several advantages to using liposomes as drug carrier systems including biodegradability, the ability to carry both hydrophilic and hydrophobic payloads, improving protein stabilization, and cell targeting.^[20-27] However, liposomes have several drawbacks including a lack of stability to the wide pH range found in biological systems, a lack of long-term storage ability, and the need to formulate specific concentrations of the structural components such as lipids and cholesterol in order to achieve the most stable system.^[28, 29] Liposomes also undergo oxidative and hydrolytic degradation resulting in the loss of structure and the unregulated release of cargo molecules. Recently, the groups of Brinker and Bein have utilized surface charge properties to demonstrate that a lipid bilayer can be stabilized on the surface of mesoporous silica particles and used to carry drug molecules.^[12, 13] New work by Brinker et al. also demonstrates the ability of silica particles encased in lipid bilayers to target specific cells.^[30] Work by Ho and coworkers demonstrates the ability of a covalently bound inner leaflet and hydrophobically attached outer leaflet can result in material that is capable of interfacing with cells.^[14]

Herein, we report the synthesis, characterization and biological activity of a lipid-bilayer supported MSN (LB-MSN). The biocompatibility of the phosphorylated head group is explored by using pure coatings of one of four phosphorylated dipalmitoylglycerols including phosphatidylcholine (PC), phosphatidylethanolamine (PE), phosphatidic acid sodium salt (PA) and cardiolipin (CL) (**Figure 1**).

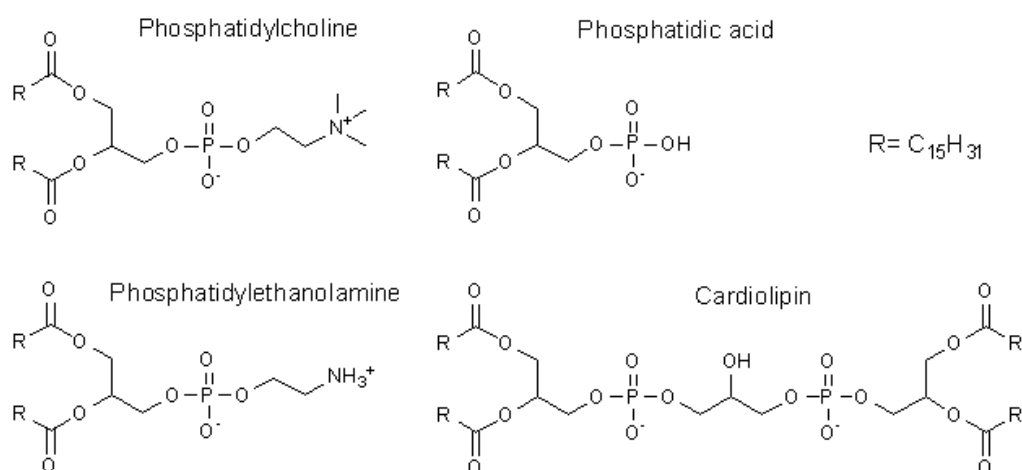
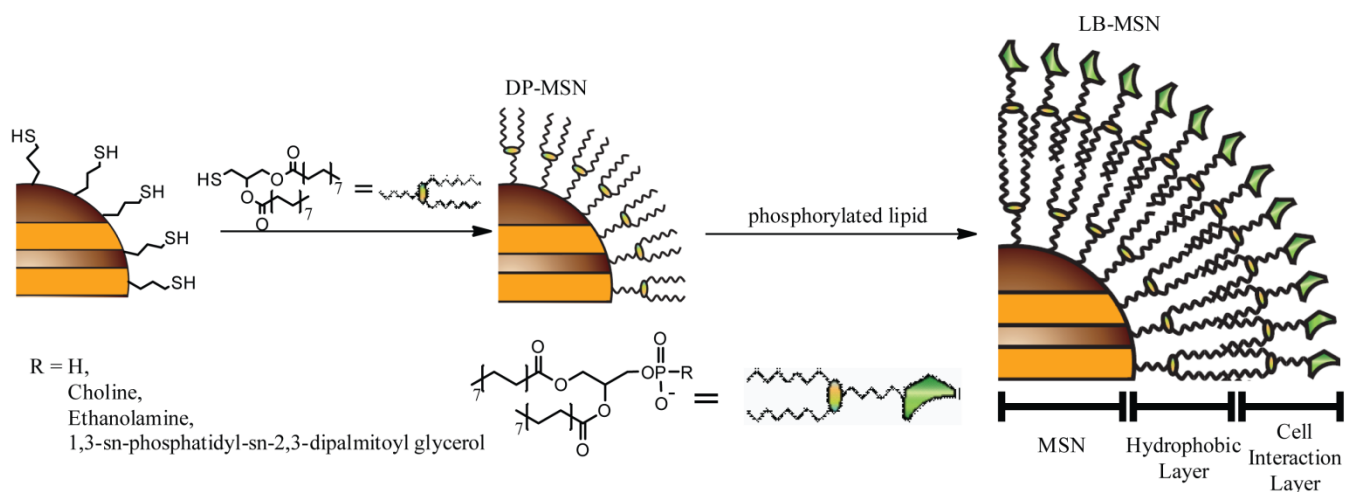


Figure 1. Phosphorlyated lipids comprising the cell-interaction layer of the LB-MSNs studied.

These lipids differ in structure, charge, and cellular location and function and provide valuable insight into the importance of the formulation of the cell interaction layer (CIL) of the carrier particle. An illustration describing the assembly of LB-MSN can be seen in **Scheme 1**.



Scheme 1. Synthesis of lipid bilayer functionalized mesoporous silica nanoparticles (LB-MSN) showing layer-by-layer assembly of the material.

We also demonstrated the ability of our system to release a model compound (fluorescein) upon cleavage of the hydrophobic dipalmitoyl monolayer (DP) with the disulfide reducing agent, dithiothreitol (DTT). Using confocal fluorescence microscopy, we tracked the internalization of fluorescently labeled LB-MSN. Finally, we examined the relative cell

populations in several control experiments to show that phosphorylated lipids and MSN have a unique, synergistic effect in cellular interaction.

Experimental

Dipalmitoylphosphatidyl choline and dipalmitoylphosphatidyl ethanolamine were used as received from Avanti Polar Lipids Inc. Dipalmitoylphosphatidic acid, cardiolipin, palmitic acid, dimethylaminopyridine, dicyclohexylcarbodiimide (DCC), 3-mercaptopropyltrimethoxysilane (MPTMS) and 1-thiol-2,3-propanediol (TPD) were used as received from Sigma-Aldrich. 2,2'-dipyridyl disulfide was used as received from TCI America. Hoechst 33342 nucleus stain was purchased from Molecular Probes. Powder X-ray diffraction patterns were obtained on a Rigaku Ultima IV X-ray diffractometer using Bragg-Brentano geometry using Cu K- α radiation and a 2.2 kW X-ray beam. Nitrogen sorption isotherms were measured using a Micromeritics Tristar 3000 sorption analyzer. Isotherms are interpreted using the Brunauer, Emmett and Teller (BET) method to calculate surface area and the Barrett, Joyner, and Halenda (BJH) method to determine pore diameters and volumes. TEM micrographs were obtained on a Philips CM-30 using 110 kV accelerating voltage and ζ -potential of LB-MSN were obtained on a Malvern Zetasizer.

Synthesis of 1-thiol-2,3-dipalmitoylpropane (TDPP): In 100 mL of dry dichloromethane, 1.08 g (10 mmol) of TPD, 2.27 g (11 mmol) of DCC and 2.82 g (11 mmol) of palmitic acid were added sequentially. Dimethylaminopyridine (5-10 mg) was then added as a catalyst and the reaction was allowed to stir overnight at room-temperature. The reaction mixture was filtered twice to remove precipitated dicyclohexylurea and extracted with 2 x 100 mL of 0.01 M HCl and one 100 mL of distilled water. The organic layer was dried over anhydrous Na₂SO₄, filtered and the solvent was removed under reduced pressure. The residue was dissolved in ethanol and the product, 1-thiol-2,3-dipalmitoylpropane (TDPP) was recovered by recrystallization from ethanol. TDPP is recovered in 83 % yield and spectral data match those found in the literature.^[31]

Synthesis of dipalmitoyl functionalized MSN (DP-MSN): MSN was synthesized using our previously reported procedure and dried *in vacuo* for 6 h at 110 °C.^[32] The MSN

surface was functionalized by grafting MPTMS at a concentration of 100 mM in refluxing, anhydrous toluene under an argon atmosphere. The functionalized particles are removed via filtration and dried overnight (MP-MSN). MP-MSN (1.0 g) is placed in 50 mL of dry methanol and 2.20 g of 2,2'-dipyridyl disulfide is added and the mixture is stirred overnight at room-temperature. The resulting yellow mixture was filtered and washed with excess methanol and freeze-dried for several hours to yield pyridyl-disulfide MSN. The pyridyl-disulfide MSN was resuspended in 50 mL of dry methanol and 0.540 g (5.0 mmol) of TDPP was added and stirred overnight at room temperature. Particles were filtered from the yellow mixture and washed with excess methanol to yield DP-MSN and freeze dried overnight.

Synthesis of lipid bilayer MSN (LB-MSN): In a typical synthesis, approximately 10 mg of DP-MSN is placed in a small vial with 10 mL of chloroform and sonicated for 10 minutes to ensure good dispersion. To this suspension 3 - 4 mg of the desired phosphorylated lipid was added. The solvent was removed under reduced pressure to associate the phosphorylated lipid with the hydrophobic surface of DP-MSN, the material was freeze dried for approximately 3 hours. The dried material was resuspended in pH 7.4 phosphate buffer (ionic strength 10 mM) without NaCl and shook intermittently over the next 30 minutes. This step was repeated two additional times to remove excess phospholipid. The resulting LB-MSN was immediately used in further experiments or freeze-dried and stored at -20°C to prevent degradation of the phosphorylated head groups of the CIL.

Fluorescein loaded LB-MSN: In order to prepare fluorescein loaded LB-MSN, a methanol solution containing 250 mM of fluorescein and 2,2'-dipyridyl disulfide is added to 250 mg of MP-MSN and stirred overnight. After filtering, the powder was collected and placed in a methanol solution containing 250 mM of fluorescein and 0.90 g of the capping agent, TDPP, and stirred overnight at room temperature. The solution was filtered and the powder lyophilized overnight.

The cell lines used in this study are immortalized HeLa (CCL-2) and normal mouse liver cells (CRL-6447) received from ATCC. Both cell lines were maintained in T-75 culture flasks using Dulbecco's Modified Eagle Medium (DMEM) with 100 U mL^{-1} penicillin, $100\text{ }\mu\text{g mL}^{-1}$ streptomycin, $2\text{ }\mu\text{M}$ L-alanyl glutamine and $100\text{ }\mu\text{g mL}^{-1}$ gentamicin. Media used in HeLa culture was further modified with 10% (v/v) donor equine serum while media used for

NLC was modified with 10% (v/v) fetal bovine serum. Cells were grown in an environmentally controlled incubator with a 5.5 % CO₂ atmosphere and a temperature of 37 °C and were subcultured every 3-4 days. All cytotoxicity measurements were obtained using a Millipore Guava flow cytometer. Cell toxicity measurements were carried out by first seeding six-well plates with 1x10⁵ cells mL⁻¹ of media and allowing 24 hrs for the cells to attach to the plate surface. Cells were then exposed to varying concentrations of MSN particles between 200 µg mL⁻¹ and 25 µg mL⁻¹ for 36 hours. Particle toxicity was recorded as the change in viable cell population from a control population that was not exposed to MSN particles. Confocal fluorescence micrographs were obtained using a Leica SP5 II confocal microscope. Cells were introduced to Wilco Glass Bottom dishes (GWSt-3512) at a concentration of 5x10⁴ cells mL⁻¹ and allowed to attach to the surface of the plate for approximately 24 hours. The cells were then exposed to media containing Hoechst 33342 dye for 30 minutes and then washed with fresh media. After washing, a 100 µg mL⁻¹ suspension of FITC labeled LB-MSN particles in modified DMEM media are then added to the cells and then immediately observed using confocal microscopy.

Results and Discussion

The material structure characteristics of MSN and DP-MSN were first examined by XRD, TEM, nitrogen sorption, TGA, and zeta potential. In **Figure 2A**, XRD patterns indicate that the hexagonal pore structure of the particle was well maintained through all synthetic steps. Reduced intensity of the d_{100} , d_{110} , and d_{200} XRD peaks in the surface functionalized MSN are due to the pore-filling effects leading to a decrease in contrast between the pores and the framework as previously reported.^[4] In order to determine whether the pores are chemically accessible and to obtain the surface area, pore volume, and pore size of the MSN, the adsorption and desorption of nitrogen were measured (**Figure 2B**). Analysis of the nitrogen adsorption/desorption isotherms indicate that the material has a

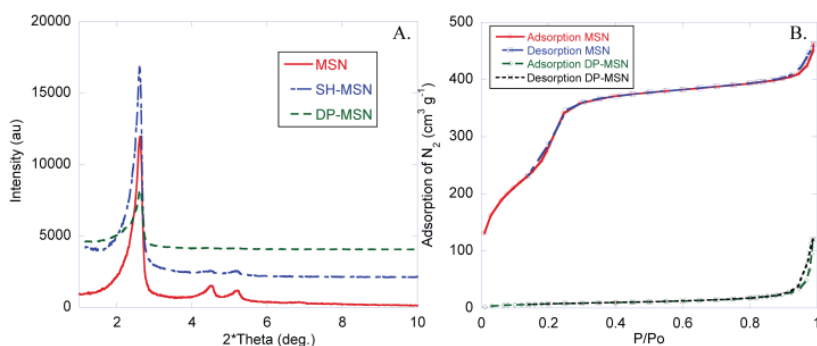


Figure 2. A.) X-ray diffraction pattern of MSN, SH-MSN and DP-MSN. The intensities of the scans have been offset for clarity. B.) Nitrogen adsorption and desorption isotherms of MSN and DP-MSN showing that after the addition of the DP layer the pores of MSN are blocked. Surface areas of MSN and DP-MSN are $1050 \text{ m}^2 \text{ g}^{-1}$ and $49 \text{ m}^2 \text{ g}^{-1}$, respectively.

typical type IV isotherm with a surface area of $1029 \text{ m}^2 \text{ g}^{-1}$ and a pore volume of $0.85 \text{ cm}^3 \text{ g}^{-1}$ by the BET method. A narrow pore diameter distribution (2.4 nm) was calculated by applying the BJH calculation to the adsorption isotherm and confirmed by TEM analysis. After capping the MSN with DP, the surface area significantly decreased to $49 \text{ m}^2 \text{ g}^{-1}$. Utilizing the t-plot method developed by de Boer the external surface area of MSN was estimated to be approximately $50 \text{ m}^2 \text{ g}^{-1}$.^[33] The results of these analyses, along with the XRD results, indicate that the pores were completely blocked by DP, encapsulating guest molecules before the CIL was added to the DP-MSN. Parallel channels were observed in the TEM images of the MSN, DP-MSN, and LB-MSN indicating the MCM-41 type pore structure was not destroyed by attachment the organic lipids to the surface. Transmission electron microscopy investigations of the MSN with both the DP and CIL moieties also provided direct visual evidence of the total coverage of the MSN (**Figure 3**). Due to contrast restraints with the surface bound organic layer and the MSN in the TEM, we were unable to visualize the DP and LB layers on the MSN. In order to observe the presence of the DP and LB layer, samples of MSN, DP-MSN, and LB-MSN were each exposed to a 2% (w/w) solution of uranyl acetate. Uranyl acetate binds to the oxygen containing phosphate groups of the lipids in the CIL of the LB-MSN. The LB-MSN (**Figure 3f**) stained in this manner show greater contrast with a dark ring around the particle while DP-MSN, which lacks phosphate groups (**Figure 3e**) appear identical to the unstained control micrograph (**Figure 3a**).

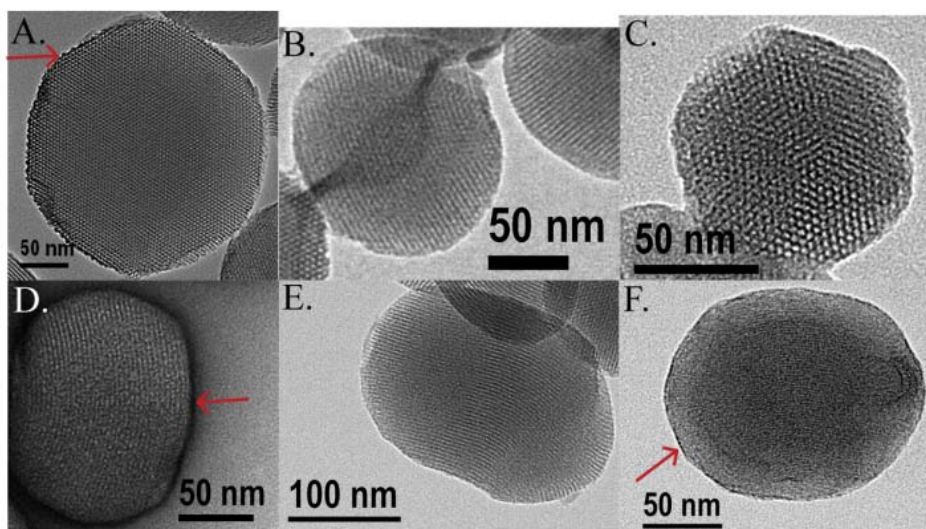


Figure 3. TEM micrographs showing MSN unstained and stained with uranyl acetate (A. and D.), unstained and stained DP-MSN (B. and E.) and unstained and stained LB-MSN (C. and F.). Arrows have been added clarify locations of high contrast due to uranium staining.

Unstained samples of LB-MSN show that the pore structure of the LB-MSN was maintained (**Figure 3c**).

In order to test the ability of DP molecules to be cleaved from the surface of MSN and release the fluorescein from the pores in a controlled manner, fluorescein loaded LB-MSN was exposed to various concentrations (0.5 mM, 1 mM and 2 mM) of the disulfide-reducing molecule, dithiothreitol [34]. The release of fluorescein from the pores of LB-MSN was dependent on the concentration of the disulfide reducing trigger (**Figure 4**).^[34] The fluorescein loaded LB-MSN exhibited approximately 15%

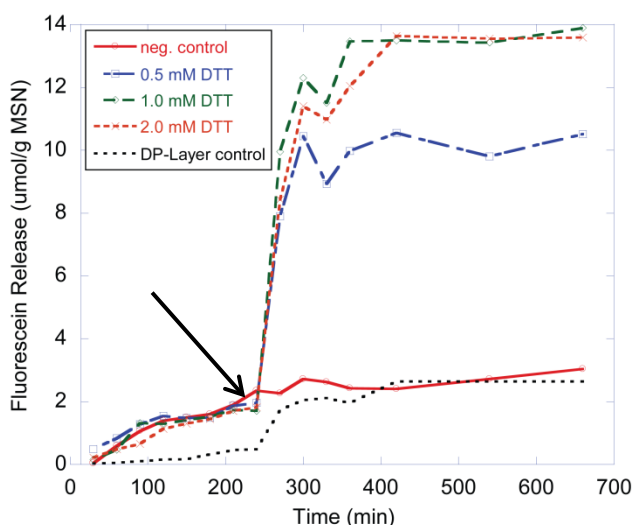


Figure 4. Controlled release of fluorescein from LB-MSN using dithiothreitol disulfide reducing agent is introduced at 240 min (black arrow). Control sample is LB-MSN with loaded fluorescein but no disulfide reducing molecule is added, DP-layer control is described in the supporting information.

release of fluorescein in 10 mM PBS in 10 h prior to the addition of the DTT. This result suggests that the lipid bilayer is an efficient, but somewhat permeable cap for encapsulating fluorescein. The addition of DTT to the aqueous suspension of LB-MSN triggered a rapid release of the encapsulated fluorescein. Within 1.5 hr, nearly 100% of the total release was reached in the experiment with the greatest DTT concentration (2 mM). In previous studies demonstrating controlled release of guest molecules from the pores through cleavage of disulfide linked caps, release was generally completed within 24-72 h post addition of the disulfide reducing agent.^[4, 35] Release of fluorescein from LB-MSNs using glutathione as the disulfide reducing agent is described in the supporting information. A calibration curve was established for fluorescein and it was calculated that LB-MSNs are capable of releasing approximately 14 μmol fluorescein g^{-1} LB-MSN into a 10 mM, pH 7.4 PBS solution.

Incubation of LB-MSN with both HeLa and normal liver cells (NLC) was performed to examine the biocompatibility and cytotoxicity of the MSN-lipid system. The flow cytometry results, in **Figure 5**,

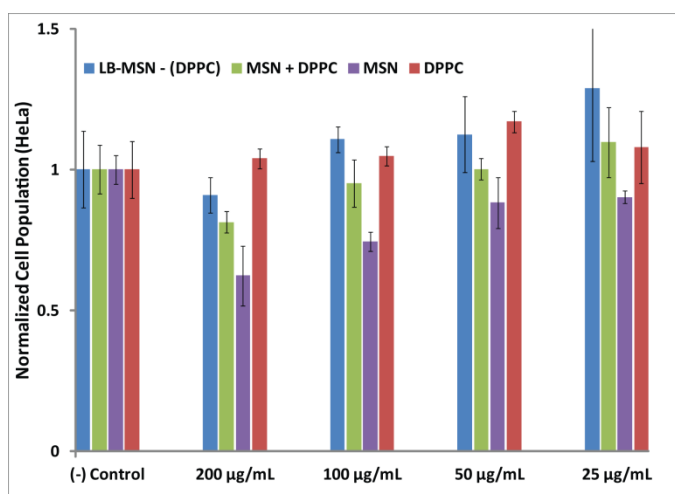


Figure 5. Cytotoxicity of varying concentrations of MSNs in HeLa cells. While the DPPC control sample shows increased cell populations at all concentrations, comparisons of LB-MSN (DPPC) and the DPPC control and of MSN and MSN + DPPC indicate that DPPC is more effectively delivered to the cell when chemically supported by MSN. Growth data is normalized against the growth of the negative control, cells not exposed to LB-MSN.

demonstrate increased biocompatibility of LB-MSNs with a CIL of dipalmitoylated PC over controls containing MSN and MSN physically mixed with DPPC. In fact, the cells incubated in the presence of LB-MSN (DPPC) showed greater cell populations at some concentrations than the negative control that did not have any MSNs present. Specifically, it was observed that LB-MSNs functionalized with PC actually enhanced the growth of both HeLa and NLC at LB-MSN concentrations below $200 \mu\text{g mL}^{-1}$. Research into possible biochemical pathways leads to the hypothesis that the observation of enhanced growth is due to the increased availability of diacylglycerol phosphatidylcholine (DAG-PC). While this indicates that higher concentrations of LB-MSNs would provide increased cell proliferation over lower concentrations, it is hypothesized that the toxicity of these particles at high concentrations mediate this effect.^[36-38] The hydrolysis of DAG-PC by phospholipase D (PLD) results in diacylglycerols (DAGs) and phosphatidylcholine (PC).^[39] Phospholipase D has been found to be active in most cells during endocytosis and can be found at increased concentrations in many cancer cell types. Additionally, PLD has also been shown to cooperate with several tyrosine kinases in order to increase cell survival and proliferation.^[40] Diacylglycerols have been shown to be potent upregulators of protein kinase C activity resulting in stimulation of

the ras/raf/MEK/MAPK mitogenic pathway^[41]. It has been determined that when cells accumulate a critical concentration of phosphatidylcholine, the transcription factor Sp1 binds to the proximal promoter of cytidylyltransferase- α resulting in DNA transcription during the S-phase of mitosis.^[42] However, without sufficient co-factors for enzyme pathway activation it was determined that PLD is saturated with DPPC at low concentrations and that enzymatic turnover to DAG and PC is very low even when 98% of the enzyme is bound to DPPC substrate.^[43] This indicates that even though a high local concentration of DPPC may be achieved in cells, very little additional DAG and PC are generated at these high concentrations, resulting in little increase to mitogenic signaling. If only a small amount of mitogenic up-regulation is achieved through DPPC activation, then proliferation is not expected to completely negate the intrinsic cytotoxic effects of the material.

In order for a particle to be considered as a drug delivery system, the particle must be able to enter cells. To determine if LB-MSN are able to enter cells, we covalently labelled LB-MSN with fluorescein isothiocyanate (LB-MSN-F) and examined the cells of interest using confocal fluorescence microscopy. In order to assess whether the LB-MSN were internalized, we examined both HeLa and NLCs shortly after adding a suspension of LB-MSN-F to the cells growing on the glass slide. We utilized a nucleus staining dye to be certain that the focal plane being observed intersected a cell. We also utilized an endosomal dye to attempt to identify the mode of internalization of LB-MSN-F. Overlay of the confocal images at the same z-distance showed both the nucleus (blue) and the LB-MSN-F (green) indicating that the LB-MSN-F are inside of the cells due to the close proximity to the nucleus (**Figure 6a & 6d**). The images overlaying the red and green channels identifying the location of the endosomes and LB-MSN-F must be considered inconclusive, this is due to the possibility that the lipophilic dye used to stain the endosomes eventually mixes with the LB-MSN which could potentially result in dual labeling of the particle (**Figure 6c & 6f**).

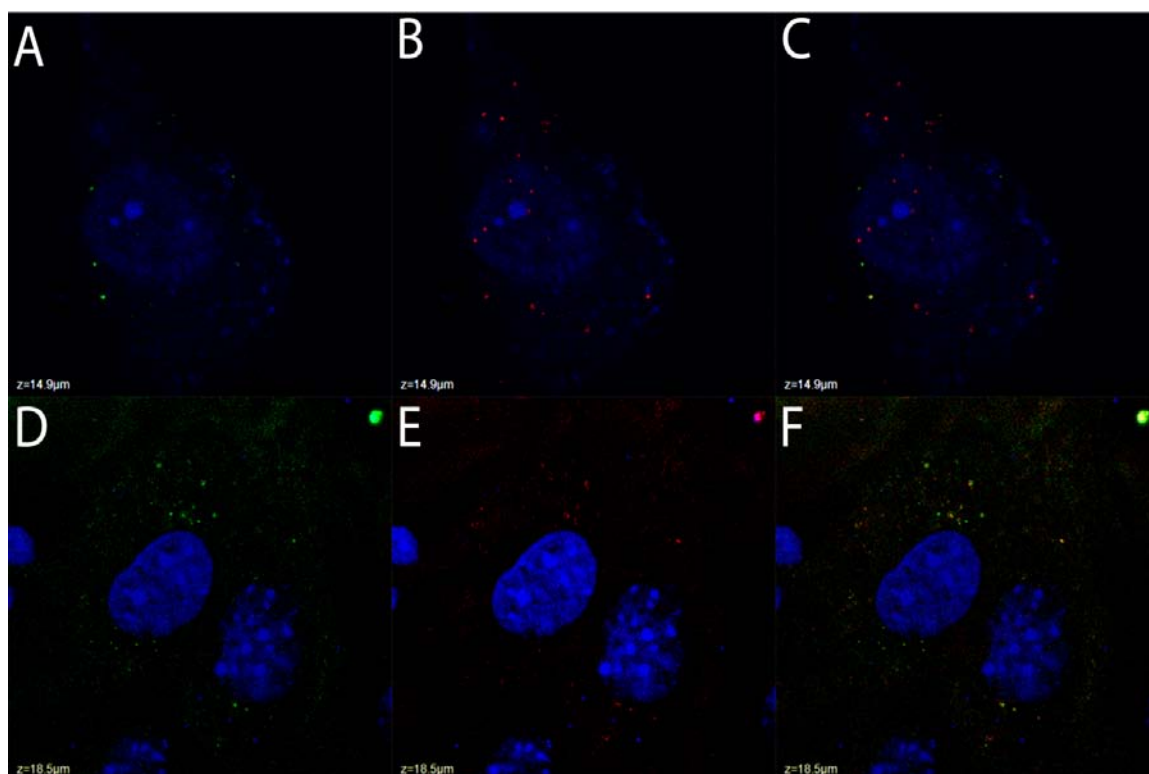


Figure 6. Confocal fluorescence microscopy images of HeLa (A, B, C) and NLC (D, E, F) showing internalized LB-MSN particles (green), endosomes (red) and cell nuclei (blue). Images A and D show only green fluorescent particles, images B and E show only red endosomes and images C and F show overlays of the two channels.

Thermogravimetric analysis (TGA) data obtained from PC-MSN was used to determine the total amount of PC present on a sample of LB-MSN (supporting information).²⁶ TGA analysis of DP-MSN shows that approximately 20% of the mass of the particle is composed of 1-thiol-2,3-dipalmitoyl propane (TDP). LB-MSNs examined by TGA showed a 40% by mass of TDP and CIL combined, resulting in approximately 20% of the total mass of the LB-MSN coming from the CIL. This data was then used to design a control experiment in which HeLa and NLCs were exposed to concentrations of free DPPC equivalent to concentrations bound to the surface of LB-MSN. This experiment shows that free DPPC at similar concentrations found on the external surface of the LB-MSN has negligible effect on the growth rate of HeLa or NLC lines.^[44] Biocompatibility data of MSN and DP-MSN were obtained in order to determine the effectiveness of the CIL in remediating

particle toxicity.³⁰ In contrast, a direct comparison of the cytotoxicity of all LB-MSN materials at $100 \mu\text{g mL}^{-1}$ demonstrates optimal biocompatibility upon the incorporation of a complete lipid bilayer system composed of a terminal choline group on the surface of MSN (**Figure 7**), in fact this sample showed a 20% increased

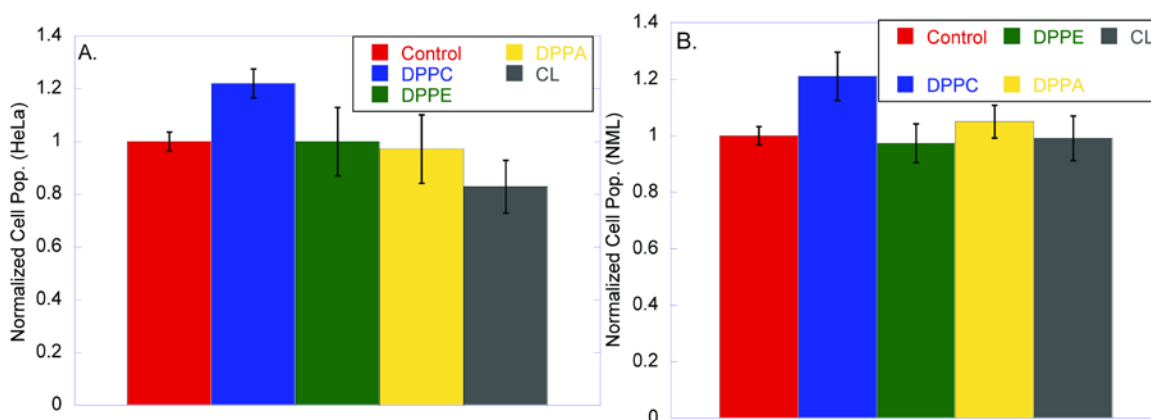


Figure 7. Cytotoxicity measurements of LB-MSNs with different phosphorylated lipids in the CIL in HeLa (A.) and Normal Liver Cells (NLC, B.). All cell populations are for a 36 hour exposure of $100 \mu\text{g(LB-MSN)} \text{ mL}^{-1}$ of cell culture medium. Experiments detailing the cytotoxicity of LB-MSNs across a range of concentrations for each CIL head-group are available in the supporting information. Growth data is normalized against the growth of the negative control, cells in normal growth media.

cell proliferation over the negative control. Finally, in order to determine whether the nature of the polar headgroup of the phospholipids attached to the MSN affected cellular function, phosphatidylethanolamine (PE), phosphatidic acid (PA), and cardiolipin (CL) were all investigated for cytotoxicity in HeLa and NLC (supporting information). We expected the following trend in biocompatibility based on biological aspects of the various phospholipids $\text{PC} > \text{PA} > \text{PE} > \text{CL}$ including the ζ -potential of LB-MSN suspensions (**Table 1**). While phospholipids with the PA and PE headgroups are also found in cell membranes, the total amount present on these cells is only several percent and were not expected to influence cell proliferation. It has been reported that PA and PE containing phospholipids with two palmitoyl chains are not as effective at up-regulating mitosis pathways as phospholipids containing the natural C16-C18 saturated and C18-C20 unsaturated lipid chains.^[45]

Phospholipid	ζ -potential (mV)	Error (mV)
PC	-12.6	± 2.3
PA	-26.7	± 0.8
PE	-28.6	± 1.8
CL	-65.8	± 2.9

Table 1. Zeta -Potentials of LB-MSNs bearing different phosphorylated headgroups in the cell interaction layer (CIL).

In contrast to data from the PC headgroup toxicity studies, materials containing CL-lipids cause a decrease in the cell population. This is thought to be due to the fact that CL containing lipids are most often found on the inner leaflet of mitochondria. When the cell begins to undergo apoptosis, CL binds to cytochrome C resulting in a non-native conformation which provides a direct channel for H₂O₂ to access the heme region of the protein.^[46] Binding of cytochrome C in this manner has been shown to be an essential step in continuing the apoptosis cascade in many cell types.^[47]

Conclusion

To summarize, we have successfully synthesized a mesoporous silica nanoparticle supported lipid bilayer system with a high degree of dispersability and the ability for rapid and diverse CIL functionalization. Cytotoxicity experiments show that our system is biocompatible and the degree of compatibility can be altered by changing the composition of the CIL. Additionally, we have shown that it is possible to release a model molecule, fluorescein, from the pores of LB-MSN via a chemically triggered disulfide reduction. Finally, we proved, utilizing confocal fluorescence microscopy, that LB-MSNs containing PC in the CIL enter HeLa and NLCs very rapidly. All of these data indicate that lipid bilayer

coated-MSNs could potentially be used to design a drug delivery system capable of controlled release.

II. Haemocompatibility of lipid bilayer functionalized large-pore mesoporous silica

During the proceeding decade, research into materials for use as pharmaceutical delivery devices has seen considerable growth. However, questions regarding toxicity and circulation of these systems have not been fully answered, and for many nanomaterials the information available is inadequate. One of the major issues surrounding the safety and efficacy of such delivery platforms is that of haemocompatibility. A material capable of releasing a pharmaceutical compound on demand is neither safe nor effective if damage is produced among circulating red blood cells (RBCs). The deleterious effects of a RBC-incompatible system could potentially range from bruising at the inoculation site, immunogenic response, and embolism which can lead to infarction and stroke. In order to minimize these risks, covalently-linked lipid-bilayer functionalized large-pore mesoporous silica has been developed. These hybrid materials are shown to be capable of interfacing with RBCs without damaging the cells even at relatively high concentrations. Additionally, a small change in outer bilayer composition is shown to produce toxic effects without resulting in haemolysis.

Introduction

The necessity to minimize cytotoxic effects of promising pharmaceutical molecules and increase the efficacy of existing pharmaceuticals has lead to the development of many types of drug delivery devices. Among these, silica based particles have been extensively researched in regards to their ability for releasing a cargo upon exposure to the correct stimulus, which can include such triggers as pH, light, disulfide reducing agents, enzymes and magnetic fields.^[48-56] While drug release and even cell-specific targeting have been demonstrated, there is still a need to fully understand how nanoparticle systems will affect other areas of the body besides the intended target.^[57-59] The majority of recent work has been to decrease fouling caused by non-specific protein binding and to increase the haemocompatibility of device surfaces by using by using pendant PEG groups.^[60-62] However, particles and surfaces that have been prepared to mimic the surface charge or protein composition of the red blood cell or the use of erythrocyte ghosts to reduce toxicity

and increase circulation times have been studied for several decades. A powerful strategy for obtaining biocompatible particles is to enclose the particle in within a lipid bilayer structure. Lipid bilayer coated particles have been shown to be effective immunoadjuvants, drug delivery devices, and as a platform for biologically active saccharide to bind with cholera toxin.^[63, 64] Additionally, this method has proven effective in modeling RBCs for studying protein insertion and structure via NMR and for studying phagocytosis of healthy and sickle RBCs.^[65, 66] Future advancements in silica-particle-based therapeutics will require definitive knowledge of in-vivo effects, especially haemocompatibility.

With the goal of synthesizing a nanodevice capable of safely interfacing with human RBCs, we investigated the properties of lipid bilayer-coated large-pore mesoporous silica nanoparticles (LB-l-MSN). Currently, haemotoxicity reports on silica nanoparticle systems (SNPs) are limited to morphological effects of the particles on haemocompatibility and biodistribution.^[67-69] To the best of our knowledge, using mixtures of phosphorylated lipids and cholesterol to mimic the surface of red blood cells on mesoporous silica particles has not been published. Previous reports have shown that MSNs possessing small pores and small, regular particle sizes (e.g. 100 – 200 nm) are haemocompatible to concentrations of 100 µg/mL.^[68] In contrast, solutions of l-MSNs (\approx 800 nm) do cause significant haemolysis detected by UV-vis analysis and the naked eye, an observation also seen by Hudson et al. in regards to a similar SBA-15 mesoporous silicate.^[70] This incompatibility with RBCs has been theorized to be due to interactions between the negatively charged l-MSN particle and positively charged phosphatidylcholine lipids in the outer RBC membrane. As the size of the particle increases, less energy is required to deform the RBC membrane allowing for more contact between RBC and particle. Examinations of flow cytometry data in this study indicate a high degree of association between particles and RBC; however TEM evidence indicates that LB-l-MSNs are not internalized by the RBC, which is in contrast to the observed behaviour of l-MSNs in our previous study.

Experimental Section

Large pore MSNs (1-MSN) were synthesized via our previously reported procedure.^[71] The surfactant Pluronic P-104 (7.0 g) was added to a solution of water (164 g) and 4 M HCl (109 g) and stirred at exactly 55 °C for one hour in a sealed Erlenmeyer flask. Tetramethylorthosilicate (TMOS, 10.64 g) was then added at once and the mixture is stirred for an additional 24 hours at 55 °C. The mixture is then added to a Teflon lined autoclave and treated at 105 °C for 24 hours. The product was then isolated via filtration, washed sequentially with water and methanol and then lyophilized overnight before further modification. Surfactant is removed via calcination; the 1-MSN is placed inside a furnace and slowly ramped (1.5°/min) to 550 °C and allowed to stand at that temperature for 4 hours. The material is then characterized via powder X-ray diffraction and nitrogen sorption analysis (BET and BJH methods). Particles labeled with fluorescein are prepared by mixing 2 mg of fluorescein isothiocyanate with 7 µL of 3-aminopropyltrimethoxysilane in 2 mL of anhydrous acetonitrile or DMSO and allowed to react for 10 minutes. The mixture is then directly added to 1.0 g of 1-MSN stirring in 50 mL of anhydrous toluene at 115 °C and allowed to react overnight. The product is then collected via filtration, washed with methanol and lyophilized overnight resulting in fluorescein labeled 1-MSNs (1-[f]MSN).

The lipid-bilayer functionalized particles are synthesized according to our previously reported method. Particles with surfactant removed (1.0 g) are dried in vacuo overnight at 110 – 115 °C, the flask is then back-filled with argon. A solution of anhydrous toluene (50 mL) and 100 mM mercaptopropyltrimethoxysilane (MPTMS) is then quickly added to the flask and stirred at 115 °C for 24 hours. The product is then filtered and washed with copious amounts of methanol to remove any unreacted MPTMS and is then dried in vacuo for approximately 8 hours. The product (1.0 g) is then resuspended in 50 mL of alumina-dried methanol and 2,2'-dipyridyl disulfide is added and the mixture stirred overnight. The product is again filtered and washed with copious amounts of methanol and then immediately resuspended in 50 mL of alumina-dried methanol and 1-thiol-2,3-dipalmitoylpropane (0.540 g) is then added to the flask and allowed to stir for an additional 24 hours. The product is filtered, washed with methanol, and lyophilized overnight resulting in a highly hydrophobic

dipalmitoyl functionalized I-MSN (DPI-MSN). This hydrophobic I-MSN is then placed into a solution of containing 1 mg/mL of the desired bilayer constituents in chloroform. In this study we have examine the effects of a simple dipalmitoyl phosphatidylcholine bilayer and one that more closely mimics the surface of the red blood cell, possessing a composition of 40% dipalmitoylphosphatidyl choline, 10 % dipalmitoylphosphatidyl ethanolamine, and 50% cholesterol by weight (mRBC).^[72, 73] During a typical synthesis, 10 mg of DPI-MSN is placed into a 20 mL glass scintillation vial and chloroform/outer layer solution added so that there is a total of 3 mg of membrane constituent, chloroform is then added to a total of 10 mL. The mixture is then sonicated for several seconds and allowed to stand approximately 30 minutes with intermittent shaking. The chloroform is then removed via rotary evaporation and 10 mL pH 7.4 phosphate buffer (no NaCl, 15 mM P_i) is added. The mixture is sonicated again for several seconds to detach the particles from the wall of the vial and then allowed to stand another 30 minutes with intermittent shaking. Mixtures are then transferred to glass centrifuge tubes and particles are sedimented at 1500 RPM for 10 minutes. The phosphate buffer is decanted, an additional 10 mL of buffer is added, the particles are then resuspended with mechanical shaking and centrifuged a second time. After the second decantation of the buffer, the particles are ready to be used in further experiments.

Approximately 4 mL of human blood sample (ethylenediamine tetraacetic acid stabilized) was freshly collected from the Occupational Medicine office, Ames Laboratory and was centrifuged at 1600 rpm for 5 minutes. The plasma and buffy coat layers were removed and the remaining RBCs were washed with sterile isotonic PBS. After washing the RBCs five times with PBS, no traces of plasma were seen in the supernatant solution. The packed RBCs were used for all the experiments.

For labeling with PKH26 (red fluorescent cell linker kit, Sigma, USA), 100 μ L of packed RBCs were suspended in 1 mL of diluent C and then mixed with 1 mL of diluent C containing 4 μ M PKH26 followed by incubation at room temperature in the dark for 5min. The reaction was stopped by adding 1 mL of plasma (heat inactivated at 57 °C in oil bath for 1h beforehand). The stained RBCs were then centrifuged at 1600 rpm for 5 min followed by

six washing cycles with PBS to remove the excess and free pKH26 dye. The labeled RBCs were used for flow cytometry analysis and confocal fluorescence microscopy.

For haemolysis experiment, 200 μL of packed RBCs were diluted to 4 mL with PBS (5% hematocrit) and the diluted RBC suspension (0.2 mL) was mixed with 0.8 mL of 1-MSN suspensions in PBS at 25, 50, 100 $\mu\text{g}/\text{mL}$ concentrations. Water and PBS (0.8mL) incubated with 0.2 mL diluted RBC suspension served as positive and negative control, respectively. All the mixtures were gently vortexed and incubated at room temperature for 2 h. The mixtures were then centrifuged at 1600 rpm for 5 min. The supernatant was transferred to a cuvet and the absorbance was measured at 541 nm by Agilent UV-visible spectrometer. The following formula was used to calculate the percent haemolysis of RBCs. A table of the haemolysis results is available in the SI.

$$\text{Haemolysis \%} = \frac{\text{Sample Abs.} - \text{Neg. Control Abs.}}{\text{Pos. Control Abs.} - \text{Neg. Control Abs.}} \times 100$$

200 μL of PKH26 labeled RBCs at 5×10^6 cells per mL were mixed with 200 μL of FITC-1-MSN suspensions in PBS at 20 $\mu\text{g}/\text{mL}$ to make the final nanoparticle concentration 10 $\mu\text{g}/\text{mL}$ and incubated at room temperature for 2h. An aliquot of sample (10 μL) was mounted in between two plastic coverslips and imaged using

The diluted RBC suspension (0.2 mL) was mixed with 0.8 mL of 1-MSN suspensions in PBS at 25, 50, 100 $\mu\text{g}/\text{mL}$ concentrations and incubated at room temperature for 2 h. The samples were then fixed by adding a 1% glutaraldehyde solution in PBS dropwise over 5 min and further incubated at 37 $^{\circ}\text{C}$ for 1.5 h, followed by postfixation with 2% osmium tetroxide in PBS for 1.5 h. The RBCs were then dehydrated in increasing concentrations of ethanol (50, 60, 70, 80, 90, 95 and 100%) for 15 min each. 10 μL of cell suspensions were dropped onto plastic coverslips, dried, and coated with iridium before viewing under a FEI Quanta 250 FEG scanning electron microscope.

The same procedure for preparing samples for SEM imaging was also used for preparing, fixing and dehydrating the samples followed by staining with 1% uranyl acetate in

70% ethanol at room temperature overnight. The cells were washed three times with pure acetone and embedded in Epon. The embedded samples were sectioned in 80 nm thick slices on a Leica Ultracut sliding ultramicrotome. Thin sections were supported on copper grids with carbon film and examined in a Tecnai G2 F20 microscope operated at 200 kV.

Results and Discussion

In this study, two lipid bilayer compositions (mRBC and DPPC) were tested for haemocompatibility and compared with our previously published data. Physical measurements were obtained including TEM, SEM, XRD and nitrogen sorption isotherms confirming an expected spherical morphology and 2D-hexagonal pore structure (See Supporting Information). Zeta-potential measurements of l-MSNs, DPPC-l-MSNs and mRBC-l-MSNs are summarized in Table 1. At physiological pH, silanol groups ($pK_a \approx 4$) on the particle surface are deprotonated, imparting a negative charge to the particle. The haemolytic activity of LB-l-MSNs on RBCs was observed using UV-Vis measurements

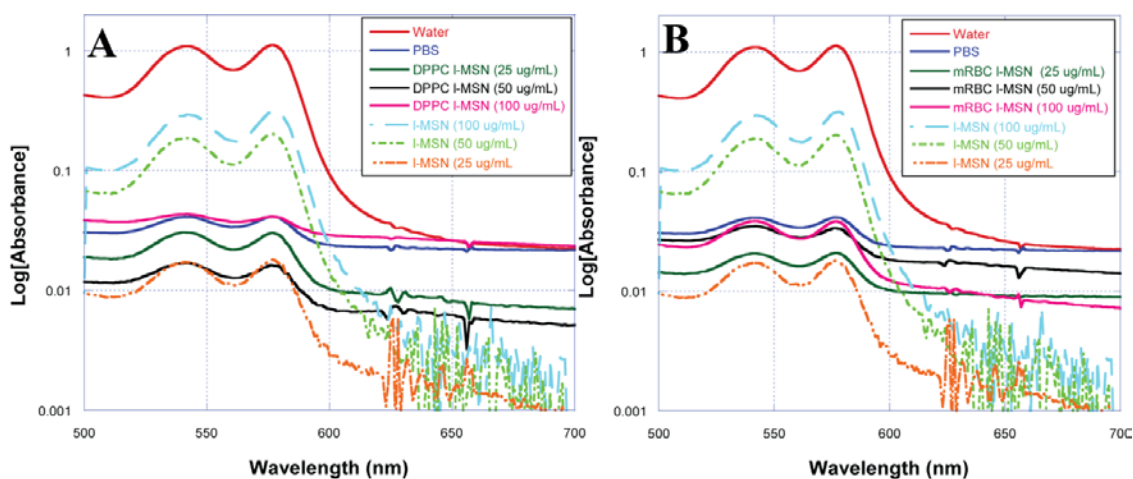


Figure 1. UV-Vis spectra of test for haemolytic activity of LB-l-MSNs. Spectra have been plotted on a Log y-axis for better visualization of traces. Uncoated l-MSNs show high haemolytic activity, roughly 40% of the positive haemolysis control of RBCs in water. In contrast, both LB-l-MSNs in A. (DPPC) and B. (mRBC) show haemolytic activity near or below that of the negative haemolysis control, RBCs in PBS buffer. The baselines of l-MSNs are shifted due to scattering of yellow-red wavelengths by particles.

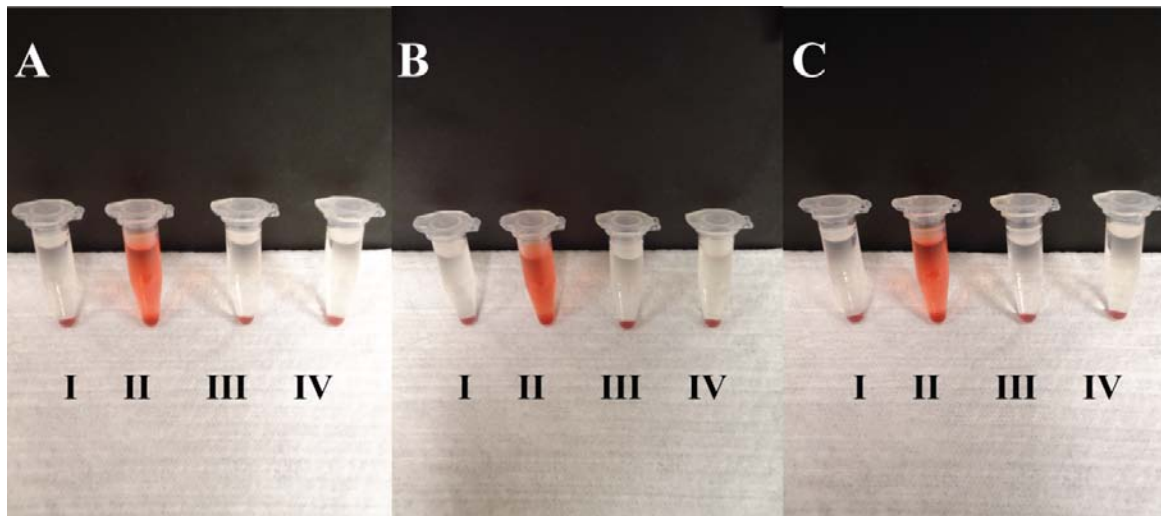


Figure Y. Photographs of the results of haemolysis assays in figure X. Labels I, II, III, and IV correspond to red blood cells under the following conditions; PBS, water, PBS with DPPC l-MSN, and PBS with mRBC l-MSN respectively. The panels A, B and C correspond to experiments with differing concentrations of MSN (25 $\mu\text{g/mL}$, 50 $\mu\text{g/mL}$, and 100 $\mu\text{g/mL}$ of particles respectively). Only the positive haemolysis control sample showed any significant visible haemolysis.

(Fig. 1) and regular photography (Fig. 2). Surprisingly, l-MSNs functionalized with lipid bilayer architecture do not cause any measurable haemolysis above that of the negative control. Visual inspection of the haemolysis experiments shows a clear color differential between samples with small and large amounts of haemolysis. Studies on other particle systems has determined that increasing positive charge of the particle leads to decrease in haemolysis.^[74] This may be due to the attraction between the negative surface charges of the particle and the positively charged choline-lipids that make up the majority of the RBC outer membrane. The ion interaction provides enough energy to cause a deformation of the RBC membrane which may result in spiculation or haemolysis of RBCs.^[68] Additional studies have also shown that RBCs in an acidic environment are more prone to crenation which can then lead to the generation of spicules.^[75, 76] Acidic silanol groups on the surface of MSN may potentially create acidic microenvironments upon association with the RBC membrane promoting membrane deformation and eventually spiculation. While LB-l-MSNs have been shown to cause virtually no haemolysis, this may have been to low association of particles with RBCs. In order to determine the amount of particles associated with RBCs, flow cytometry measurements of fluorescein labeled LB-l-MSNs mixed with PKH26 labeled

RBCs were performed. A series of controls was carefully selected to ensure that signals from RBCs associated with LB-I-MSNs do not overlap with signals from unassociated cells. The results of these experiments indicate that all of the particles in solution are closely associated with RBCs (Figure 2). Interestingly, while LB-I-MSNs are observed to produce a unique signal (I-MSN (-) samples), this signal was not observed when particles were mixed with RBCs, indicating that all LB-I-MSNs are associated with RBCs. Since it is possible that the dye labeling RBCs could become adsorbed by LB-I-MSNs, controls (I-MSN(+)) were established in which MSNs were exposed to PKH26. Measurements from flow cytometry show no signals in the gated region for PKH26 and LB-I-MSNs can be observed in the normal region for fluorescein labeled particles (Supplemental Info). Further evidence demonstrating the haemocompatibility of LB-I-MSNs, specifically mRBC I-MSN, was observed during SEM measurements of fixed RBCs (Figure 4). The series of

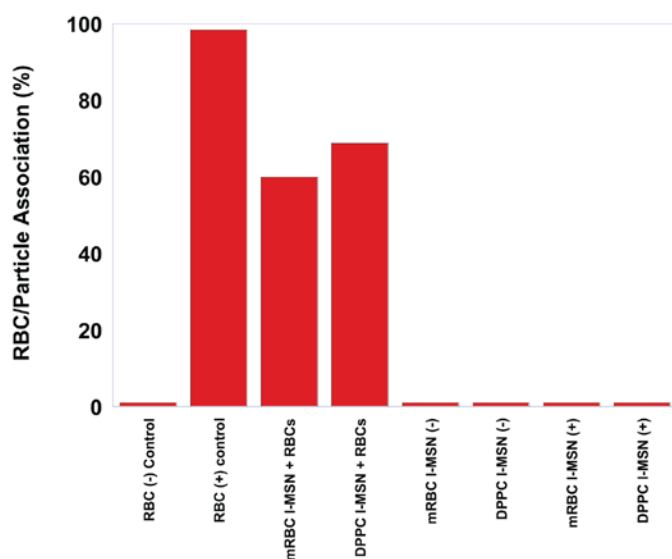


Figure 3. The results of flow cytometry measurements. RBC (-) and (+) controls confirm positive labelling by PKH26 marker. Samples mRBC and DPPC I-MSNs were evaluated based on the number of RBCs that were observed to also be positive for fluorescein fluorescent signals. mRBC and DPPC I-MSN (-) and (+) controls show that fluorescein-labelled particles do not exhibit and fluorescent signals in the region expected for PKH26.

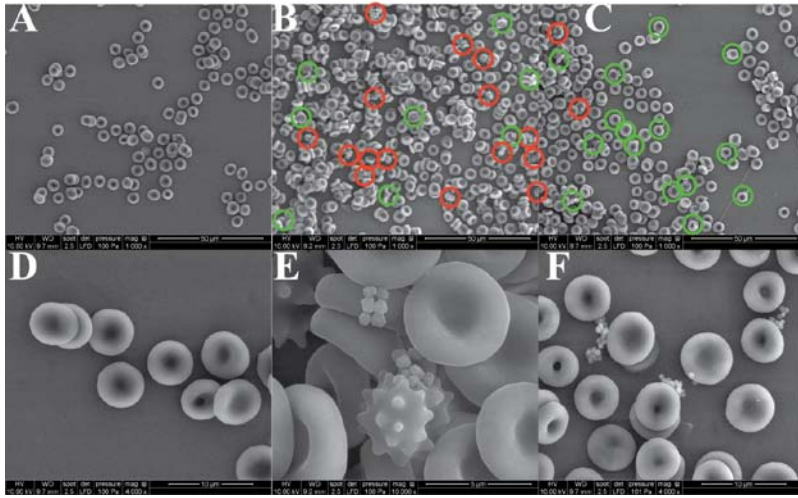


Figure 4. SEM micrographs of RBCs. Cells in panels A and D are control populations not exposed to MSNs. RBCs in panels E and F are exposed to concentrations of DPPC I-MSNs at 50 µg/mL, cells associated with particles show a large amount of damage in the form of spicules. Panels C and F show RBCs exposed to concentrations of mRBC I-MSNs at 50 µg/mL. RBCs in these images appear largely undamaged even when clearly associated with particles.

micrographs illustrates how changes in the composition of the outer bilayer of MSNs can affect the RBC morphology. In our previous study by Zhao et al., I-MSNs have been shown to be associated with spiculated RBCs under SEM observation. The control population of RBCs (Fig. 4A and D) shows only normal discocytes, while RBCs exposed to DPPC I-MSNs show a large proportion of spiculated cells of echinocyte phase II and III associated with the particles (red circles)(Fig. 4B and E).^[77] A smaller proportion of RBCs which do not appear to be damaged can be observed with particles on their surfaces (green circles). When the composition of the particle lipid bilayer was changed to mRBC, the majority of cells observed appear as normal discocytes and spiculation of cells appeared to proceed no further than echinocyte I phase (Fig. 4C and F). \

While initial haemolysis and flow cytometry data showed good haemocompatibility of DPPC I-MSNs, the SEM micrographs prove that due to the large amount of damaged cells, DPPC coating would have adverse affects on the ability of RBCs to deform when passing through capillaries, leading to possible clots and necrosis. There is also evidence in recent toxicological studies that shows a sharp increase in silicon concentration of the spleen

and liver shortly after the administration of MSNs, especially when the dose is given intravenously.^[36, 67] The close association of MSNs and RBCs observed with flow cytometry coupled with the sharp increase Si concentrations of the spleen indicate that RBCs are being spiculated and removed from circulation in the spleen by normal biological process.^[78] In contrast to DPPC l-MSNs, particles coated with mRBC do not appear to cause spiculation of RBCs by SEM analysis. This evidence coupled with the lack of haemolysis and close association of particles and RBCs indicates that mRBC coated particles may be better candidates as drug delivery devices due to a more biocompatible coating.

During the course of our previous study, TEM observations showed that l-MSNs were enveloped by the RBC membrane.^[68] While there are several systems that utilize the interior of the red blood cell to deliver cargo, this was not the intended purpose of the LB-l-MSN drug delivery system. Instead, by using mRBC coatings we hoped to avoid deformation of RBCs at all. Micrographs of LB-l-MSNs show markedly less local deformation than unfunctionalized l-MSNs(Figures 5 - 7). Similar to SEM observations, mRBC l-

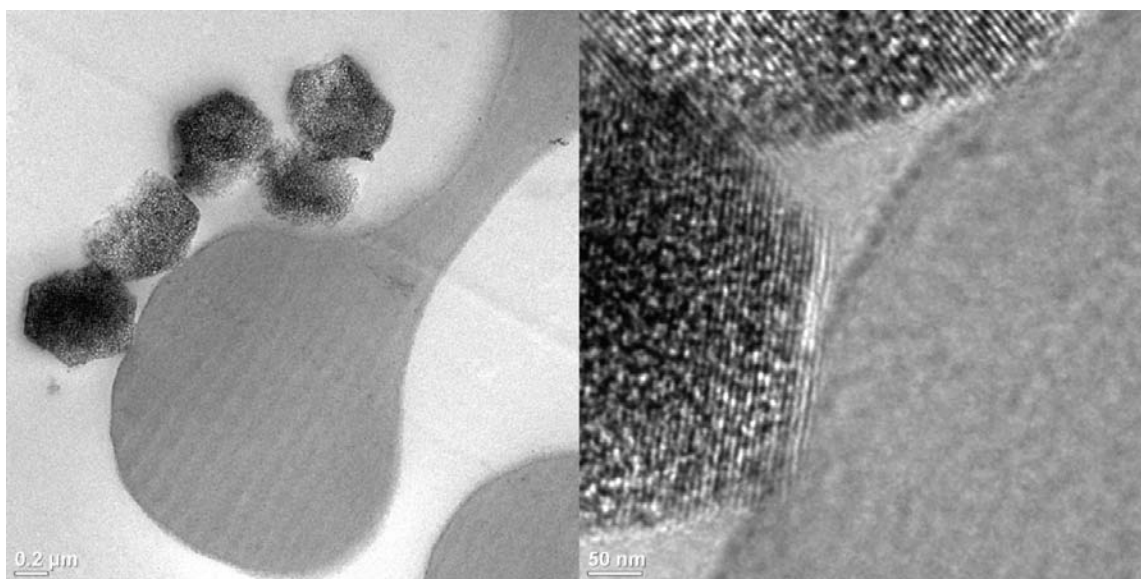


Figure 5. Large Pore MSNs coated with phospholipids which roughly approximate the RBC membrane. MSN's are shown to be in contact with the red blood cell membrane, however deformation of the red blood cell membrane, spiculation of the cell and endocytosis of the particle is not observed.

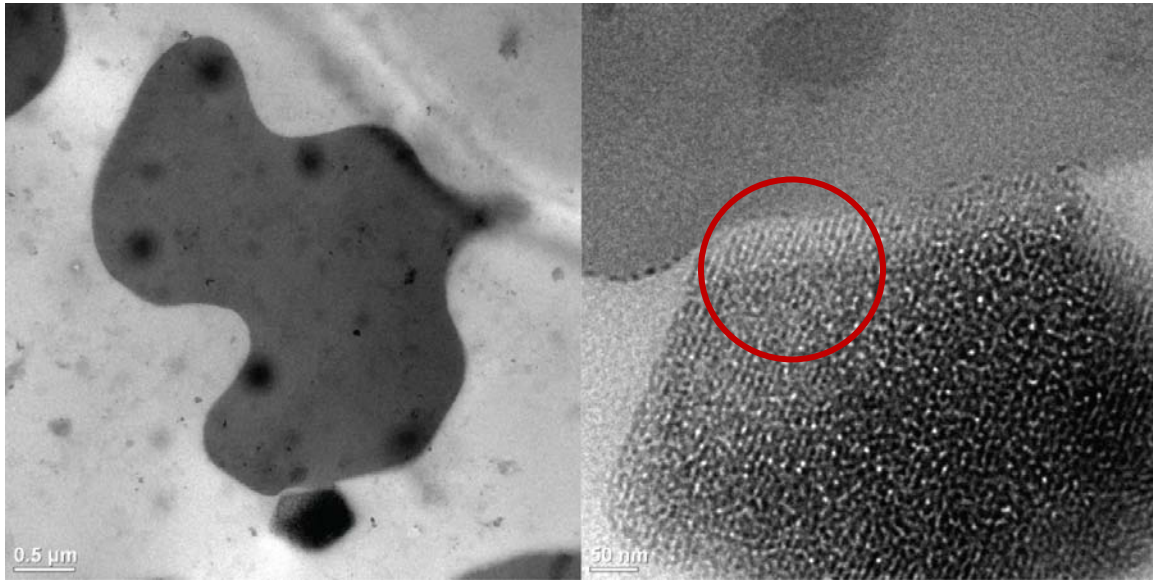


Figure 6. Large pore MSNs coated with only dipalmitoylphosphatidylcholine (DPPC). MSN is shown to be in contact with a spiculated cell. Deformation of the red blood cell membrane is also observed at the corner of the particle (highlighted). Unlike uncoated LP-MSNs, endocytosis of the particles is not observed in TEM images.

MSNs in contact with RBCs do not appear to cause spiculation and DPPC I-MSNs appear in contact with spiculated RBCs. In contrast to our previous study, neither mRBC nor DPPC coated I-MSN was observed to be engulfed by the RBC membrane.

Conclusion

Biomimicry is one of the most powerful tools that scientists have for exploring the human body and treating our various diseases and ailments. This is clearly shown by affecting a seemingly minor change in the lipid bilayer composition of I-MSNs. By altering the composition of the particle-supported outer bilayer to one which more closely matches the composition of a red blood cell, we were able to transform the LB-I-MSN system from one with a serious incompatibility (causing RBC spiculation) to a system that appears completely biocompatible. This study also outlines the importance of establishing guidelines for determining biocompatibility, as the haemolysis assay to determine deleterious effects of the particles on RBCs used by most researchers did not detect the change in RBC morphology that could lead to potentially harmful effects should similar mesoporous silica systems be tested *in vivo* or, in the long term, actual human test subjects. Adoption of

guidelines regarding nanoparticle toxicity evaluation, in addition to saving lives of current and future workers and researchers in these fields, may prove to save millions of dollars in the testing of systems that appear compatible except for a small difference that may not appear under the majority of currently applied tests.

References

- [1] J. L. Vivero-Escoto, I. I. Slowing, B. G. Trewyn, V. S. Y. Lin *Small*. **2010**, 6, 1952-1967.
- [2] Y. Zhao, J. L. Vivero-Escoto, I. I. Slowing, B. G. Trewyn, V. S. Y. Lin *Expert Opin. Drug Delivery*. **2010**, 7, 1013-1029.
- [3] S. Angelos, E. Johansson, J. F. Stoddart, J. I. Zink *Adv. Funct. Mater.* **2007**, 17, 2261-2271.
- [4] C.-Y. Lai, B. G. Trewyn, D. M. Jeftinija, K. Jeftinija, S. Xu, S. Jeftinija, V. S. Y. Lin *J Am Chem Soc.* **2003**, 125, 4451-4459.
- [5] M. Manzano, M. Colilla, M. Vallet-Regi *Expert Opin. Drug Del.* **2009**, 6, 1383-1400.
- [6] D. R. Radu, C.-Y. Lai, K. Jeftinija, E. W. Rowe, S. Jeftinija, V. S. Y. Lin *J. Am. Chem. Soc.* **2004**, 126, 13216-13217.
- [7] B. G. Trewyn, S. Giri, I. I. Slowing, V. S. Y. Lin *Chem. Commun. (Cambridge, U. K.)*. **2007**, 3236-3245.
- [8] J. Yu, H. Zhao, L. Ye, H. Yang, S. Ku, N. Yang, N. Xiao *J. Mater. Chem.* **2009**, 19, 1265-1270.
- [9] Y.-L. Zhao, Z. Li, S. Kabehie, Y. Y. Botros, J. F. Stoddart, J. I. Zink *J. Am. Chem. Soc.* **2010**, 132, 13016-13025.
- [10] H. M. Geysen, R. H. Meleon, S. J. Barteling *Proc. Natl. Acad. Sci. U. S. A.* **1984**, 81, 3998-4002.
- [11] H. Kitano *Nat. Rev. Drug Discovery*. **2007**, 5, 202-210.
- [12] V. Cauda, H. Engelke, A. Sauer, D. Arcizet, C. Brauchle, J. Radler, T. Bein *Nano Lett.* **2010**, 10, 2484-2492.
- [13] J. Liu, X. Jiang, C. Ashley, C. J. Brinker *J. Am. Chem. Soc.* **2009**, 131, 7567-7569.
- [14] L.-S. Wang, L.-C. Wu, S.-Y. Lu, L.-L. Chang, I. T. Teng, C.-M. Yang, J.-a. A. Ho *ACS Nano*. **2010**, 4, 4371-4379.
- [15] A. E. Garcia-Bennett *Nanomedicine (London, U. K.)*. **2011**, 6, 867-877.
- [16] R. Solaro, F. Chiellini, A. Battisti *Materials*. **2010**, 3, 1928-1980.
- [17] C. E. Ashley, E. C. Carnes, G. K. Phillips, D. Padilla, P. N. Durfee, P. A. Brown, T. N. Hanna, J. Liu, B. Phillips, M. B. Carter, N. J. Carroll, X. Jiang, D. R. Dunphy, C. L. Willman, D. N. Petsev, D. G. Evans, A. N. Parikh, B. Chackerian, W. Wharton, D. S. Peabody, C. J. Brinker *Nature Materials*. **2011**, 10, 389-397.
- [18] J. Fan, G. Fang, X. Wang, F. Zeng, Y. Xiang, S. Wu *Nanotechnology*. **2011**, 22, S455102/455101-455102/455111, S455102/455101-S455102/455117.

- [19] S. G. Patil, S. G. Gattani, R. S. Gaud, S. J. Surana, S. P. Dewani, H. S. Mahajan *Pharma Rev.* **2005**, 3, 53-58.
- [20] A. Samad, Y. Sultana, M. Aqil *Curr. Drug Delivery.* **2007**, 4, 297-305.
- [21] S. Hatziantoniou, C. Demetzos *Stud. Nat. Prod. Chem.* **2008**, 34, 173-202.
- [22] N. Allon, A. Saxena, C. Chambers, B. P. Doctor in Liposomal drug delivery constructs targeted by lipid-conjugated peptide ligands, Vol. (Ed.^Eds.: Editor), (United State Army, USA). City, **2009**, pp.20pp , Cont -in-part of U S Ser No 339,404.
- [23] M. N. Jones *Adv. Drug Del. Rev.* **1994**, 13, 215-249.
- [24] N. Yamazaki, Y. Jigami, H.-J. Gabius, S. Kojima *Trends Glycosci. Glycotechn.* **2001**, 13, 319-329.
- [25] K. K. Matthay, T. D. Heath, C. C. Badger, I. D. Bernstein, D. Papahadjopoulos *Cancer Res.* **1986**, 46, 4904-4910.
- [26] M. Mizuno, J. Yoshida *Drug Delivery Sys.* **1995**, 10, 399-403.
- [27] V. P. Torchilin *Nat Rev Drug Discov.* **2005**, 4, 145-160.
- [28] A. Gabizon Alberto, H. Shmeeda, S. Zalipsky *J. Liposome Res.* **2006**, 16, 175-183.
- [29] T. Lian, R. J. Ho *J. Pharm. Sci.* **2001**, 90, 667-680.
- [30] C. E. Ashley, E. C. Carnes, G. K. Phillips, D. Padilla, P. N. Durfee, P. A. Brown, T. N. Hanna, J. Liu, B. Phillips, M. B. Carter, N. J. Carroll, X. Jiang, D. R. Dunphy, C. L. Willman, D. N. Petsev, D. G. Evans, A. N. Parikh, B. Chackerian, W. Wharton, D. S. Peabody, C. J. Brinker *Nature Materials.* **2011**, 10, 389-397.
- [31] L. Moroder, H.-J. Musiol, G. Siglmüller *Synthesis.* **1990**, 1990, 889-892.
- [32] S. Huh, J. W. Wiench, J.-C. Yoo, M. Pruski, S. Y. Lin Victor *Chem. Mater.* **2003**, 15, 4247-4256.
- [33] J. H. de Boer, B. C. Lippens, B. G. Linsen, J. C. P. Broekhoff, A. van den Heuvel, T. J. Osinga *Journal of Colloid and Interface Science.* **1966**, 21, 405-414.
- [34] F. Michelet, R. Gueguen, P. Leroy, M. Wellman, A. Nicolas, G. Siest *Clin. Chem.* **1995**, 41, 1509-1517.
- [35] S. Giri, B. G. Trewyn, M. P. Stellmaker, V. S. Y. Lin *Angew Chem, Int Ed.* **2005**, 44, 5038-5044.
- [36] T. Liu, L. Li, X. Teng, X. Huang, H. Liu, D. Chen, J. Ren, J. He, F. Tang *Biomaterials.* **2011**, 32, 1657-1668.
- [37] M. Al Shamsi, M. T. Al Samri, S. Al-Salam, W. Conca, S. Shaban, S. Benedict, S. Tariq, A. V. Biradar, H. S. Penefsky, T. Asefa, A.-K. Souid *Chemical Research in Toxicology.* **2010**, 23, 1796-1805.
- [38] H. Zhang, T. Xia, H. Meng, M. Xue, S. George, Z. Ji, X. Wang, R. Liu, M. Wang, B. France, R. Rallo, R. Damoiseaux, Y. Cohen, K. A. Bradley, J. I. Zink, A. E. Nel *ACS Nano.* **2011**, 5, 2756-2769.
- [39] E. J. Murphy, T. A. Rosenberger, Lipid Mediated Signaling, Taylor and Francis Group, LLC, Boca Raton, **2010**.
- [40] D. A. Foster, L. Xu *Molec. Canc. Res.* **2003**, 1, 789-800.
- [41] N. R. Murray, L. J. Thompson, A. P. Fields, The Role of Protein Kinase C in Cellular Proliferation and Cell Cycle Control, R.G. Landes Company, Austin, **1997**.
- [42] C. Banchio, L. M. Schang, D. E. Vance *J. Biol. Chem.* **2003**, 278, 32457-32464.
- [43] L. G. Henage, J. H. Exton, H. A. Brown *J. Biol. Chem.* **2006**, 281, 3408 - 3417.
- [44] J. Zhu, J. Tang, L. Zhao, X. Zhou, Y. Wang, C. Yu *Small*, 6, 276-282.

- [45] W. H. Moolenaar, W. Kruijer, B. C. Tilly, I. Verlaan, A. J. Bierman, S. W. de Laat *Nature*. **1986**, 323, 171-173.
- [46] A. A. Kapralov, I. V. Kurnikov, I. I. Vlasova, N. A. Belikova, V. A. Tyurin, L. V. Basova, Q. Zhao, Y. Y. Tyurina, J. Jiang, H. Bayir, Y. A. Vladimirov, V. E. Kagan *Biochemistry*. **2007**, 46, 14232-14244.
- [47] Z. T. Schug, E. Gottleib *Biochim. Biophys. Acta*. **2009**, 1788, 2022-2031.
- [48] Q. Gan, X. Lu, Y. Yuan, J. Qian, H. Zhou, X. Lu, J. Shi, C. Liu *Biomaterials*. **2011**, 32, 1932-1942.
- [49] C.-H. Lee, S.-H. Cheng, I. P. Huang, S. Souris Jeffrey, C.-S. Yang, C.-Y. Mou, L.-W. Lo *Angewandte Chemie (International ed. in English)*. **2010**, 49, 8214-8219.
- [50] S. Febvay, D. M. Marini, A. M. Belcher, D. E. Clapham *Nano Letters*. **2010**, 10, 2211-2219.
- [51] J. L. Vivero-Escoto, I. I. Slowing, C.-W. Wu, V. S. Y. Lin *Journal of the American Chemical Society*. **2009**, 131, 3462-3463.
- [52] A. Bernardos, L. Mondragon, E. Aznar, M. D. Marcos, R. Martinez-Manez, F. Sancenon, J. Soto, J. M. Barat, E. Perez-Paya, C. Guillem, P. Amoros *ACS Nano*. **2010**, 4, 6353-6368.
- [53] K. Patel, S. Angelos, W. R. Dichtel, A. Coskun, Y.-W. Yang, J. I. Zink, J. F. Stoddart *Journal of the American Chemical Society*. **2008**, 130, 2382-2383.
- [54] C.-Y. Lai, G. Trewyn Brian, M. Jeftinija Dusan, K. Jeftinija, S. Xu, S. Jeftinija, S. Y. Lin Victor *Journal of the American Chemical Society*. **2003**, 125, 4451-4459.
- [55] Z. Luo, K. Cai, Y. Hu, L. Zhao, P. Liu, L. Duan, W. Yang *Angewandte Chemie, International Edition*. **2011**, 50, 640-643, S640/641-S640/648.
- [56] V. K. Varadan, L. Chen, J. Xie, *Nanomedicine: Design and applications for Magnetic Nanomaterials, Nanosensors and Nanosystems*, John Wiley & Sons, Ltd, West Sussex, United Kingdom, **2009**.
- [57] K. Cheng, S. R. Blumen, M. B. MacPherson, J. L. Steinbacher, B. T. Mossman, C. C. Landry *ACS Applied Materials & Interfaces*. **2010**, 2, 2489-2495.
- [58] D. Brevet, M. Gary-Bobo, L. Raehm, S. Richeter, O. Hocine, K. Amro, B. Loock, P. Couleaud, C. Frochot, A. Morere, P. Maillard, M. Garcia, J.-O. Durand *Chemical Communications (Cambridge, United Kingdom)*. **2009**, 1475-1477.
- [59] M. Fisichella, H. Dabboue, S. Bhattacharyya, G. Lelong, M.-L. Saboungi, F. Warmont, P. Midoux, C. Pichon, M. Guerin, T. Hevor, J.-P. Salvétat *Journal of Nanoscience and Nanotechnology*. **2010**, 10, 2314-2324.
- [60] Z. Guo, S. Meng, W. Zhong, Q. Du, L. L. Chou *Appl. Surf. Sci.* **2009**, 255, 6771-6780.
- [61] N. Gulati, R. Rastogi, A. K. Dinda, R. Saxena, V. Koul *Colloids Surf., B*. **2010**, 79, 164-173.
- [62] S. R. Meyers, M. W. Grinstaff *Chemical Reviews*. **2011**.
- [63] A. M. Carmona-Riveiro *International Journal of Nanomedicine*. **2010**, 5, 249 - 259.
- [64] S. Moura, A. Carmona-Ribeiro *Cell Biochemistry and Biophysics*. **2006**, 44, 446-552.
- [65] R. Mani, S. D. Cady, M. Tang, A. J. Waring, R. I. Lehrer, M. Hong *Proc. Natl. Acad. Sci. U. S. A.* **2006**, 103, 16242-16247.
- [66] M. A. Symes, H. M. Patel *Biochem. Soc. Trans.* **1992**, 20, 327S.
- [67] X. Huang, L. Li, T. Liu, N. Hao, H. Liu, D. Chen, F. Tang *ACS Nano*. **2011**, 5, 5390-5399.

- [68] Y. Zhao, X. Sun, G. Zhang, B. G. Trewyn, I. I. Slowing, V. S. Y. Lin *ACS Nano*. **2011**, 5, 1366-1375.
- [69] M. Joglekar, R. Roggers, B. Trewyn. **in preparation**.
- [70] S. P. Hudson, R. F. Padera, R. Langer, D. S. Kohane *Biomaterials*. **2008**, 29, 4045-4055.
- [71] T.-W. Kim, I. I. Slowing, P.-W. Chung, V. S.-Y. Lin *ACS Nano*. **2010**, 5, 360-366.
- [72] N. Mohandas, P. G. Gallagher *Blood*. **2008**, 112, 3939-3947.
- [73] M. Narla in Red Blood Cell Membrane Dynamics and Organization, Vol. 18.2 (Ed. Eds.: Editor), Wolters Kluwer Health, City, **2010**.
- [74] R. Shelma, C. P. Sharma *Colloids and Surfaces B: Biointerfaces*. **2011**, 84, 561-570.
- [75] R. Sergey V *Biochimica et Biophysica Acta (BBA) - Biomembranes*. **2010**, 1798, 1767-1778.
- [76] M. Rasia, A. Bollini *Biochimica et Biophysica Acta (BBA) - Biomembranes*. **1998**, 1372, 198-204.
- [77] G. Lim H. W., M. Wortis, R. Mukhopadhyay *Proceedings of the National Academy of Sciences*. **2002**, 99, 16766-16769.
- [78] R. E. Mebius, G. Kraal *Nature Reviews Immunology*. **2005**, 5, 606-616.

Chapter 3: Synthesis of New Materials using the Hydrolysis and Condensation of Alkoxysilane Precursors

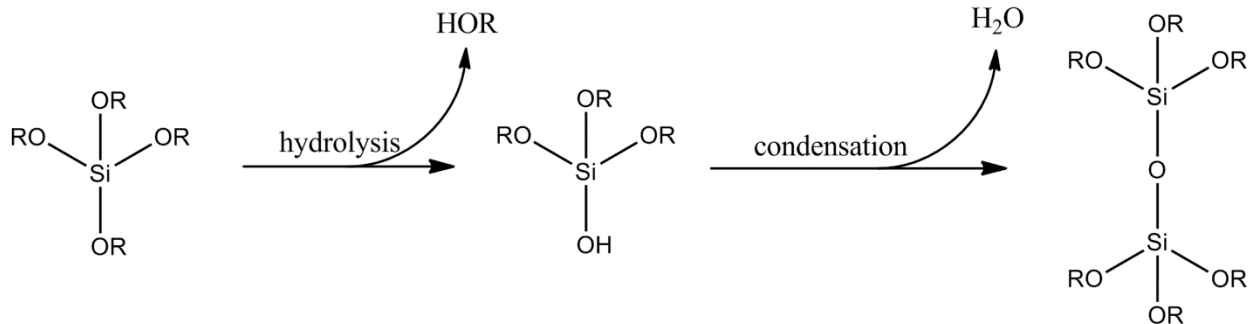
Introduction

The “bottom-up” synthesis of new materials represents a powerful driving force in science and technology research today. This synthetic method provides a fine degree of control for assembling highly ordered materials. Of particular interest are mesoporous silica particles (MSPs). Bottom up synthesis of MSPs allows for the control of particle morphology, size, surface area, pore size and pore volume. Additionally, the methods are generally tolerant to a large variety of functional groups, allowing for organic transformation of the MSP surfaces in order to achieve synthetic and scientific goals.

The general method of MSP synthesis, utilized by researchers across the world, requires control of two main factors. The first is control over the templating agent. Altering concentrations of the organic templating agent will influence the MSP’s morphology, particle size, and pore size.^[1-4] The second factor requiring fine control is reaction kinetics of the silica precursor or precursors. The rate of Si-O-Si bond formation also has the ability to influence the physical properties of the final product.^[5] Modifying the organic functional groups, in addition to framework properties, enables MSPs to function in a wide variety of applications including (bio)chemical analysis, catalysis, therapeutic devices, energy storage/generation devices, and templates for other materials.^[6]

Our approach uses a two step mechanism for producing the Si-O-Si bond; hydrolysis and condensation of an alkoxysilane precursor (Scheme 1). The rates of these two reactions are mainly controlled by adjusting the pH of the solution or the alkoxy groups of the silicon precursor. Counterions in acids or bases used to adjust the pH have also been shown to have an effect on the physical characteristics of the particle.^[7, 8] This range of effective working

pHs indicates that silicate materials are stable from pH 2 – 11 and indeed synthesis is performed across all of these pH ranges.



Scheme 1. Stepwise hydrolysis and condensation of an alkoxy silane precursor. Single silane molecules may undergo multiple hydrolysis steps before beginning condensation or silica oligomers undergo further hydrolysis of unreacted alkoxy groups until all alkoxy groups have been converted to Si-O-Si or Si-OH bonds.

I. Synthesis of a New Mesoporous Silica Nanoparticle from Water in Oil Emulsion

Introduction

The original impetus for this project was three-fold; first was the development of a truly spherical large-pore (pore diameter > 7 nm) mesoporous silica nanoparticle (MSN). The second was to develop reaction conditions that could be modified in order to accommodate the later synthesis of particles with different metal-oxide frameworks via condensation method. Lastly, we desired a fast, low-temperature method to generate a truly spherical particle. The current synthesis of large pore mesoporous silica particles takes 72 hours and relies on high temperatures to achieve large pore size, resulting in a particle that is actually a hexagonal prism. It was for these reasons that water-in-oil (W/O) emulsion was chosen as the synthetic medium. In terms of morphological control, W/O emulsion allows for control of the particle size through control of the water droplet “reactor” size. Stabilization for the water droplet is provided by an amphiphilic block copolymer. Since the silica precursors in the hydrolysis and condensation reaction are hydrophilic, formation of the MSN occurs totally within the water droplet.^[9] Several examples of mesoporous silica materials formed in W/O emulsions have been previously published, however the majority of these studies employ non-ionic multi-bloc copolymers.^[10-13]

Experimental

The surfactant, cetyltrimethylammonium bromide (CTAB), silica precursor, tetraethylorthosilane (TEOS), decane, and citric acid were purchased from Sigma Aldrich and used as received. Arlcel P-135 (AP, Cithrol™), an ABA diblock copolymer (A = polyhydroxystearate, B = 30-polyethyleneglycol) employed as an emulsion stabilizer was generously donated by Croda International Plc.

All materials in this study were prepared via the following synthetic method; first, a stock solution containing the appropriate weight% of CTAB was added to a flask. Secondly, the appropriate volume ratio of decane was added. The solution was allowed to stir rapidly to form the W/O emulsion, for solutions containing higher concentrations of CTAB and/or AP, mild heating was required to dissolve all constituents (flasks were then allowed to cool to room temp. before subsequent additions of reagents). This was followed by the addition of AP, citric acid and ammonium hydroxide and with stirring to homogenize reactants. Finally TEOS was added rapidly to the flask and stirred for 24 hours. Reaction mixtures were then centrifuged at 9000 g for 15 min. and the decane layer was decanted and saved for repurification. Methanol was then added to the remaining mixture and centrifuged again at 9000 g for 15 min., the supernatant was decanted and washed twice more with methanol and once with acetone before being placed in a lyophilizer and dried overnight. A complete list of all experiments performed is available in appendix C.

The materials were characterized via the following methods; the first, X-Ray diffraction (XRD), was performed on a Rigaku Ultima IV powder X-ray system utilizing $2\theta/\theta$ geometry and equipped with a copper target ($\lambda = 1.54 \text{ \AA}$) operated at 2.2 kW. The second method of characterization was transmission electron microscopy (TEM). Microtomed samples were embedded in an epoxy resin and then sliced to 80 nm thickness using a Leica Ultracut sliding ultramicrotome. Thin sections and particle samples were supported on copper grids with carbon film and examined in a Tecnai G2 F20 microscope

operated at 200 kV. Scanning electron micrographs were obtained using a FEI Quanta 250 FEG scanning electron microscope

Results and Discussion

In order to establish the phase behavior of the silicate particle product, several experiments were designed and carried out including variation in TEOS concentration, CTAB concentration, synthesis temperature, oil-to-water ratio and weight percentage of AP stabilizer. The initial evaluation of the materials in these experiments was performed by powder XRD. The first set of experiments was performed by varying the concentration of CTAB around the value for the second critical micelle concentration (transition from micelles to long rods in hexagonally packed arrays).^[14] Surprisingly, a material with some of the desired characteristics including a pore size of 7 nm was obtained in this first attempt (**Fig. 1**). It was not immediately clear from the analysis of the XRD pattern whether or not the pore system in the material was of a 2D cubic or hexagonal structure due to the fact that when the hkl-indices for the peaks were compared with 2θ values derived from calculations did not result

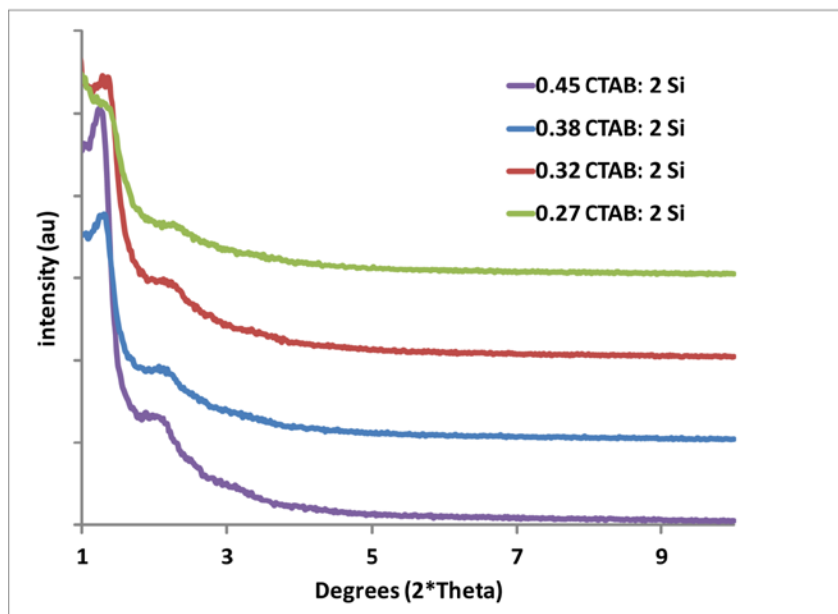


Figure 1. Powder X-ray diffraction pattern of materials synthesized using variations in CTAB concentrations. The ratio of CTAB to silica precursor can be seen in the figure legend.

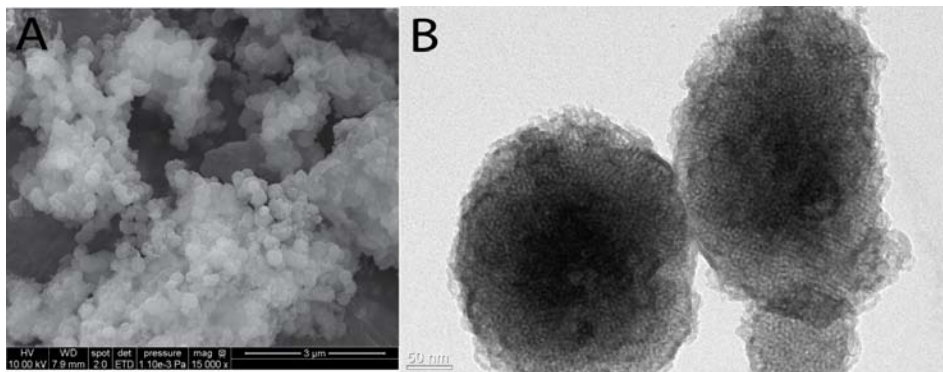


Figure 2. SEM (A) and TEM (B) micrographs of material 78-1 detailing the random particle morphology and pore structure.

in a positive match for either cubic or hexagonal pore arrangement. Further analysis of the morphology using SEM and TEM observations revealed that this initial set of particles also possessed a wide distribution of particle sizes (**Fig. 2A**) and the pore structure did not appear to be uniform across all particles (**Fig. 2B**). In addition, the particle morphology was not limited to spheres or sphere-like particles and instead included ovoid particles and monolithic particles possessing no mesostructure. The next step was to control the amount of TEOS added to the solution, the presence of monolithic particles indicated that the capacity of the water phase of the emulsion to contain the current amount of TEOS had reached the saturation point. The results of the experiment yielded a particle with the most ordered structure and uniform morphology of any of the following studies (**Fig. 3**). The peak position

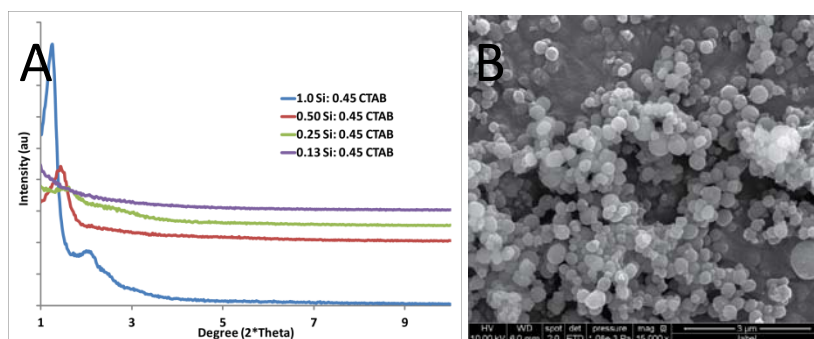


Figure 3. X-Ray diffraction patterns for 79 series of reactions (A) in which the concentration of TEOS is varied. The figure legend shows the mol ratio of silica precursor to CTAB structure directing agent. Panel B shows the SEM micrograph of the material 79-1.

data obtained from the XRD pattern of these materials resulted in a relatively good match for a hexagonally close packed array of pores (**Tab. 1**). The incomplete matching of peak positions to hkl- indices led to samples of 79-1 to be embedded in an epoxy resin and microtomed so that thin slices of the particle could be examined to test whether multiple phases were still observable (**Fig. 4**). A third set of samples was prepared in which the weight% of AP was varied to determine if particle morphology could be better controlled by altering the amount of emulsion stabilizer. The peaks recorded in the powder XRD patterns did not shift position indicating that AP does not play an active role in determining the pore structure of the mesoporous silicate material (**Fig. 5**).

To determine what role AP is performing in these experiments; SEM and TEM micrographs of the materials were examined (**Fig. 6**). This set of micrographs confirms that AP concentration affects the morphology of the particle. In the sample where the smallest weight percentage of AP is used, a spherical morphology is achieved but the particle size is found to vary from 200 nm up to 2 μm (**Fig. 6A and 6C**). In the samples where the largest weight percentage of AP is used, a uniform particle size is obtained however the morphology deviates from spherical (**Fig. 6B and 6D**).

Table 1. Calculations of the expected peak positions of an array of pores matching either 2D hexagonal or cubic phases. Cubic arrangement appears to give the closest values for calculated peak positions.

2-D hexagonal							
hkl - values			Calculations		Actual Peak Position		
h	k	l	2*Theta	d-spacing	2*Theta	d-spacing	
1	0	0	0.62	7.09	1.26	7.00	
1	1	0	1.08	5.02	2.10	4.20	
2	0	0	1.25	3.55	2.50	3.53	
2	2	0	2.16	2.51	3.08	2.87	
Cubic							
hkl - values			Calculations		Actual Peak Position		
h	k	l	2*Theta	d-spacing	2*Theta	d-spacing	
1	0	0	1.23	7.18	1.26	7.00	
1	1	0	1.74	5.08	2.10	4.20	
2	0	0	2.46	3.59	2.50	3.53	
2	2	0	3.48	2.54	3.08	2.87	

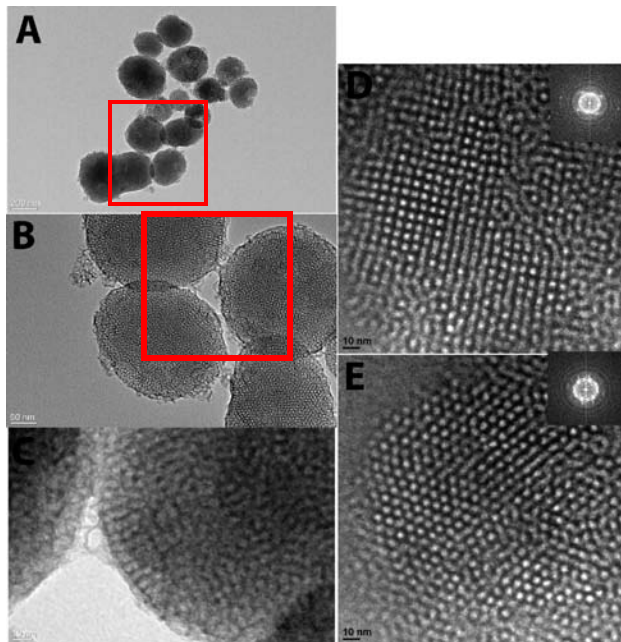


Figure 4. TEM images of particles in experiment number 79-1 at increasing magnifications of 10 kX (A), 42 kX, and 160 kX. The red box shows the area examined in the images of increased magnification. Images of samples embedded in epoxy and then microtomed, the particle in panel D shows a cubic pattern with a matching fourier transform of the diffracted electrons (inset) while panel E shows a particle with a visually hexagonal pattern though the fourier transform of diffracted electrons for this sample is inconclusive (inset).

In addition the edges of the particle are also roughened and the micrographs show that many of the particles are not completely formed or broken.

Despite the fact that uniform morphology and a regular pore structure had been discovered in earlier experiments, further tests of temperature were carried out to ensure that room temperature synthesis was providing the best overall structure (**Fig. 7**). The results of this experiment clearly show that any increase in synthesis temperature results in the degradation of long range pore ordering followed eventually by the total loss of pores in the material. Finally a synthetic phase diagram was derived

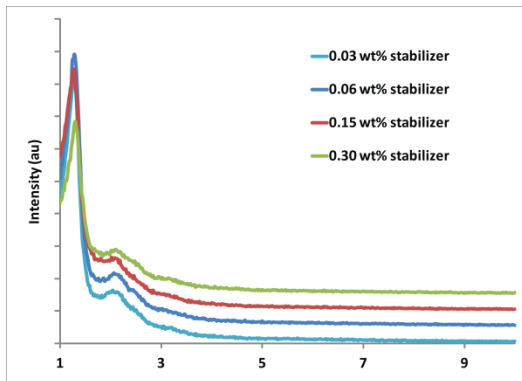


Figure 5. Powder XRD pattern of mesoporous materials prepared with different concentrations of emulsion stabilizer AP. Samples 82-1, 82-2, 82-3, 82-4 correspond to 0.03 wt%, 0.06 wt%, 0.15 wt% and 0.30 wt% (decane) respectively.

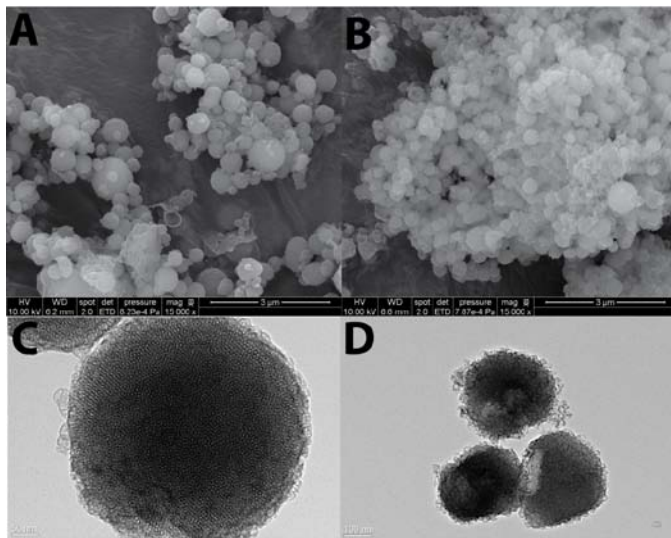


Figure 6. Micographs of materials synthesized using 0.03% wt (A and C) and using 0.30% wt (B and D) of emulsion stabilizing molecule, AP. Particle diameter varies greatly in A and C, while the spherical morphology is degraded in B and D.

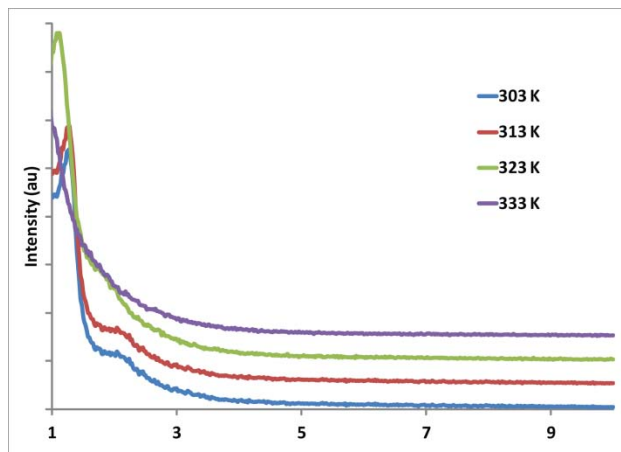


Figure 7. Powder XRD pattern showing the effect of increasing temperature on the pore structure of mesoporous silica particles. The sample 80-1, 80-2, 80-3 and 80-4 are synthesized at 30°C, 40°C, 50°C, and 60°C respectively. Intensity values are offset for clarity.

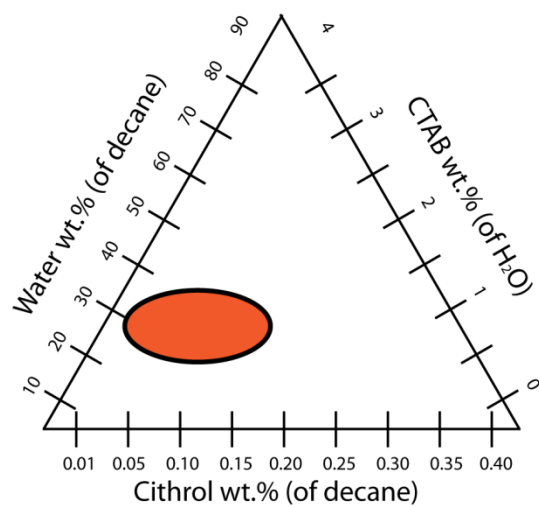


Figure 8. Phase diagram for the synthesis of ca. 7 nm pore diameter mesoporous silica spheres. The orange oval represents conditions which produce the desired product.

using the observations from the various analytical techniques (**Fig. 8**). A spherical mesoporous silica particle was successfully synthesized and characterized. Additionally a phase diagram was developed for to describe the conditions at which this particle could be synthesized. The spherical nature of the particle should enable the material to interact with biological systems without causing undue toxicity. In addition the increased pore size above the normal diameter from the MCM-41 type mesoporous silica particles pores (approx. 3 nm) should enable future researchers to encapsulate larger molecules such as proteins or enzymes in the pores.

II. Synthesis and Morphology Control of a Periodic Mesoporous Organosilica Derived from Benzobisoxazole-Bridged Alkoxysilanes

Introduction

Periodic mesoporous organosilicas (PMOs) represent a large class of materials originating from a common molecular precursor with the basic structure $(\text{RO})_3\text{Si}-\text{R}'-\text{Si}(\text{OR})_3$. These precursors are capable of producing highly ordered structures on both the molecular and supra-molecular levels. On the supramolecular level, a wide range of morphologies have been synthesized from films to spherical particles, each with a range of pore sizes and pore arrangements.^[15-18] PMOs have also been reported containing a variety of organic groups that impart the materials with distinctive characteristics. Organic groups having been successfully incorporated into PMOs include simple alkanes, alkenes, alkynes, metal complexes and conjugated molecules including benzene, naphthalene and anthracene derivatives.^[19-26] Furthermore, it has been proven that several PMOs are capable of performing or enhancing catalytic reactions, temperature responsive materials and light harvesting materials.^[26-28] PMO materials with luminescent properties have been recently reviewed by Tani et al. indicating that interest in luminescent PMOs and their usefulness in a variety of devices have been increasing.^[29]

This current work focuses on the synthesis and morphology control of a PMO material containing 2,6-bis(methyl(3-aminopropyltriethoxy-silane))benzo(1,2-d,4,5-d')bisoxazole (MASBB) as the organic bridging group (Scheme 1).

Scheme 1. Synthesis silsesquioxane precursor via $\text{S}_{\text{N}}2$ of MASBB and 3-aminopropyltriethoxysilane.

Benzobisoxazoles (BBOs) represent a class of materials already researched as robust materials for alternative energy and mechanical applications; however the ability to process these materials into functioning devices such as solar cells and ballistic materials is generally an expensive and laborious process involving specialized hardware and strong acids.^[30-32] Despite these limitations poly-benzobisoxazole based diodes are receiving increased attention due to their excellent ability to transfer electrons.^[33] Many of the important sensing and photoreactive attributes displayed by BBO based polymers are due to the π - π stacking effects of adjacent polymer chains.^[34] By incorporating BBOs into the pores of our PMOs we hope to be able to generate materials with many of the same opto-electric properties as BBO based polymers.

All PMO materials were synthesized under the same general procedures which are as follows: synthesis of precursor silsesquioxane by S_N2 reaction with 3-aminopropyltriethoxysilane followed by purification of PMO precursor via vacuum distillation. An aqueous solution of cetyltrimethylammonium bromide (CTAB) and NaOH is then added to the still hot PMO precursor, followed by addition of tetraethylorthosilicate (TEOS). The molar ratio of Si : CTAB : NaOH : H₂O, in solution are as follows: 1 : 0.748 : 6.795 : 1385. The solution is then stirred at 105°C for 4 days followed by condensation of the solution via adjustments of the pH between 9 and 11 with concentrated HCl. Hydrothermal aging at 120°C in sealed Teflon bottles was carried out on several samples in attempts to further control the final morphology of the PMO. The CTAB template was removed via high vacuum at 200°C and template extracted materials were compared with as-synthesized materials via TGA analysis in order to confirm removal of the surfactant and retention of MASBB group. X-Ray powder diffraction patterns, TEM micrographs and nitrogen sorption isotherm experiments were used to characterize the PMO materials. MASBB-based PMOs can be synthesized in such a way as to yield a crystalline organic phase and regular mesopores as shown in the powder XRD patterns in Figure 1.

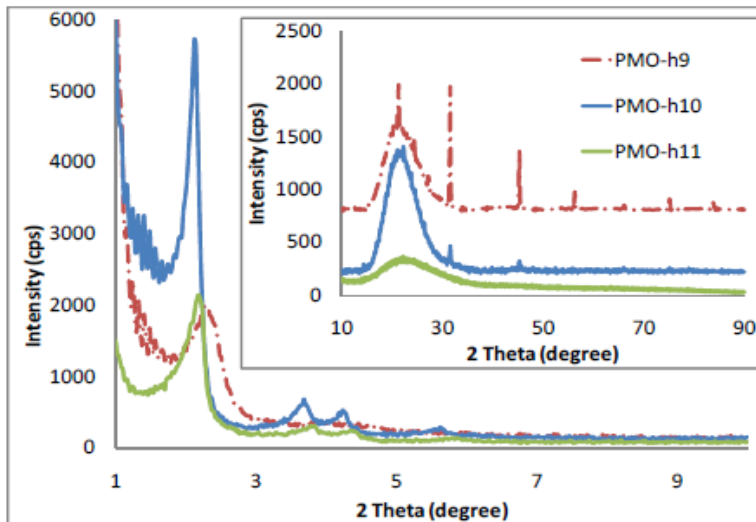


Figure 1. XRD pattern for materials synthesized with pH adjustment at 100°C and 24 hours of aging. Scan from 1 – 10 degrees 2 theta indicating mesoporosity of the material. The inset shows a scan from 10 – 90 degrees 2 theta indicating crystalline BBO domains.

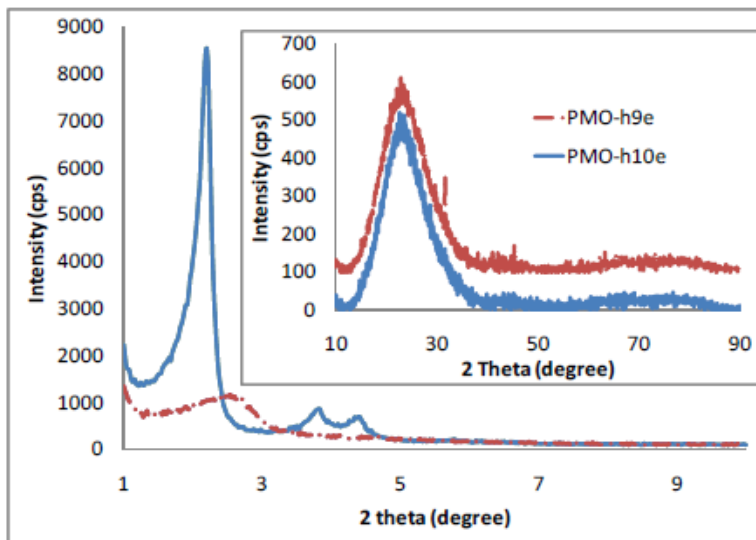


Figure 2. XRD patterns for template-extracted materials. Scan from 1 – 10 degrees 2 theta indicating mesoporosity of the material after template extraction. The inset shows a scan from 10 – 90 degrees 2 theta indicating retention of crystalline MASBB domains after template extraction.

The results of X-ray diffraction experiments show that mesoporosity of the materials is obtained in all samples while extended hexagonal ordering is only accessible at hydrolysis conditions of pH 10 to 11. Crystallinity of the benzobisoxazole moiety can be obtained from hydrolyzing the homogenized solutions at a pH range of 9 to 10 (Figure 1). Calcination at

temperatures higher than 200 °C both with and without the presence of vacuum results in the collapse of both mesopores and the dissociation of the crystalline domains in all materials. TEM analysis of the synthesized materials yields the following trends; sphere shaped materials resulted from high temperature condensation while a rod morphology is obtained from samples which are condensed at room temperature (Figure 3). Hollow silicate materials have been synthesized previously using very basic conditions or swelling agents.^[35-37]

In this study we have also successfully synthesized hollow PMO materials by hydrothermally aging the PMO-h11 or PMO-r10 solutions for 8 or more hours (Figure 4).

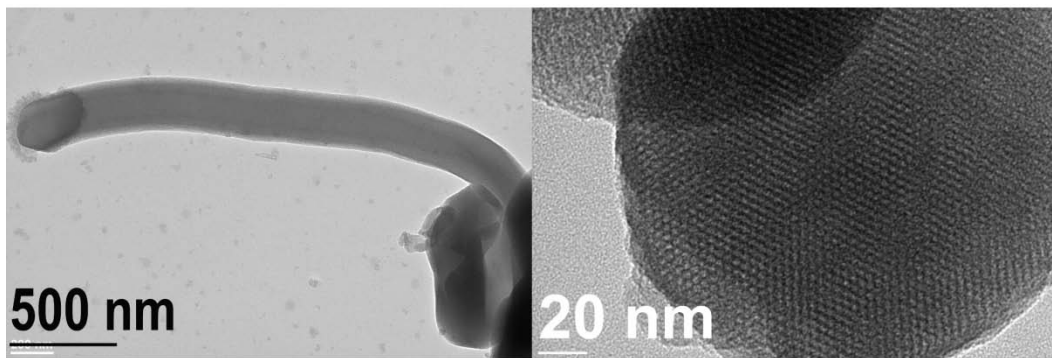


Figure 3. TEM micrograph showing the effect of condensation temperature on PMO morphology, (a.) room temperature condensation at pH 10 and (b.) 100 °C condensation at pH 10

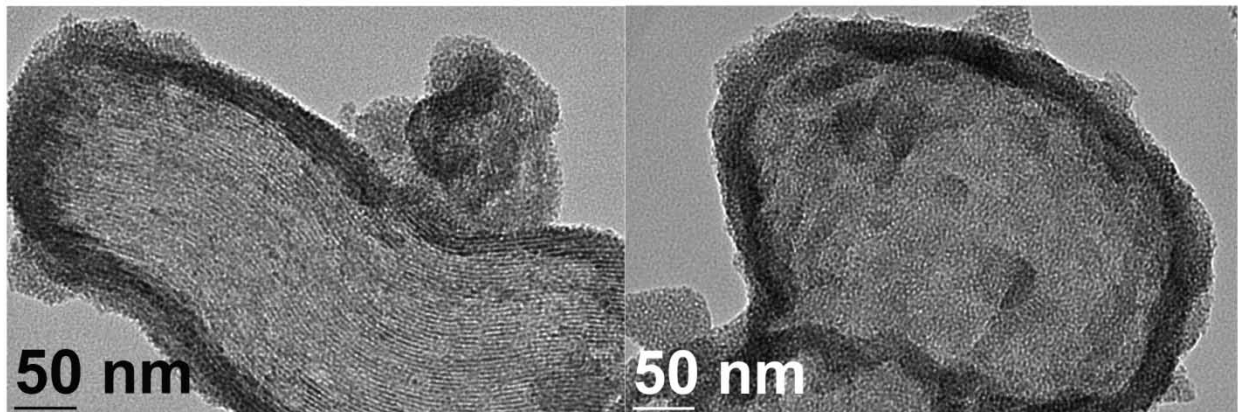


Figure 4. TEM micrograph showing the effect of aging on PMO morphology, (a.) room temperature condensation at pH 10 followed by 24 hour hydrothermal treatment, (b.) 100 °C condensation at pH 11 followed by 24 hour hydrothermal treatment.

In order to demonstrate a potential application of MASBBO-PMOs as chemical sensors, an experiment was carried out to determine the amount of fluorescence quenching that could be achieved by exposing the materials to 100 μ M solutions of the common

explosive taggants 3-nitrotoluene (3-NT) and nitromethane (NM) in acetonitrile. Both of these molecules exert room temperature vapor pressures well above that of TNT or other plastic explosive and are thusly used in the detection of explosives.^[38-40] The pi interactions of the benzobisoxazole moiety and nitro group of the selected molecules results in fluorescence quenching of the MASBBO-PMO. The UV-vis spectrum of MASBBO-PMO was first obtained in aqueous solution and in THF, and an absorption edge at 295 nm was selected as the fluorescence excitation wavelength. Excitation of MASBBO-PMO at 295 nm results in two excitation peaks, one centered at 335 nm and the other at 440 nm (**Fig. 5**).

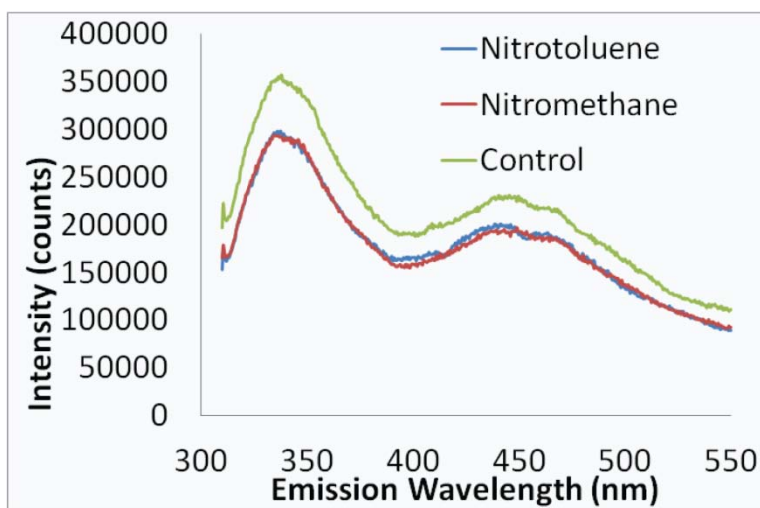


Figure 5. Fluorescence measurements of MASBB-PMO (250 µg/mL) exposed to 100 µM taggant/acetonitrile solutions and in acetonitrile (control).

The total amount of quenching observed for 3-NT treated PMO is $20\% \pm 3.5\%$ at 335 nm and $22\% \pm 5.6\%$ at 440 nm. The total amount of fluorescence quenching for the NM treated PMO is $20\% \pm 1.2\%$ at 335 nm and $21\% \pm 1.4\%$. MASBBO-based PMOs have been successfully synthesized and their morphology and crystallinity carefully controlled using a variety of synthesis conditions. This research provides a framework under which other PMOs may be prepared in order to take advantage forced-ordering of small molecules due to confinement. These future materials may be used on opto-electronic, sensing and other devices.

Conclusion

Two new mesoporous silicates have been successfully synthesized and characterized by a variety of techniques. The first structure is an improvement over the current large pore mesoporous silica nanoparticles in that the total synthesis time has been cut by approximately two thirds, the morphology of the particle is truly spherical and the structure can be generated at room temperature using materials with less total cost (if the decane is recovered and reused). The second type of particle represents a new class of potential electronic materials. Further experiments are required to determine whether or not it is possible to synthesize such a particle with a larger array of photo-active functional groups. Future research would develop a particle which may find applications in both solar cell development and light-emitting diodes.

References

- [1] L. Chen, Y. M. Wang, M.-Y. He *J. Porous Mater.* **2011**, 18, 211-216.
- [2] S. Che, Y. Sakamoto, O. Terasaki, T. Tatsumi *Chem. Mater.* **2001**, 13, 2237-2239.
- [3] D. Zhao, J. Sun, Q. Li, G. D. Stucky *Chem. Mater.* **2000**, 12, 275-279.
- [4] C.-Y. Mou, H.-P. Lin *Pure Appl. Chem.* **2000**, 72, 137-146.
- [5] B. Tan, S. E. Rankin *The Journal of Physical Chemistry B.* **2006**, 110, 22353-22364.
- [6] J. H. Kim, J.-S. Yu *Phys. Chem. Chem. Phys.* **2010**, 12, 15301-15308.
- [7] B. Tian, X. Liu, B. Tu, C. Yu, J. Fan, L. Wang, S. Xie, G. D. Stucky, D. Zhao *Nat Mater.* **2003**, 2, 159-163.
- [8] C. V. Teixeira, H. Amenitsch, P. Linton, M. Lindén, V. Alfredsson *Langmuir.* **2011**, 27, 7121-7131.
- [9] G. Fornasieri, S. Badaire, R. Backov, O. Mondain-Monval, C. Zakri, P. Poulin *Adv. Mater. (Weinheim, Ger.)* **2004**, 16, 1094-1097.
- [10] Y.-G. Lee, C. Oh, S.-K. Yoo, S.-M. Koo, S.-G. Oh *Microporous Mesoporous Mater.* **2005**, 86, 134-144.
- [11] J. L. Blin, R. Bleta, J. Ghanbaja, M. J. Stebe *Microporous Mesoporous Mater.* **2006**, 94, 74-80.
- [12] J. L. Blin, J. Grignard, K. Zimny, M. J. Stebe *Colloids Surf., A.* **2007**, 308, 71-78.
- [13] N. Andersson, B. Kronberg, R. Corkery, P. Alberius *Langmuir.* **2007**, 23, 1459-1464.
- [14] T. Shikata, H. Hirata, T. Kotaka *Langmuir.* **1987**, 3, 1081-1086.
- [15] B. D. Hatton, K. Landskron, W. Whitnall, D. D. Perovic, G. A. Ozin *Advanced Functional Materials.* **2005**, 15, 823-829.
- [16] Y. Yang, A. Sayari *Chemistry of Materials.* **2008**, 20, 2980-2984.
- [17] J. Morell, M. Gungerich, G. Wolter, J. Jiao, M. Hunger, P. J. Klar, M. Froba *Journal of Materials Chemistry.* **2006**, 16, 2809-2818.
- [18] Y. Liang, E. S. Erichsen, M. Hanzlik, R. Anwander *Chemistry of Materials.* **2008**, 20, 1451-1458.
- [19] T. Asefa, M. J. MacLachlan, N. Coombs, G. A. Ozin *Nature.* **1999**, 402, 867-871.

- [20] H. Li, M. Xiong, F. Zhang, J. Huang, W. Chai *The Journal of Physical Chemistry C*. **2008**, 112, 6366-6371.
- [21] C. Baleizao, B. Gigante, D. Das, M. Alvaro, H. Garcia, A. Corma *Chemical Communications*. **2003**, 1860-1861.
- [22] M. Kuroki, T. Asefa, W. Whitnal, M. Kruk, C. Yoshina-Ishii, M. Jaroniec, G. A. Ozin *Journal of the American Chemical Society*. **2002**, 124, 13886-13895.
- [23] J. Morell, G. Wolter, M. Fröba *Chemistry of Materials*. **2005**, 17, 804-808.
- [24] Y. Goto, N. Mizoshita, O. Ohtani, T. Okada, T. Shimada, T. Tani, S. Inagaki *Chemistry of Materials*. **2008**, 20, 4495-4498.
- [25] M. A. Wahab, C. He *Langmuir*. **2008**, 25, 832-838.
- [26] H. Peng, J. Tang, L. Yang, J. Pang, H. S. Ashbaugh, C. J. Brinker, Z. Yang, Y. Lu *Journal of the American Chemical Society*. **2006**, 128, 5304-5305.
- [27] S. Shylesh, C. Srilakshmi, A. P. Singh, B. G. Anderson *Microporous and Mesoporous Materials*. **2007**, 99, 334-344.
- [28] M. Rat, M. H. Zahedi-Niaki, S. Kaliaguine, T. O. Do *Microporous and Mesoporous Materials*. **2008**, 112, 26-31.
- [29] T. Tani, N. Mizoshita, S. Inagaki *Journal of Materials Chemistry*. **2009**, 19, 4451-4456.
- [30] J. H. Armstrong, S. Wiedeman, L. M. Woods in *Monolithically integrated diodes in thin-film photovoltaic devices*, Vol. (Ed.^Eds.: Editor), (Global Solar Energy, Inc., USA). City, **2003**, pp.26 pp.
- [31] Y.-H. So, S. J. Martin, B. Bell, C. D. Pfeiffer, R. M. Van Effen, B. L. Romain, S. M. Lefkowitz *Macromolecules*. **2003**, 36, 4699-4708.
- [32] X. Liu, X. Xu, Q. Zhuang, Z. Han *Polymer Bulletin*. **2008**, 60, 765-774.
- [33] M. M. Alam, S. A. Jenekhe *Chemistry of Materials*. **2002**, 14, 4775-4780.
- [34] P. Guo, S. Wang, P. Wu, Z. Han *Polymer*. **2004**, 45, 1885-1893.
- [35] L. Yin, Z. Shen, J. Niu, J. Fu *Materials Letters*. **2009**, 63, 2212-2214.
- [36] Z. Feng, Y. Li, D. Niu, L. Li, W. Zhao, H. Chen, L. Li, J. Gao, M. Ruan, J. Shi *Chemical Communications*. **2008**, 2629-2631.
- [37] S. Z. Qiao, C. X. Lin, Y. Jin, Z. Li, Z. Yan, Z. Hao, Y. Huang, G. Q. Lu *The Journal of Physical Chemistry C*. **2009**, 113, 8673-8682.
- [38] K. J. Balkus Jr, T. J. Pisklak, G. Hundt, J. Sibert, Y. Zhang *Microporous and Mesoporous Materials*. **2008**, 112, 1-13.
- [39] A. Lan, K. Li, H. Wu, D. H. Olson, T. J. Emge, W. Ki, M. Hong, J. Li *Angewandte Chemie International Edition*. **2009**, 48, 2334-2338.
- [40] M. E. Germain, T. R. Vargo, P. G. Khalifah, M. J. Knapp *Inorganic Chemistry*. **2007**, 46, 4422-4429.

Chapter 4: Synthesis of a New Imidazole-Derived Copper Ligand for Copper Assisted Azide/Alkyne Cycloaddition

Introduction

N-heterocyclic carbenes (NHCs) represent a specific type of Fischer carbenes and have shown a diverse and expanding chemistry, specifically as ancillary ligands. Coordination of NHC ligands to a variety of metal centers has led to the generation of efficient and selective catalysts (reference, cite Grubbs obviously). Moreover, numerous methods for the synthesis of NHCs have been reported (reference), which has allowed for, among other things, the development of solid-supported NHC complexes. It is this diversity of catalytic reactions that makes NHC chemistry so attractive for heterogeneous catalysis (HC). Utilizing a single carbene ligand numerous groups have shown it possible to catalyze over a dozen different reactions including Suzuki coupling (Pd),^[1] amide bonds from alcohols (Ru),^[2] hydroalkoxylation (Au),^[3] transfer hydrogenation (Ir),^[4] and O-arylation of aryl bromides (Rh).^[5, 6] The same NHC ligand can also be used to create pharmaceutically active compounds.^[7] One of the main goals of HC is to develop new “green” catalysts, which can be used in benign/aqueous solvents and are easily recoverable and recycled; to this effect we are attempting to develop a novel solid-supported Cu (I) NHC catalyst for the 1,4-dipolar azide/alkyne cycloaddition (CuAAC).

The Imidazole Derived NHC Ligand

The existence of stable NHC compounds was theorized in the 1960's by Wanzlick et al. followed shortly thereafter by the first isolation of stable NHC-transition metal complex in the 1970's by the groups of Wanzlick and Öfele.^[8-10] However, it was not until 1991 that the first stable diaminocarbene was synthesized by Arduengo et al.^[11, 12] The difficulty in preparation was owed to the propensity of diaminocarbenes to dimerize unless bulky R₂ groups were used to prevent dimer formation. Later it was discovered that adequate

electronic stabilization of the carbene through σ -withdrawing atoms at the 4 and 5 positions yields stable, free NHCs by reducing the basicity of the carbene lone-pair.^[13] NHCs first gained notoriety as replacements for phosphine ligands and other strongly σ -donating ligands such as cyclopentadienyl. A review by Crabtree highlights some differences between phosphine ligands and NHC ligands.^[14] One difference lies in the shape of the ligands. Phosphines are cone-shaped whereas NHCs are fan shaped resulting in much more steric interaction in the case of bis-chelating NHC ligands.

NHCs are regarded as Fischer-type carbene complexes. Fischer carbenes exist in the singlet ground state with a filled sp^2 -orbital and a vacant p orbital on the carbene carbon. In contrast, Schrock carbenes are found in a triplet ground-state and contain one electron in both the sp^2 and p carbene orbitals (Figure 1A). A Fischer carbene is usually seen when there is a difference of greater than 40 kJ/mol between the

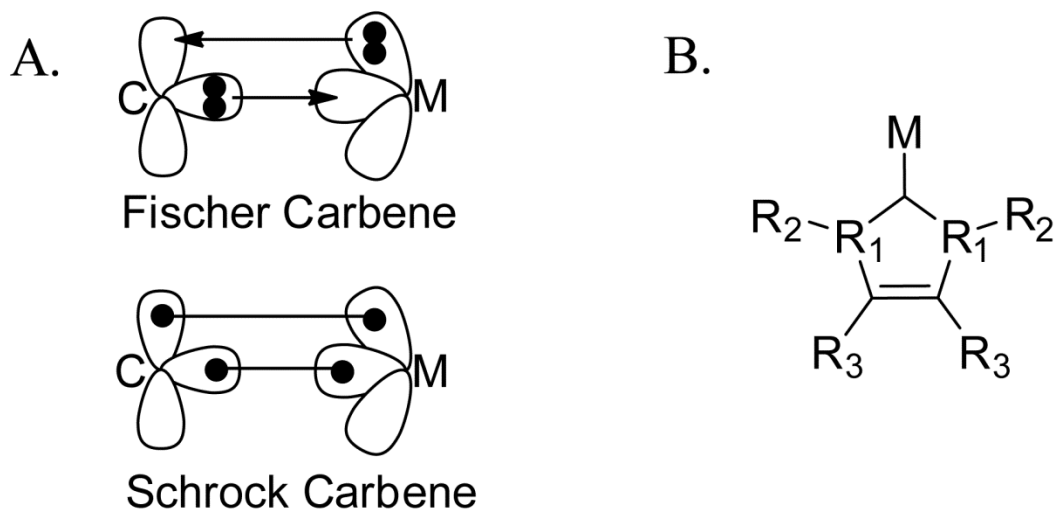


Figure 1. A. Illustration of the differences in bonding between Fischer and Schrock carbenes. Fischer carbenes reside in a singlet ground state while Schrock carbenes have a triplet ground state. B. Representation of imidazole outlining important areas of substitution in the molecule.

singlet and the triplet state. Owing to their different electronic structures, Fischer and Schrock carbenes interact differently with metal centers and the resulting carbene complexes display different reactivities. Fischer carbenes are L-type ligands, which do not formally oxidize the metal center. Moreover, the vacant p orbital on Fischer carbenes render them capable of π -

back bonding to the metal center and susceptible to attack from nucleophiles. Schrock carbenes are X_2 type ligands that formally oxidize the metal center by two, similar to O^{2-} .^[15] Unlike Fisher carbenes, Schrock carbenes tend to behave as nucleophiles. Although NHCs derived from 1,3-imidazoles are usually classified as Fisher carbenes, there are two scenarios where they more closely resemble Schrock-type carbenes. The two scenarios arise when switching from π -donating groups at R_1 to π -accepting groups and by decreasing the oxidation state of the metal complex, thereby increasing the energy of the metal d_{π} -orbitals and reducing overlap with the empty π -accepting orbitals of the carbene (**Fig. 1B**).^[15]

Traditionally, the electron donating ability of a ligand has been quantified using the Tolman electronic parameter (TEP).^[16] In these experiments the carbonyl stretch of a $M(CO)_xL$ (where L is the ligand of interest) compound is measured. The TEP measures the amount of π -backbonding from the metal into the carbonyl. By increasing the amount of σ -donating character from ligand L to the metal increases the amount of π -backbonding between the metal and the CO ligand. Metal to carbon π -backbonding causes the strength of the carbon-oxygen bond to decrease, resulting in lower frequencies of the carbonyl main stretching mode. The bond dissociation energies or TEP values for $M(CO)_xNHC$ systems are usually compared with %V (percent metal volume buried) with a rough degree of correlation. In the case where significant discrepancies were found between TEP and %V, attempts to refine the correlation by measuring ΔH of CO dissociation often show greatly different energies for ligands having nearly identical TEP values. One study by Gusev shows the theoretical TEPs for 76 different NHC ligands bonded to a $Ni(CO)_3$ complex and adds a steric factor that more thoroughly explains aberrations in the data such as the propensity for 1,3-di-*t*-butyl substituted NHC complexes to eliminate CO while imidazoles with 1,3-diisopropyl substituents do not, despite having nearly identical TEP values.^[17] In addition to steric contributions, Gusev's study finds that electron donating and withdrawing substituents in the 4,5 positions also have significant contributions to the carbonyl stretching frequency.

Further electronic-structure/function relationships are provided by Khamrov, whose work seeks to outline how both σ and π contributions at the 4 and 5 positions of imidazole effect the catalytic efficiencies of rhodium and palladium NHC complexes.^[18] The Rh-

catalyzed hydroboration of substituted acetylenes with pinacolborane yielded clear trends for the phenylacetylene substrate. When σ -withdrawing groups were substituted at positions 4 and 5, reaction yields increased compared to those with analogous π -withdrawing substituents. However, no trend was detected for the reaction with the 1-hexyne substrate. While overall Heck-coupling efficiencies were low, an important distinction was observed during kinetic studies. Unsubstituted NHCs were expected to be better than 4,5-functionalized catalysts owing to their electron rich structure which increases the rate of the oxidative addition of an aryl halide to Pd.^[19] Indeed, fast saturation kinetics were observed for the unsubstituted NHC, but with strongly withdrawing CN substituents at the 4 and 5 positions, the life of the catalyst increased by almost 5-fold resulting in nearly 20% greater conversion. The cyano groups were theorized to stabilize the electron rich Pd⁰ resting state of the catalyst from unwanted oxidation.^[18] These reactions demonstrated the extraordinary tunability of NHC ligand.

While catalytic reactions with NHC coordination compounds were shown to undergo many of the same types of reactions traditionally accomplished with phosphine ligands, additional chelating groups bound to the NHC backbone can help to improve yields and make catalytic molecules more specific for different types of reactions.^[20] Additionally, NHC ligands with chiral or bulky substituents were shown to be effective for enantio- and stereoselective catalysis. NHC pincer ligands have been synthesized with pyridyl, amine, thiol and phosphine chelating groups. Most of these studies use nickel, palladium or ruthenium as the coordinated metal, and relatively little information exists on copper-based pincer chemistry.^[21-24] Results for some of these studies are summarized in Table 1. Palladium and nickel based catalysts have proven themselves effective for several types of reactions. Several reviews of existing imidazole-derived NHC catalysts are available.

Entry	Metal	Ligand	Reaction	Yield	EE	E/Z	reference
1	Pd	Am-C-Am	Suzuki	17-38%	a	b	Liao ^[25]
2	Pd	S-C-S	Suzuki/Miyaura	64-88%	a	b	Fliedel ^[26]
3	Pd	P-C-P	hydroamination	67-99%	22-75%	b	Gischig ^[22]
4	Pd	Py-C-Py	polymerization	n ≈ 37 ^c	a	b	Chen ^[27]
5	Pd	Py-C-Py	Suzuki/Miyaura	99%	a	b	Chen ^[28]
6	Ni	Py-C-Py	Kumada-Corriu	60-99%	a	b	Chen ^[28]
7	Cu	O-C-O	conj. addition	99%	46-72%	1 : 9 - 20 : 1 ^d	Kehrli ^[29]
8	Rh	Py-C-Py	t-hydrogenation	40-100%	0-83%	b	Newman ^[30]
9	Rh	Py-C-Py	hydrogenation	0-99%	0-83%	b	Newman ^[30]

Table 1. Various reactions catalyzed by NHC-pincer complexes. Abbreviations for NHC ligands are as follows; Am – amido, S – sulfur, P – phosphine, Py – pyridyl, O – ether. ^a EE not reported, ^b E/Z not reported, ^c average molecular repeat of polymer, ^d ratio of 1,2 : 1,4 substituted products.

Heterogeneous NHC Catalysis

The success of NHC molecules as catalysts has led to the development of several heterogeneous systems including polymer, organometallic structures and silica-supported catalysts.^[31, 32] Significant contributions to the field of solid supported NHC catalysts are summarized in Table 2. Application of silica supported ruthenium-NHC complexes to hydrogen transfer reactions resulted in product yields and selectivities that were comparable to the analogous homogeneous system.^[33] For the cyclopropanation of (blank with blank), a heterogeneous asymmetric Ru-NHC system was more enantioselective than the corresponding homogeneous catalyst, albeit with decreased reactivity and longer times.^[34] Promising catalytic results were also reported for silica supported palladium NHC complexes. Reports in heterogeneous Pd-NHCs for Suzuki couplings of phenyl iodides have shown excellent conversions in short times (20-50 minutes) and mild temperatures.^[35] The catalyst was shown to be able to be recycled up to 6 times with only a 10% loss in overall conversion efficiency. Suzuki couplings of phenyl bromides also showed excellent conversion efficiencies although required longer times for more electron donating phenyl bromides. The same system was used for Heck couplings with high coupling efficiencies in short times but temperatures of 130°C were required for completion. Additionally, the solid support greatly

allowed for facile recycling of the catalyst. Complexes grafted to SBA-15 (2D-hexagonal pores, ≈ 8 nm) showed only modest recyclability (4 trials) before significant loss of activity in Suzuki coupling, while complexes grafted to SBA-16 (3D-cubic pores, ≈ 8 nm) showed high activity in up to 10 trials for Suzuki couplings and up to 8 trials in Heck couplings.

Entry	Support	Metal	Ligand	Reaction	mol % cat.	Yield	Trials ^b	EE	E/Z	reference
1	MCM-41 ^a	Ru	C-Py-Am	hydrogenation		70 - 100%	-	5-98%	d	del Pozo ^[34]
2	MCM-41 ^a	Ru	C-Py-Am	cyclopropanation		10 - 100%	-	5-77%	1:1 - 100:1	del Pozo ^[33]
3	MCM-41 ^a	Ru	C-Py-N	Dehydrogenation		0 - 100%	-	c	d	del Pozo ^[33]
4	silica	Pd	R-C-R	Suzuki	0.2	79 - 84%	2	c	d	Tyrrell ^[36]
5	SBA-16 ^a	Pd	R-C-R	Suzuki	0.01	87 - 99%	10	c	d	Yang ^[37]
6	SBA-15 ^a	Pd	R-C-R	Suzuki	0.01	98%	3	c	d	Yang ^[37]
7	silica	Pd	R-C-R	Suzuki	0.01	95%	2	c	d	Yang ^[37]
8	SBA-16 ^a	Pd	R-C-R	Heck	0.01	76 - 97%	8	c	d	Yang ^[37]
9	MCM-41 ^a	Pd	R-C-R	Suzuki	0.05 - 1.0	93 - 100%	6	c	d	Alam ^[35]
10	MCM-41 ^a	Pd	R-C-R	Hydrogenation	0.0001	100%	3	c	> 80% ^e	Liu ^[38]
11	silica	Pd	R-C-C-R	Heck	0.0001	78 - 96%	4	c	d	Karimi ^[39]
12	MOF	Pd	R-C-R	conj. Umpolung	-	46 - 84%	5	c	01:01.5	Rose ^[32]
13	MOF	Pd	C-C	Strecker	4	51 - 99%	3	c	c	Choi ^[40]

Table 2. Various reactions catalyzed by metal-NHC complexes immobilized on solid substrates. MOF = Metal Organic Framework. ^a designates a specific mesoporous silicate. ^b Trials in which catalyst activity dropped below 50% of the starting activity are dropped from the total count. ^c EE data unavailable. ^d E/Z data unavailable. ^e represents selectivity of propanol over propanal products

Han et al. recently prepared a collection of imidazolium-ionic liquid based NHCs linked to an amorphous silica particle with 2D-hexagonal pore framework. Their work showed that the ionic liquid Pd-NHCs had a equal efficiencies to Pd/C for hydrogenating 1-hexene and cyclohexene but showed approximately 20% more conversion with allyl alcohol as the substrate with 1-propanol/propanal selectivities more than 5% greater than Pd/C.^[38] With increases in the types and synthetic pathways to NHC molecules and the advantages of

heterogeneous and “green” catalysis, this area is expected to greatly increase in scope over the next decade.

Copper Catalyzed Azide/Alkyne Coupling (CuAAC) Reactions

For over a decade the CuAAC reaction has been one of the best studied of the “click” reactions. The reaction has proven to be useful in a wide variety of conditions with a wide variety of substrates. The azide/alkyne coupling reaction has been employed to attach molecules to surfaces and to synthesize new materials; the catalysts have also been shown to be effective when immobilized onto solid supports. Azide/alkyne coupling reactions have been successfully performed using a variety of simple copper salts alone. The addition of ancillary ligands also allow the synthesis of molecules impossible when using only simple copper salts.^[41] Amine, phosphine and NHC ligands have been utilized to affect the rates and selectivities of some CuAAC reactions.

CuAAC reactions have been proposed to proceed via a variety of different reactions pathways depending on copper precursor, ligand, base and solvent used.^[42-46] In all cases, it is widely regarded that ligands generally help to protect Cu (I) species from oxidation and basic amine ligands add electron density to the metal center (Figure 2).^[47] Additional electron density was hypothesized to accelerate the rate of the triazole forming step.^[50]

In general, multi-dentate ligands provide the best acceleration due to their ability to stabilize the resting form of the catalyst. The best examples of accelerating ligands to date are those molecules with structures $(Hy)_3N$. Early results by Fokin indicate that tris-(benzyltriazolylmethyl)amine (TBTA) provides the most protection from aerobic conditions coupled with a strong rate-enhancement effect.^[51] Although strongly donating ligands were proposed to increase reaction rate, the use of strongly-coordinating multi-dentate ligands such as tris-pyridylamine and tris-methylcarboxylamine resulted in slower CuAAC reactions.^[52] It is thusly theorized that weak-binding ligands are necessary to permit binding

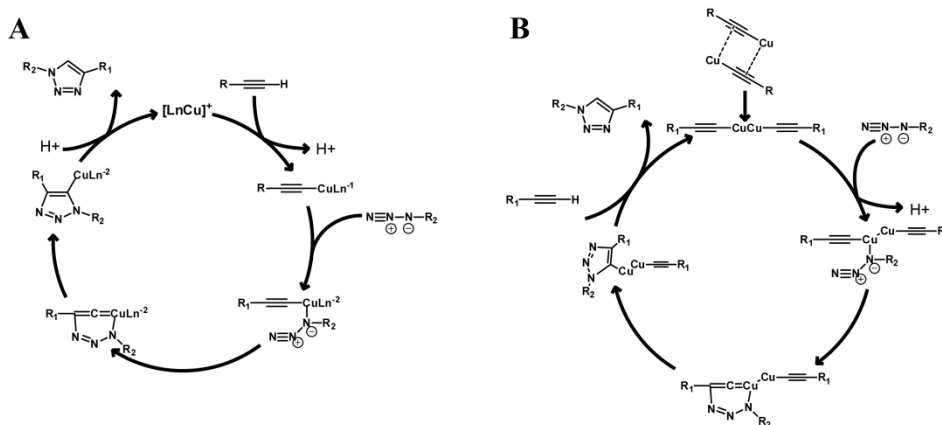


Figure 2. A. Original CuAAC reaction mechanism proposed by Sharpless and Fokin in 2002.^[47] B. One of several recently proposed reaction mechanisms with a dinuclear copper complex. The dinuclear complex is in response to observed second order rate constants with respect to copper and the difference in reactivities of mono and bis-alkyne substrates. The copper molecules may be directly bonded or bridged by ligands, depending on the reaction conditions.^[48, 49]

of the substrate to the catalyst. Multi-denticity is required to keep the metal atom in the coordination environment of the ligand. Furthermore, in this study, it was found that tridentate ligands with a bulky side group (table 3. Ent #) and ligands bearing pendant carboxylic acid groups increased reaction rates relative to those using the TBTA ligand. The rate enhancement was explained using the preferred coordination geometry of Cu (I) complexes; the strongly chelating carboxylic acid displaces an imidazole ligand providing better overall geometry for substrate binding. Carboxylic acids have also been shown to increase the rate of imidazole protonation in CuAAC reactions leading to an overall increase in reaction rate.^[53] In the case of a non-bonding R-group, the ligand is more able to maintain the tetrahedral geometry of Cu (I) while protecting the Cu center from oxidation and allowing the substrate to bind without the displacement of ligand.

While rare in the literature, Cu complexes bearing NHC ligands have been found to catalyze CuAAC reactions. The most effective catalyst was (SIMes)CuBr, which afforded products in yields up to 98% in approximately 20 minutes reaction times under optimized conditions.^[54] This ligand has also been shown to be effective at catalyzing the reactions between azides and internal alkynes, presumably through strong σ -donating character of the NHC helping to stabilize the Cu-alkyne π -complex.^[55]

Heterogeneous CuAAC Catalysts

One of the main driving forces behind the development of a heterogeneous CuAAC system is the reactions wide use in biochemical applications where copper concentrations must be tightly controlled and can quickly reach toxic levels.^[56, 57] The overall versatility and reliability of the CuAAC reaction naturally lends itself to studies in heterogeneous systems. Active catalysts have been prepared on a number of substrates including polymer, charcoal, silica and MOFs.^[58-61] Important studies on heterogeneous CuAAC are summarized in Table 4. Although reports of silica supported CuAAC catalysts are quite rare, the systems that have been developed gave promising results.

Entry	Support	Ligand	mol % cat.	Yield	Trials ^b	reference
1	polymer	TBTA	0.001	a	7	Lammens ^[58]
2	polymer	-	-	66 - 98%	-	Buckley ^[49]
3	charcoal	-	10	92 - 99%	3	Lipshutz ^[59]
4	zeolite	-	10	52 - 94%	-	Chassaing ^[62]
5	zeolite	-	-	57 - 98%	4	Beneteau ^[63]
6	MOF	-	0.1	37 - 99%	2	Luz ^[64]
7	SiO ₂	BPA	0.05 - 1.5	86 - 99%	5	Megia-Fernandez ^[65]
8	SiO ₂	DEA	1	29 - 70%	3	Cabrero-Antonino ^[66]
9	SiO ₂	Cu ₃ N	-	60 - 91%	5	Lee ^[67]
10	SiO ₂	PEI(Cu)	-	60-98%	3	Veerakumar ^[60]

Table 4. Various CuAAC reactions using heterogeneous copper catalysts. ^bThe number of trials reported are the number of subsequent reactions that can be run before the product synthesized drops below 50% of the original value.

Two recent reports use copper nanoparticles immobilized on silica. The first example uses simple copper nanoparticles stabilized with polyethylenimine on simple silica spheres.^[60] Results of cycloaddition reactions show greater than 90% yields for a variety of substituted azides. Additionally, this catalyst was evaluated for C-S cross coupling with high yields (>80%) for all substrates. The second example utilizes copper nitride particles immobilized on mesoporous silica.^[67] This system also incorporates a superparamagnetic Fe₃N for the magnet-assisted removal of the catalyst. Moderate yields of cycloaddition

products (72 – 91%) were obtained for sets of highly substituted azides and alkynes. Reaction times for this catalyst were excessive with some systems requiring 14 days for 82% yields. The shortest reaction time in the study was 12 hours for the triazole product containing 1,4-bisphenyl substitution. The only example ligand accelerated CuAAC on mesoporous silica comes from the work of Cabrero-Antonino et al.^[66] This group synthesized a hybrid silica/organic structure using either a diethylamine (DEA)(sodium ascorbate added to reduce Cu (II)) or a Tröger base silsequioxane molecule as the copper chelating moiety. Product yields were low for the two systems with DEA producing a 70% yield and the Tröger base resulting in a 53% yield in 24 hour reactions.

It is noteworthy that the three studies of CuAAC catalysts on silica were all reported within the last year, indicating a new interest in this area of research. Additionally, the reported yields for all silica systems were lower than those for homogeneous systems, which allows for much additional room to synthesize and optimize new silica supported CuAAC catalysts. Considering the promise shown for NHC accelerated CuAAC and the preliminary reports of silica supported “click” catalysts, we endeavored to synthesize several unique 1,3-bispyridyl substituted imidazolium molecules for their eventual application as catalysts (Figure 4). In addition, we hypothesize that due to the fact that the CuAAC ligand in this

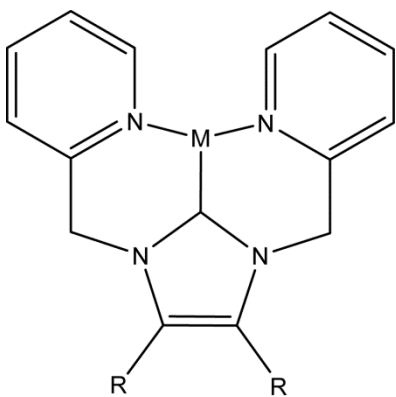


Figure 4: The structure of the final products in this study. The 4,5-substitution ‘R’ can be any organic molecule allowing for the tethering of the ligand to the mesoporous silica support. In the case of CuAAC reactions M = Cu.

study will be immobilized on the solid support, mechanistic work in determining whether a bi-nuclear or mono-nuclear copper transition species will also be possible. The structure pictured in Fig. 4 is unreported except when positions 4 and 5 are hydrogen. Currently, several linking moieties have been hypothesized which will allow for relationships between 4,5 substitution and catalytic efficiency and/or product distribution to be drawn.

The ability for NHC ligands to catalyze such a wide variety of reactions and the general utility and dependability of CuAAC reactions has led to the proposal of a heterogeneous system comprising a copper coordinated NHC ligand linked to the surface of a mesoporous silica nanoparticle (MSN). In addition, MSN supported catalysts have been shown to be able to catalyze tandem reactions that are normally in which the catalysts are incompatible, such as subsequent acid-base reactions.^[68] Furthermore MSN supported catalysts have also been shown to be effective at providing enantioselectivity as well as being able to increase product yield through secondary functionalization of the silica surface.^[69, 70] These attributes, in addition to the arguments of catalyst recovery and recyclability have led us to propose this new NHC-MSN system. The project is in currently in its rudimentary stages and no supported catalyst has been synthesized however, important precursors have been synthesized and a test of the ability for the 1,3-methylpyridine-(4,5-H,H)-imidazole copper ligand to catalyze the CuAAC reaction have been performed.

Experimental

Silver oxide, potassium iodide, potassium periodate, potassium chloride, sodium carbonate and 12 M HCl were purchased from Sigma Aldrich and used without further purification. 1H-imidazole-4,5-dicarboxylic acid and 1H-imidazole-4,5-dimethanol were purchased from TCI America and used without purification. Ammonium hexafluorophosphine and 2-bromomethylpyridine were purchased from Acros Organics and used without further purification. Finely powdered copper metal was received in an unmarked vial as a donation from the Larock group. Water used is purified with a Millipore® system until 18 Mohm resistance is reached.

Potassium iododichloride (KICl₂) solution: Synthesis of this solution was accomplished using the published procedure by Larsen *et al.*^[71] In a 2-neck one liter flask, 71 g (0.33 mol.) of potassium iodate, 40 g of potassium chloride and 5 mL of concentrated hydrochloric acid is added to 80 mL of water and allowed to dissolve. To an Erlenmeyer flask, 111 g (0.66 mol.) of potassium iodide is dissolved in 90 mL of water and then placed in an addition funnel; the flask is washed once with 10 mL of water. To a second addition funnel, 170 mL of conc. hydrochloric acid is added. The two addition funnels are fixed to the 2-neck one liter flask equipped with a stir bar and then reagents are added dropwise simultaneously. It was found to be vitally important to control the rate of addition so that it takes 3-4 hour to complete each addition in order to avoid excess generation of heat and the subsequent release of chlorine gas, attempting to cool the reaction in an ice bath results in the precipitation of solid I₂. Water is then added to the solution to make 500 mL, resulting in a 2 M solution of KICl₂.

1H-4,5-diiodoimidazole (1): Synthesis of this precursor was carried out according to the procedure published by Garden *et al.*^[72] An aqueous solution of imidazole (30 mmol, 0.3 M) is added dropwise to 37 mL of the 2 M KICl₂ solution via addition funnel. After addition the reaction is stirred an additional 6 hours and 2 M NaOH is added to the flask until the solids are completely dissolved. The solution is then adjusted to pH 10 by dropwise addition of concentrated HCl. This results in the precipitation of the desired product which is then recrystallized from methanol to afford the purified 4,5-diiodoimidazole in 90% yield.

1,3-methylpyridineimidazole bromide (2): Synthesis of this ligand was accomplished by first placing 500 mg (7.34 mmol) of imidazole and 3.46 g (32.6 mmol) sodium carbonate (dibasic) in 160 mL of anhydrous acetonitrile and stirring for 30 minutes. To the suspension, 4.12 g (16.3 mmol) of 2-bromomethylpyridine is added and the mixture heated to reflux and allowed to react for 48 hours under argon atmosphere. Acetonitrile is then removed via rotovap and the sticky solid is dissolved in a minimum of CH₂Cl₂. This solution is then placed in a one liter beaker and the CH₂Cl₂ is allowed to evaporate leaving a purple/red film. This film is then triturated in approx. 500 mL of THF to afford the final product in approximately 75% yield.

1,3-methylpyridineimidazole silver bromide (2a): This compound is synthesized by dissolving 1,3-methylpyridineimidazole bromide in methanol and adding 1.5 equivalents of Ag_2O . This solution is stirred for four hours and then filtered to remove excess Ag_2O to give the product.

1,3-methylpyridineimidazole silver hexafluorophospine (2b): 1,3-methylpyridineimidazole silver bromide is dissolved in water and 2 equivalents of ammonium hexafluorophospine are added to the flask and allowed to stir for 2 hours. The product appears as an oil in the bottom of the flask and is extracted into CH_2Cl_2 . The organic layer is dried over MgSO_4 , filtered and rotovapped to yield the desired product.

1,3-methylpyridineimidazole copper hexafluorophospine (2c): 1,3-methylpyridineimidazole silver hexafluorophospine is added to a flask containing acetonitrile and excess powdered copper. This reaction is allowed to stir overnight and is then filtered to remove excess copper and precipitated AgBr salts. The filtrate is then rotovapped to dryness to yield the desired product.

1,3-methylpyridine-4,5-diiodoimidazolium bromide (3): Synthesis of this ligand was accomplished by first placing 500 mg (1.56 mmol) and 735 mg (6.94 mmol) of disodium carbonate in 80 mL of anhydrous acetonitrile and stirring for 30 minutes. To the suspension is added 877 mg (3.47 mmol) 2-bromomethylpyridine and the mixture is heated to reflux and allowed to react for 48 hours under argon atmosphere. Acetonitrile is then removed via rotovap and the sticky solid is dissolved in a minimum of CH_2Cl_2 . This solution is then added dropwise to ice cold diethyl ether and filtered. The product is unstable to light and atmosphere and is decanted under an argon atmosphere and redissolved in methypyrrolidone to be used immediately in the next reaction step.

1,3-methylpyridine-4,5-di(acetyltrimethylsilyl)imidazolium bromide

CuAAC catalysis: In a 20 mL scintillation vial containing 10 mL of water, 50 mg (0.159 mmol) of catalyst is added followed by 1.0 mmol of phenylacetylene, 1.0 mmol of benzylchloride, and 1.0 mmol of sodium azide. This mixture is allowed to stir for 24 hours and is then extracted with ether to remove the catalyst. The aqueous layer is then extracted 3

times with ethylacetate and the organic layer is dried over MgSO_4 and filtered. The filtered solution is rotovapped to dryness and the crude is collected and analyzed via proton NMR to determine whether or not product is present in the mixture.

Results and Discussion

Of the compounds synthesized in this project, only compound 2c was tested for to determine whether catalysis of the CuAAC reaction could be achieved. To this effect, it was observed that the catalytic reaction did proceed, albeit not to completion (figure 5). It is hypothesized that the main reasons behind the incomplete reaction were two-fold; the first reason being the lack of solubility of the catalytic ligand itself. While an excess (10 mol%) of the catalyst is added to the aqueous solution, a k_{sp} value of $10^{-3} \text{ mol L}^{-1}$ could easily reduce the amount of catalyst to less than 0.1 mol%. The second reason is the mass transfer and eventual precipitation of the triazole products. During the course of the catalytic reaction it was observed that the triazole product began to precipitate quickly from the aqueous solution. The precipitate quickly coated visible particles of catalyst resulting in a yellow waxy substance at the bottom of the reaction vessel. This precipitate could easily prevent substrates from reaching the catalyst and preventing further reaction.

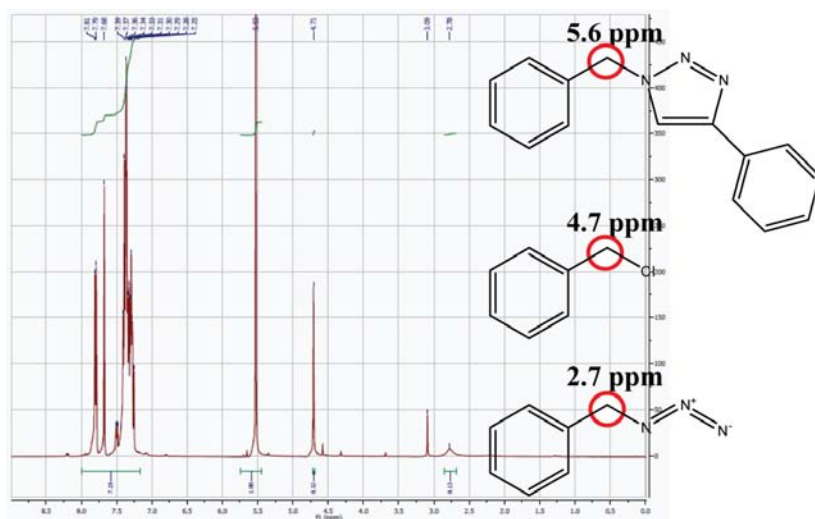
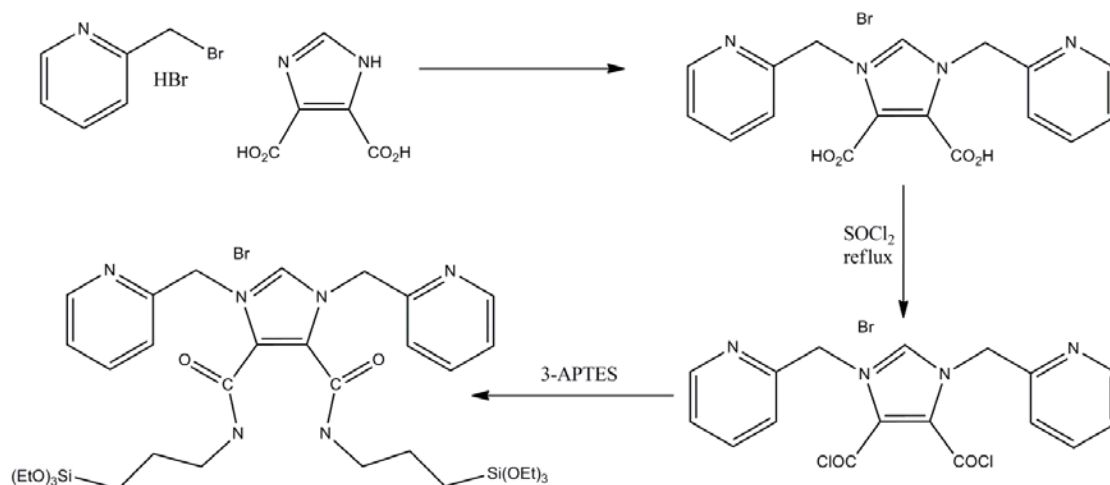


Figure 5. Proton NMR of the crude mixture resulting from the CuAAC catalytic testing using compound 2c as the catalyst.

Initially, the goal was to synthesize the ligand from 4,5-dicarboxyimidazole, this would have provided the shortest and one of the cheapest routes to a ligand capable of being incorporated into an MSN (scheme 1). Unfortunately it was discovered that reaction with 2-bromomethylpyridine resulted in



Scheme 1. Initial proposed scheme for preparation of the tridentate NHC ligand. The abbreviation 3-APTES stands for 3-aminopropyltriethoxysilane

only the monosubstituted 4,5-dicarboxyimidazole due to the deactivation of the nucleophilic nitrogens via electron withdrawing effects of the conjugated carboxyl groups. This led to the proposition of several other precursors including the following molecules seen in figure 6. It is hypothesized that molecule 3 could be reacted under Sonogashira conditions to afford

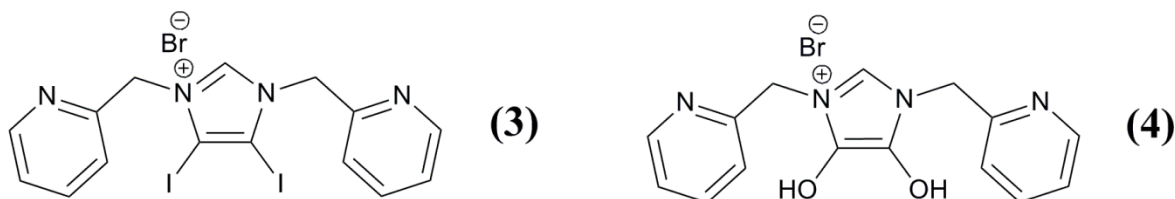
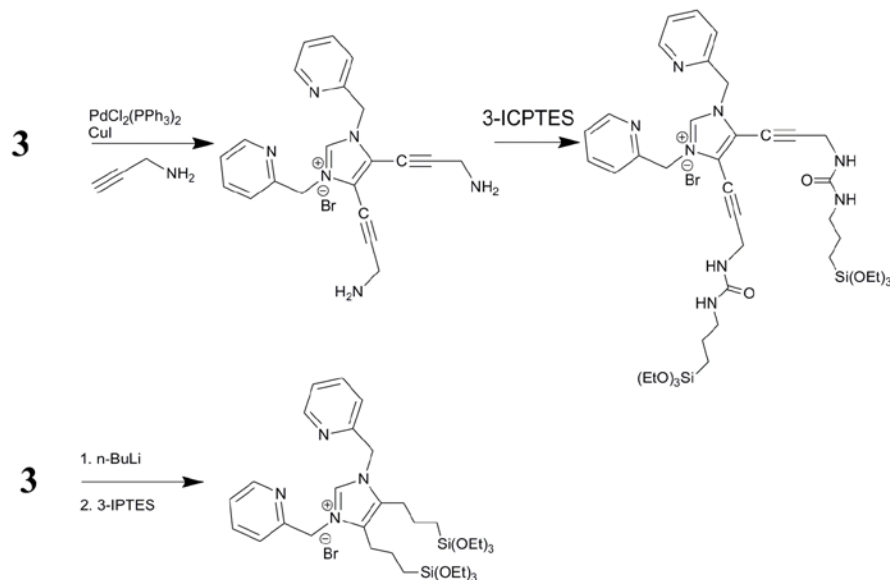


Figure 6. Molecules proposed after the initial failure to synthesize the product in step 2 of scheme 1.

the amine terminated product (scheme 2), followed by reaction with 3-isocyanatopropyltriethoxy silane to yield a product capable of being linked to an MSN. It is known that palladium will coordinate with NHC ligands over phosphine ligands which

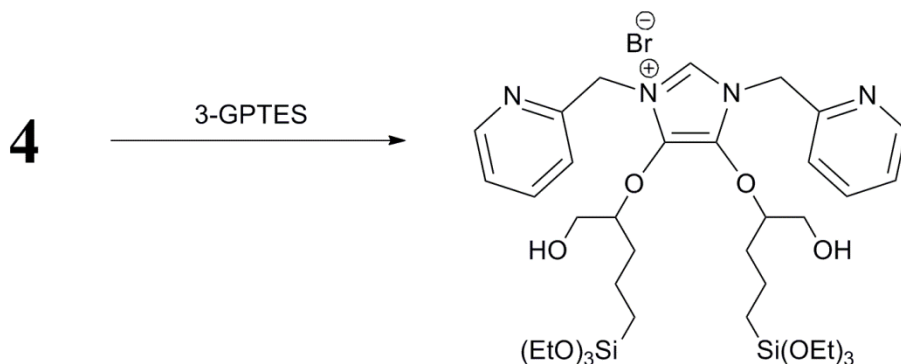
makes the first reaction in scheme 2 particularly interesting as the metallated product may be self-catalyzing as seen in the introduction where NHC-Pd complexes have been shown to be



Scheme 2. Proposed reactions to alkoxy silane terminated NHC ligands for incorporation with MSNs.

Abbreviations in the scheme are as follows: 3-ICPTES = 3-isocyanatopropyltriethoxysilane, 3IPTES = 3-iodopropyltriethoxysilane

active Sonogashira catalysts. The second reaction, lithium halogen exchange is much simpler though generating dianions on conjugated molecules is typically quite difficult (see chapter 3, section 2). Molecule 4 also presents several synthetic pathways to alkoxy silane terminated products although a simple one-step reaction is outlined in scheme 3. In this case, 4 would be added to 3-glycidoxypropyltriethoxysilane and the desired product should form



Scheme 3. The reaction of 4 with 3-glycidoxypropyltriethoxysilane (3-GPTES) to yield the desired product.

spontaneously. The substrate 3-GPTES could also be reacted with the lithiated product in scheme 2 to provide the anti-Markovnikov substituted product.

Conclusion

The successful synthesis of multiple ligand precursors enables future researchers to use different synthetic strategies in linking the tridentate-NHC ligand to the surface of MSN. In addition, while only 4,5-disubstituted products have been shown here, monosubstitution at either the 4 or 5 position would also provide another variable for study. The ability to change the metal center in the NHC ligand should also enable this system to be active for many different catalytic reactions. Furthermore, modification of the surface of the MSN should enable us to fine tune the reaction parameters to make many of the catalytic reactions enantioselective or to force away products and side products allowing the equilibrium of the reaction to be shifted toward making more product. When all of the aspects of this system are taken as a whole, this project has the potential to be one of the most powerful catalytic devices that has yet been synthesized.

References

- [1] S. K. Schneider, W. A. Herrmann, E. Herdtweck *J. Mol. Catal. A Chem.* **2006**, 245, 248-254.
- [2] C. Chen, Y. Zhang, S. H. Hong *J. Org. Chem.* **2011**, 76, 10005-10010.
- [3] R. S. Paton, F. Maseras *Org. Lett.* **2009**, 11, 2237-2240.
- [4] S. C. Zinner, C. F. Rentsch, E. Herdtweck, W. A. Herrmann, F. E. Kuehn *Dalton Trans.* **2009**, 7055-7062.
- [5] G. D. Frey, C. F. Rentsch, D. von Preysing, T. Scherg, M. Muehlhofer, E. Herdtweck, W. A. Herrmann *J. Organomet. Chem.* **2006**, 691, 5725-5738.
- [6] H. J. Kim, M. Kim, S. Chang *Org. Lett.* **2011**, 13, 2368-2371.
- [7] M. M. Jellicoe, S. J. Nichols, B. A. Callus, M. V. Baker, P. J. Barnard, S. J. Berners-Price, J. Whelan, G. C. Yeoh, A. Filipovska *Carcinogenesis*. **2008**, 29, 1124-1133.
- [8] H. W. Wanzlick *Angewandte Chemie International Edition in English*. **1962**, 1, 75-80.
- [9] H. W. Wanzlick, H. J. Schönherr *Angewandte Chemie International Edition in English*. **1968**, 7, 141-142.
- [10] Ö. K *Journal of Organometallic Chemistry*. **1968**, 12, P42-P43.
- [11] A. J. Arduengo, R. L. Harlow, M. Kline *Journal of the American Chemical Society*. **1991**, 113, 361-363.
- [12] A. J. Arduengo, M. Kline, J. C. Calabrese, F. Davidson *Journal of the American Chemical Society*. **1991**, 113, 9704-9705.

- [13] A. J. Arduengo, F. Davidson, H. V. R. Dias, J. R. Goerlich, D. Khasnis, W. J. Marshall, T. K. Prakash *Journal of the American Chemical Society*. **1997**, 119, 12742-12749.
- [14] R. H. Crabtree *J. Organomet. Chem.* **2005**, 690, 5451-5457.
- [15] R. H. Crabtree, *The Organometallic Chemistry of the Transition Metals*, John Wiley & Sons, Inc., Hoboken, New Jersey, **2005**.
- [16] C. A. Tolman *Chemical Reviews*. **1977**, 77, 313-348.
- [17] D. G. Gusev *Organometallics*. **2009**, 28, 6458-6461.
- [18] D. M. Khramov, E. L. Rosen, J. A. V. Er, P. D. Vu, V. D. Lynch *Tetrahedron*. **2008**, 64, 6853-6862.
- [19] A. F. Littke, G. C. Fu *Angewandte Chemie International Edition*. **2002**, 41, 4176-4211.
- [20] E. Peris, R. H. Crabtree *Coordination Chemistry Reviews*. **2004**, 248, 2239-2246.
- [21] J. C. C. Chen, I. J. B. Lin *Organometallics*. **2000**, 19, 5113-5121.
- [22] S. Gischig, A. Togni *Eur. J. Inorg. Chem.* **2005**, 4745-4754.
- [23] J. Berding, T. F. van Dijkman, M. Lutz, A. L. Spek, E. Bouwman *Dalton Trans.* **2009**, 6948-6955.
- [24] M. Bierenstiel, E. D. Cross *Coord. Chem. Rev.* **2011**, 255, 574-590.
- [25] C.-Y. Liao, K.-T. Chan, J.-Y. Zeng, C.-H. Hu, C.-Y. Tu, H. M. Lee *Organometallics*. **2007**, 26, 1692-1702.
- [26] C. Fliedel, A. Sabbatini, P. Braunstein *Dalton Transactions*. **2010**, 39, 8820-8828.
- [27] K.-T. Chan, Y.-H. Tsai, W.-S. Lin, J.-R. Wu, S.-J. Chen, F.-X. Liao, C.-H. Hu, H. M. Lee *Organometallics*. **2010**, 29, 463-472.
- [28] C. Chen, H. Qiu, W. Chen *J. Organomet. Chem.* **2012**, 696, 4166-4172.
- [29] S. Kehrl, D. Martin, D. Rix, M. Mauduit, A. Alexakis *Chem.--Eur. J.* **2010**, 16, 9890-9904, S9890/9891-S9890/9104.
- [30] P. D. Newman, K. J. Cavell, A. J. Hallett, B. M. Kariuki *Dalton Trans.* **2011**, 40, 8807-8813.
- [31] W. J. Sommer, M. Weck *Coordination Chemistry Reviews*. **2007**, 251, 860-873.
- [32] M. Rose, A. Notzon, M. Heitbaum, G. Nickerl, S. Paasch, E. Brunner, F. Glorius, S. Kaskel *Chem. Commun. (Cambridge, U. K.)*. **2011**, 47, 4814-4816.
- [33] C. del Pozo, M. Iglesias, F. I. Sánchez *Organometallics*. **2011**, 30, 2180-2188.
- [34] C. del Pozo, A. Corma, M. Iglesias, F. Sanchez *Green Chem.* **2011**, 13, 2471-2481.
- [35] M. N. Alam, S. M. Sarkar *React. Kinet., Mech. Catal.* **2011**, 103, 493-500.
- [36] E. Tyrrell, L. Whiteman, N. Williams *J. Organomet. Chem.* **2011**, 696, 3465-3472.
- [37] H. Yang, X. Han, G. Li, Y. Wang *Green Chem.* **2009**, 11, 1184-1193.
- [38] G. Liu, M. Hou, T. Wu, T. Jiang, H. Fan, G. Yang, B. Han *Phys. Chem. Chem. Phys.* **2011**, 13, 2062-2068.
- [39] B. Karimi, D. Enders *Organic Letters*. **2006**, 8, 1237-1240.
- [40] J. Choi, Y. Y. Yang, H. J. Kim, S. U. Son *Angew. Chem., Int. Ed.* **2010**, 49, 7718-7722, S7718/7711-S7718/7717.
- [41] J. Raushel, V. V. Fokin *Organic Letters*. **2010**, 12, 4952-4955.
- [42] S. Diez-Gonzalez *Catalysis Science & Technology*. **2011**, 1, 166-178.
- [43] S. Sun, P. Wu *The Journal of Physical Chemistry A*. **2010**, 114, 8331-8336.
- [44] L. Liang, D. Astruc *Coordination Chemistry Reviews*. **2011**, 255, 2933-2945.
- [45] S. I. Presolski, V. Hong, S.-H. Cho, M. G. Finn *J. Am. Chem. Soc.* **2010**, 132, 14570-14576.
- [46] G.-C. Kuang, P. M. Guha, W. S. Brotherton, J. T. Simmons, L. A. Stanke, B. T. Nguyen, R. J. Clark, L. Zhu *Journal of the American Chemical Society*. **2011**, 133, 13984-14001.
- [47] V. V. Rostovtsev, L. G. Green, V. V. Fokin, K. B. Sharpless *Angewandte Chemie International Edition*. **2002**, 41, 2596-2599.
- [48] V. D. Bock, H. Hiemstra, J. H. van Maarseveen *Eur. J. Org. Chem.* **2005**, 51-68.

- [49] B. R. Buckley, S. E. Dann, H. Heaney, E. C. Stubbs *Eur. J. Org. Chem.* **2011**, 770-776, S770/771-S770/744.
- [50] V. O. Rodionov, S. I. Presolski, S. Gardinier, Y.-H. Lim, M. G. Finn *J. Am. Chem. Soc.* **2007**, 129, 12696-12704.
- [51] T. R. Chan, R. Hilgraf, K. B. Sharpless, V. V. Fokin *Org. Lett.* **2004**, 6, 2853-2855.
- [52] V. O. Rodionov, S. I. Presolski, D. Díaz Díaz, V. V. Fokin, M. G. Finn *Journal of the American Chemical Society.* **2007**, 129, 12705-12712.
- [53] C. Shao, X. Wang, J. Xu, J. Zhao, Q. Zhang, Y. Hu *The Journal of Organic Chemistry.* **2010**, 75, 7002-7005.
- [54] S. Díez-Gonzalez, S. P. Nolan *Synlett.* **2007**, 2158-2167.
- [55] S. Díez-González, A. Correa, L. Cavallo, S. P. Nolan *Chemistry – A European Journal.* **2006**, 12, 7558-7564.
- [56] M. D. Best *Biochemistry.* **2009**, 48, 6571-6584.
- [57] D. C. Kennedy, C. S. McKay, M. C. B. Legault, D. C. Danielson, J. A. Blake, A. F. Pegoraro, A. Stolow, Z. Mester, J. P. Pezacki *Journal of the American Chemical Society.* **2011**, 133, 17993-18001.
- [58] M. Lammens, J. Skey, S. Wallyn, R. O'Reilly, F. Du Prez *Chemical Communications.* **2010**, 46, 8719-8721.
- [59] B. H. Lipshutz, B. R. Taft *Angew. Chem., Int. Ed.* **2006**, 45, 8235-8238.
- [60] P. Veerakumar, M. Velayudham, K.-L. Lu, S. Rajagopal *Catal. Sci. Technol.* **2011**, 1, 1512-1525.
- [61] A. Corma, E. Gutierrez-Puebla, M. Iglesias, A. Monge, S. Perez-Ferreras, F. Sanchez *Adv. Synth. Catal.* **2006**, 348, 1899-1907.
- [62] S. Chassaing, A. S. S. Sido, A. Alix, M. Kumarraja, P. Pale, J. Sommer *Chem.--Eur. J.* **2008**, 14, 6713-6721.
- [63] V. Beneteau, A. Olmos, T. Boningari, J. Sommer, P. Pale *Tetrahedron Lett.* **2010**, 51, 3673-3677.
- [64] I. Luz, i. X. F. X. Llabres, A. Corma *J. Catal.* **2010**, 276, 134-140.
- [65] A. Megia-Fernandez, M. Ortega-Munoz, J. Lopez-Jaramillo, F. Hernandez-Mateo, F. Santoyo-Gonzalez *Adv. Synth. Catal.* **2010**, 352, 3306-3320.
- [66] J. R. Cabrero-Antonino, T. Garcia, P. Rubio-Marques, J. A. Vidal-Moya, A. Leyva-Perez, S. S. Al-Deyab, S. I. Al-Resayes, U. Diaz, A. Corma *ACS Catal.* **2011**, 1, 147-158.
- [67] B. S. Lee, M. Yi, S. Y. Chu, J. Y. Lee, H. R. Kwon, K. R. Lee, D. Kang, W. S. Kim, H. B. Lim, J. Lee, H.-J. Youn, D. Y. Chi, N. H. Hur *Chem. Commun. (Cambridge, U. K.).* **2010**, 46, 3935-3937.
- [68] Y. Huang, S. Xu, V. S. Y. Lin *Angew. Chem., Int. Ed.* **2011**, 50, 661-664, S661/661-S661/613.
- [69] Y. Huang, S. Xu, V. S. Y. Lin *ChemCatChem.* **2011**, 3, 690-694.
- [70] C.-H. Tsai, H.-T. Chen, S. M. Althaus, K. Mao, T. Kobayashi, M. Pruski, V. S. Y. Lin *ACS Catalysis.* **2011**, 1, 729-732.
- [71] A. A. Larsen, C. Moore, J. Sprague, B. Cloke, J. Moss, J. O. Hoppe *Journal of the American Chemical Society.* **1956**, 78, 3210-3216.
- [72] S. J. Garden, J. C. Torres, S. C. de Souza Melo, A. S. Lima, A. C. Pinto, E. L. S. Lima *Tetrahedron Letters.* **2001**, 42, 2089-2092.

Chapter 5: General Conclusions

The field of research into the applications of mesoporous silicates has proven to be a popular avenue of study for the last two decades. The ability to functionalize these mesoporous silicates for specific applications continues to drive research, both in terms of fundamental materials research in generating new types of silicate materials for specific applications and research into probing and affecting the mechanisms of catalytic and biological systems.

The first chapter of this thesis outlines the current studies into the toxicity of mesoporous silica nanoparticles (MSNs) using *in vitro* and *in vivo* assays. Due to the variety of mesoporous silicate particles that are being evaluated, a general conclusion for the bio-safety of these nanoparticles cannot be derived. What can be derived from these studies is that current toxicological research involving MSNs (and indeed other nanoparticles) needs to be evaluated on a uniform set of standards. Nanoparticles of all types are proliferating in research and driving new fields, if toxicity standards are not decided upon early in this research, promising areas of study will be delayed due to the lack of regulatory control. Many of these lines of research are reviewed at the end of the chapter and include devices capable of targeting specific cells, improving *in vivo* imaging, and releasing pharmaceuticals in response to a particular trigger. Advances in these areas of research coupled with good regulatory controls will enable MSNs to be used as reliable prototype systems for years to come.

A new MSN functionalization for interfacing with biological system has been successfully developed and this system applied to improve the biocompatibility of MSNs with red blood cells (RBCs). The first part of chapter 2 outlines the synthesis and preliminary data involved with toxicity of a lipid bilayer coated MSN (LB-MSN). These LB-MSNs were then demonstrated to be capable of controlled release of fluorescein on exposure of the particles to a disulfide reducing agent. Additionally, the endocytosis of LB-MSN particles was observed using flow cytometry and confocal microscopy. These observations all support the hypothesis that LB-MSNs may be used as a drug delivery device. The second part of

chapter 2 highlights the ability of tuning the lipid bilayer composition to increase the biocompatibility of a large pore (I-MSN) mesoporous silica particle. In this study, the I-MSN, which had proved to be toxic towards red blood cell in an early study, is functionalized with two different compositions of lipid bilayer; one consisting entirely of lipids with phosphatidylcholine headgroups (DPPC) and the other consisting of a mixture of phosphorylated lipids (mRBC) which more accurately approximates the composition of the outer leaflet of the RBC membrane. It was shown that simply coating the I-MSN with a lipid bilayer remediates the propensity of the particles to cause haemolysis although observations with SEM indicate that damage to the cells (spiculation) is still occurring. Particles coated with the mRBC bilayer also show no haemolysis and RBCs remain largely undamaged by SEM observation. In addition to the synthesis of a new generation of potential drug delivery vehicles, we have shown that careful observations of many parameters is necessary to conclude that a material is biocompatible and that the current standard of haemocompatibility (haemolysis) may not be enough to make this evaluation.

The third chapter of this thesis details the synthesis of new types of mesoporous silicates. The first section deals with the synthesis of unfunctionalized mesoporous silica particles using water-in-oil emulsion (W/O). These emulsion systems have proven useful for generating particles with well controlled spherical morphology and regular porosity with pore diameters approaching 8 nm. In addition these particles can be synthesized at room temperature and in as little as 6 hours. This is a significant advancement over the synthesis of similar particle types which often rely on high synthesis temperatures, even higher aging temperatures and extended synthesis times of 24 hours or greater. The second part of the chapter deals with the synthesis of a new type of periodic mesoporous organosilica (PMO). This new PMO material represents a model material for future silicates containing light harvesting or light emitting conjugated organic molecules. Indeed, since this study was completed, the synthesis of a solar cell using similar of chemistry has been reported, indicating that the materials may have promise in future devices.^[1]

The final chapter of this thesis deals with the synthesis of a new N-heterocyclic carbene (NHC) derived from imidazole as a heterogeneous catalytic system. The MSN-

catalysis is being designed to affect the copper-mediated acetylene-azide cross-coupling reaction (CuAAC). While only rudimentary progress has been made with the project to date, early reports are promising as the model catalyst is capable of catalyzing this reaction homogeneously. Further work on this project will involve mostly methods to reliably affect substitution of the 4 and 5 position of the 1,3-substituted imidazole, and then to link the product to the surface of MSNs. The imidazole framework provides an NHC platform capable of coordinating a wide variety of metals, thereby allowing one ligand access to many different types of catalytic reactions. This coupled with the ability of MSNs to serve as platforms for heterogeneous catalysis should result in one of the most powerful catalytic systems in the field.

For over 20 years, mesoporous silicates have proven their usefulness in catalysis, biology, and energy applications. The main reasons for their success are the relative ease of synthesis along with the ability to modify the surface of the particle with a wide array of functional ligands. As new catalysts, biological targets, and energy harvesting/light producing molecules are discovered, scientist will be working with mesoporous silicates to see if the high surface area, controllable pore size, pore structure and particle morphology can improve the performance and possibly discover new applications of the aforementioned molecules.

References

- [1] Y. Lim, Y.-S. Park, Y. Kang, D. Y. Jang, J. H. Kim, J.-J. Kim, A. Sellinger, D. Y. Yoon *Journal of the American Chemical Society*. **2010**, 133, 1375-1382.